(2)

AD-A250 350

ATION PAGE

Form Approved
OMB No. 0704-0188

1. AGENCY USE ONLY (Leave blank)	2. REPORT DATE	3. REPORT TYPE AND DATES COVERED
	March 1992	Final Technical 1 Aug 88-30 Sept 91

4. TITLE AND SUBTITLE (U)
An Experimental Investigation of the Formation of Secondary Vortices and the Generation of Small-Scale Motion in a Spanwise Forced Plane Mixing Layer

5. FUNDING NUMBERS
PE-61102F
PR-2307/BS
SA-BS
G-AFOSR-88-0271

6. AUTHOR(S)
A. Glezer

7. PERFORMING ORGANIZATION NAME(S) AND ADDRESS(ES)
University of Arizona
Tucson, AZ 86721

8. PERFORMING ORGANIZATION REPORT NUMBER
AFOSR-TR- 92 0361

9. SPONSORING/MONITORING AGENCY NAME(S) AND ADDRESS(ES)
AFSOR/NA
Building 410
Bolling AFB, DC 20332-6448

10. SPONSORING/MONITORING AGENCY REPORT NUMBER
AFOSR-88-0271

11. SUPPLEMENTARY NOTES

12a. DISTRIBUTION/AVAILABILITY STATEMENT
Approved for public release; distribution is unlimited

12b. DISTRIBUTION CODE

13. ABSTRACT (Maximum 200 words)

The evolution of spanwise instability modes and 3-D pulsed disturbances leading to the formation of streamwise vortices in a plane mixing layer and subsequently to the onset of small-scale 3-D motion were studied in a closed-return water facility.

Streamwise vortices may result from a spanwise core instability of the primary vortices, or a spanwise instability of the nominally 2-D strain field between them. These two instability modes were excited by time-harmonic wavetrains with spanwise phase or amplitude variations, respectively, synthesized by a mosaic of surface film heaters flush-mounted on the flow partition. The appearance of the streamwise vortices is accompanied by significant distortion in the transverse distribution of the streamwise velocity component. Inflection points, which are not present in corresponding velocity distributions of the unforced flow, indicate the formation of locally unstable regions of large shear in which broadband perturbations already present in the base flow undergo rapid amplification which is followed by breakdown to turbulence and mixing transition. The core instability of the primary vortices suggests itself as viable mechanism for the continuation of the mixing process far downstream of mixing transition.

Pulsed excitation was produced by pulsed spanwise amplitude modulation of a spanwise-uniform time-harmonic carrier wave train synthesized by the surface film heaters. Schlieren visualization showed that the disturbance spreads rapidly in the streamwise and lateral directions as it is advected downstream, and causes a substantial distortion of the adjacent spanwise vortices. The evolution of the disturbance depends crucially on the phase between the modulating pulse and the carrier wavetrain. A demodulation technique was used to educe a family of modal 3-D wave packets from phase-locked streamwise velocity measurements, and allowed for detailed study of the disturbance and the propagation, amplification, and some of the nonlinear aspects of its leading modal components. The momentary increase in rms velocity fluctuations induced by the disturbance is quite striking and can be related to transient mixing enhancement.

14. SUBJECT TERMS	15. NUMBER OF PAGES
shear layer, mixing, surface heaters, hot wire sensors, spanwise nonuniform, excitation, pulsed excitation, schlieren	177
	16. PRICE CODE

17. SECURITY CLASSIFICATION OF REPORT	18. SECURITY CLASSIFICATION OF THIS PAGE	19. SECURITY CLASSIFICATION OF ABSTRACT	20. LIMITATION OF ABSTRACT

TABLE OF CONTENTS

AN EXPERIMENTAL INVESTIGATION OF THE FORMATION OF SECONDARY VORTICES AND THE GENERATION OF SMALL-SCALE MOTION IN A SPANWISE-FORCED PLANE MIXING LAYER

1. Executive Summary

The research described in the present report has been concerned with the fundamental fluid dynamics of mixing in a plane shear layer, with emphasis on novel approaches to mixing manipulation and control that utilize amplitude and phase excitation. Because shear layer flows of practical interest are subjected to temporally and spatially complex disturbances with important consequences to the mixing, our work has also focused on the pursuit of the conceptual mechanisms of mixing transition involving spanwise-nonuniform and -nonharmonic (pulsed) excitation. This work has been supported by AFOSR Grants 86-0324 and 88-0271.

Efficient mixing of chemical species in free shear flows at high enough Reynolds numbers is limited by fluid motions induced by a hierarchy of large coherent vortical structures. In the plane shear layer, mixing is accomplished by nominally two-dimensional entrainment of irrotational fluid from both streams by the spanwise vortices, and three-dimensional motion induced by packets of streamwise counter-rotating vortex pairs that form in the braid region between the spanwise vortices. Because these vortices evolve from two- and three-dimensional instabilities of the mean flow, they are manipulated in our experiments by excitation at the flow partition.

Even though the role of the streamwise vortices in the mixing process has been known for some time, the mechanisms by which the three-dimensional small-scale motions develop and lead to mixing transition has been an enigma. The present research has determined that as a result of the interaction between streamwise vortices and adjacent spanwise vortices, the mean velocity distribution in planes normal to flow

direction is significantly distorted. The appearance of a spanwise-regular pattern of inflection points at the high- and low-speed edges of the layer indicates the formation of locally unstable regions of large shear. Breakdown to turbulence is initiated in this region as a result of a rapid amplification of broadband disturbances already present in the base flow. Furthermore, mixing may be significantly intensified when the flow is subjected to spanwise-nonuniform excitation.

We have demonstrated that spanwise core deformations of the primary vortices can also lead to the formation of secondary vortical structures in the braid region. Core deformations of the primary vortices are induced by spanwise phase distortions of the excitation wave train, and the shape and strength of the induced secondary vortices vary with spanwise phase distributions. Visualization of these secondary vortical structures sheds light on the nature of "dislocations" of the primary vortices previously observed by a number of other investigators. The appearance of small-scale structures within the large coherent vortices in connection with the core deformations suggests that while the appearance of streamwise vortices in the braid region as a result of localized upstream disturbances is important for the initiation of small-scale mixing, core deformations of the primary vortices are responsible for the continuation of the mixing process far downstream of the mixing transition.

We have discovered that the plane mixing layer is extremely receptive to pulsed excitation in the braid region. The ensuing disturbance spreads rapidly in the streamwise and spanwise directions and is characterized by enhanced turbulence intensity much like a turbulent spot in a laminar boundary layer. We have developed a demodulation technique that is analogous to the wavelet transform. This technique was applied to our experimental data and has enabled us to capture dynamical features of the disturbance and the concomitant distortion of the two-dimensional base flow. The rapid spatial and temporal spreading of a pulsed disturbance in the span of the flow has been exploited in an investigation of the evolution of a temporally and spatially

regular pattern of such turbulent structures, which may be useful from the standpoint of mixing enhancement. We expect that this scheme will be a viable improvement over current technology of pulsed combustion.

The present report is comprised of three major parts. In the first part (§3), we discuss the formation and evolution of the streamwise vortices and the generation of small scale motion. In the second part (§4), we discuss the effects of spanwise-nonuniform phase excitation. Finally, the third part (§5) is concerned with pulsed excitation. Because all three parts of the present research have been conducted in the same experimental facility, we begin the report with a description of the experimental hardware and techniques.

2. Facility, Actuators, and Flow Visualization

2.1. *The Water Shear Layer Facility*

The facility is shown in figure 2.1. The entire flow is driven by a single pump powered by a 10-hp motor equipped with a solid-state speed controller. The velocity of each stream can be independently varied, and test-section velocities up to 200 cm/sec can be realized. Two interchangeable 100-cm-long test sections with cross sections of 10 cm × 22 cm and 22 cm × 22 cm are equipped with Lucite walls so that the flow can be observed from any direction. The convergence of the test section on either side of the shear layer can be adjusted easily in order to vary the streamwise pressure gradient. Two interchangeable contractions (with contraction ratios of 7:1 and 9:1) have rectangular cross sections with constant aspect ratios. Turning vanes and "turbulence manipulators" (honeycomb and screens) upstream of the contraction reduce velocity variations due to secondary flow. The turbulence level in the free streams is less than 0.15%. The replaceable trailing edges of the flow partition are configured with various mosaics of surface heaters for flow manipulation, described in §2.2.

The facility is equipped with a suite of diagnostic instrumentation. A pressure transducer is connected to two 12-port fast switches. These switches are computer-controlled and allow for monitoring of the velocity on either side of the contraction exit plane and the static pressure along the test section, as well as Pitot-static measurements of the velocity field within the test section. The water temperature is monitored and recorded by the laboratory computer via a digital thermometer. Fifteen dye injection ports are available on each side of the flow partition. A computer-controlled two-axis traverse mechanism, designed for detailed measurements of the flow field within the test section with rakes of hot-wire probes, has been installed. Twenty channels of hot-wire/film anemometry are available for simultaneous measurement of instantaneous velocity distributions. A rake of 31 hot-wire sensors, 2 mm apart and suitable for use in water, is mounted on the traverse mechanism for simultaneous cross-stream or

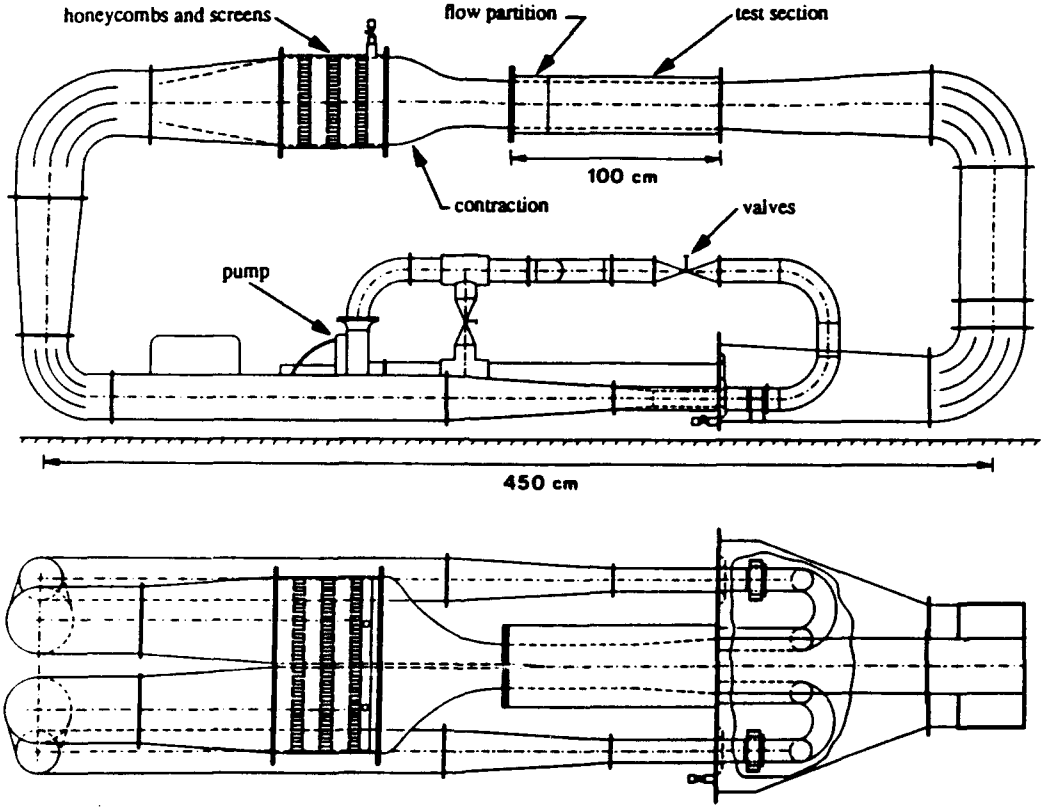
honeycombs and screens
flow partition
test section
100 cm
contraction
valves
pump
450 cm

Figure 2.1

spanwise measurement of the streamwise velocity. A Masscomp laboratory computer system, including 16 channels of 12-bit A/D, 16 channels of D/A, and 32 channels of general-purpose I/O, is dedicated to experiment control and data processing.

2.2. *Excitation by Surface Film Heaters*

Excitation of streamwise and spanwise instability modes is accomplished by either of two mosaics of surface film heating elements mounted on the flow partition. Mosaic I consists of 14 spanwise-uniform elements and two 16-element spanwise rows. Mosaic II is comprised of four spanwise-uniform elements upstream of a single 32-element spanwise row. Figure 2.2 is a schematic drawing of Mosaic II, the flow partition, and the coordinate system. (In the present work, x, y, and z are the streamwise, cross-stream, and spanwise coordinates, respectively; the corresponding velocity components are u, v, and w.) The heating elements are mounted on a standard epoxy board substrate. A thin film coating provides good heat conduction, corrosion protection, and electrical insulation. Each heating element is wired through the epoxy board (using through-hole plating) and the flow partition to a DC power amplifier. Thirty-two channels of power amplifiers, each capable of continuously driving 10 A into a load of 2-4 ohms, are available. The unit's output is limited to 2.5 kW by the power supply. Sixteen channels of power amplifiers can be directly driven by the laboratory computer via a D/A interface. This allows input of arbitrary temporal waveforms to the heaters without distortion, by compensating in software for the temperature dependence of the heater resistance and for the quadratic dependence of Joulean dissipation on input voltage. The input power to the heaters is given by $E_0(z) + E(z, t)$, where $E_0(z)$ is the mean power.

The effect of heating the surface is essentially to introduce three-dimensional vorticity perturbations into the flow partition's boundary layer by exploiting the dependence of the viscosity on temperature (Liepmann, Brown & Nosenchuck 1982). It

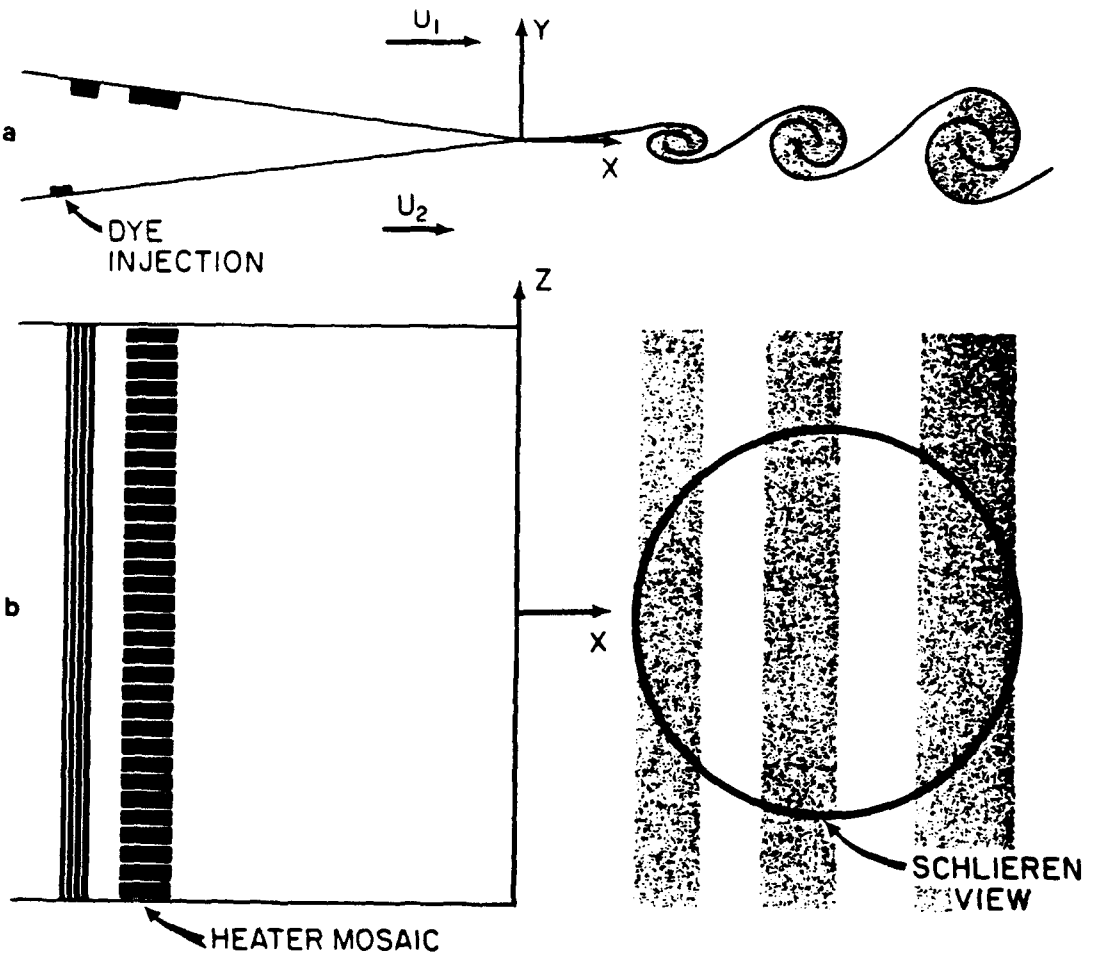

Figure 2.2

is important to recognize that small oscillations induced in the boundary layer amplify or decay according to linear stability theory. Thus, forcing a shear layer from an upstream boundary layer may not be effective if the induced waves decay appreciably before reaching the trailing edge. Hence the forcing frequency should be within the unstable (amplified) range of the boundary layer, the extent of which depends strongly on the pressure gradient. By carefully extending the flow partition into the test section, the streamwise pressure gradient can be tuned so that it becomes slightly adverse, causing the flow partition boundary layer to become less stable and more receptive to forcing.

The response of the flow to spanwise-uniform harmonic excitation over a range of forcing frequencies is deduced from power spectra $P(\nu)$ of the streamwise velocity 2.5 cm downstream of the flow partition and 1 cm above its centerline (on the high-speed side). The free-stream velocities are $U_1 = 30$ cm/sec, and $U_2 = 10$ cm/sec. These free-stream velocities are used in all the present experiments with the exception of the experiments described in §3.2. Several runs over a range of forcing frequencies ν_f were made. Figure 2.3 shows $P(\nu_f)$ as a function of ν_f, indicating the composite receptivity of the high-speed-side boundary layer and the shear layer to spanwise-uniform harmonic excitation. In connection with these measurements, it is important to note that the hot-wire probe is operated at a 4% overheat ratio, which renders it sensitive to temperature variations of the order of 0.1°C. As shown in figure 2.3, the probe does not respond to heater excitation at frequencies outside a relatively narrow bandwidth, and hence it may be concluded that shear layer temperature fluctuations associated with the surface heating are very small. Furthermore, the importance of buoyancy effects in forced convection boundary layers may be evaluated (Schlichting 1968) based on the ratio $\gamma = Gr/(Re_{\delta^*})^2$ where Gr is the local Grashoff number. For the largest surface overheat, we compute $\gamma < 10^3$. Buoyancy effects can be neglected if $\gamma << 1$.

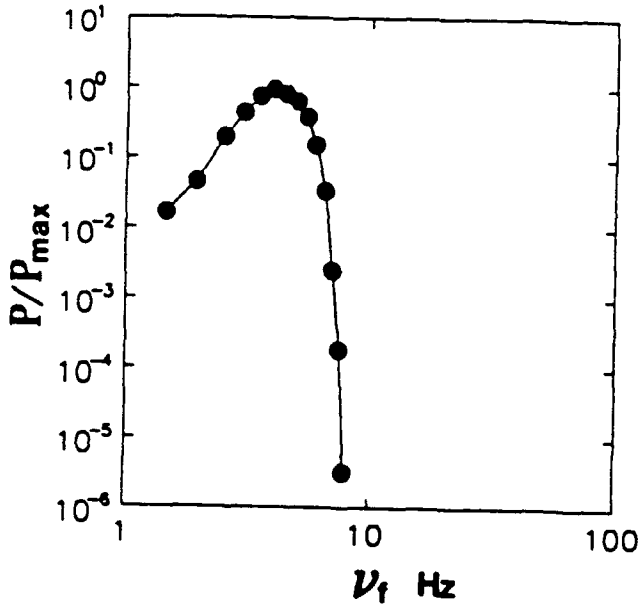

Figure 2.3

Figure 2.4 shows cross-stream profiles of the dimensionless streamwise velocity $\hat{U}(\eta) = [U(\eta) - U_2]/\Delta U$, plotted as a function of the usual similarity variable $\eta = (y - y_0)/(x - x_0)$, where $U(\eta)$ is the mean velocity measured at a number of streamwise stations, x_0 is the virtual origin, and $\Delta U = U_1 - U_2$. Here, $y_0(x)$ is the cross-stream elevation at which $U(x, y) = (U_1 + U_2)/2$, hereinafter defined as U_c. The flow is excited near the "natural" frequency and its first subharmonic (6 and 3 Hz, respectively) using spanwise-uniform excitation from Mosaic I (corresponding velocity profiles using Mosaic II are shown in figure 3.5 below). These data demonstrate that the forced shear layer spreads more in the cross-stream direction than does the unforced flow, in agreement with the findings of other investigators (e.g., Ho & Huang 1982).

In figures 2.5(*a-c*) we show power spectra $P(\nu)$ of the the streamwise velocity at $x = 10.2$ cm ($Re_\theta = 216$), 17.8 cm ($Re_\theta = 663$), and 25.4 cm ($Re_\theta = 1450$), respectively, for $y = y_0$. The Reynolds numbers at these x-stations are based on the momentum thickness

$$\theta(x) = \frac{1}{(\Delta U)^2} \int_{-\infty}^{\infty} [U(x) - U_2][U_1 - U(x)]dy \ .$$

The spectra in figures 2.5(*b,c*) correspond to spanwise-uniform harmonic excitation at $\nu_f = 6$ and 3 Hz, respectively. The establishment of small-scale motion in free shear flows is often connected with the existence of an inertial subrange in which the slope of log $P(\nu)$ versus log ν is -5/3. At sufficiently high Reynolds numbers in a homogeneous, stationary, and isotropic turbulent flow, the inertial subrange is the low wave-number part of an equilibrium range of wave numbers in which negligible viscous dissipation occurs (Batchelor 1953). Free shear flows, however, are not homogeneous and, if forced, are not statistically stationary, so the extent of the inertial subrange (which implies local isotropy) in laboratory flows is limited even at relatively high Reynolds numbers (Champagne 1978). Furthermore, mixing transition does not

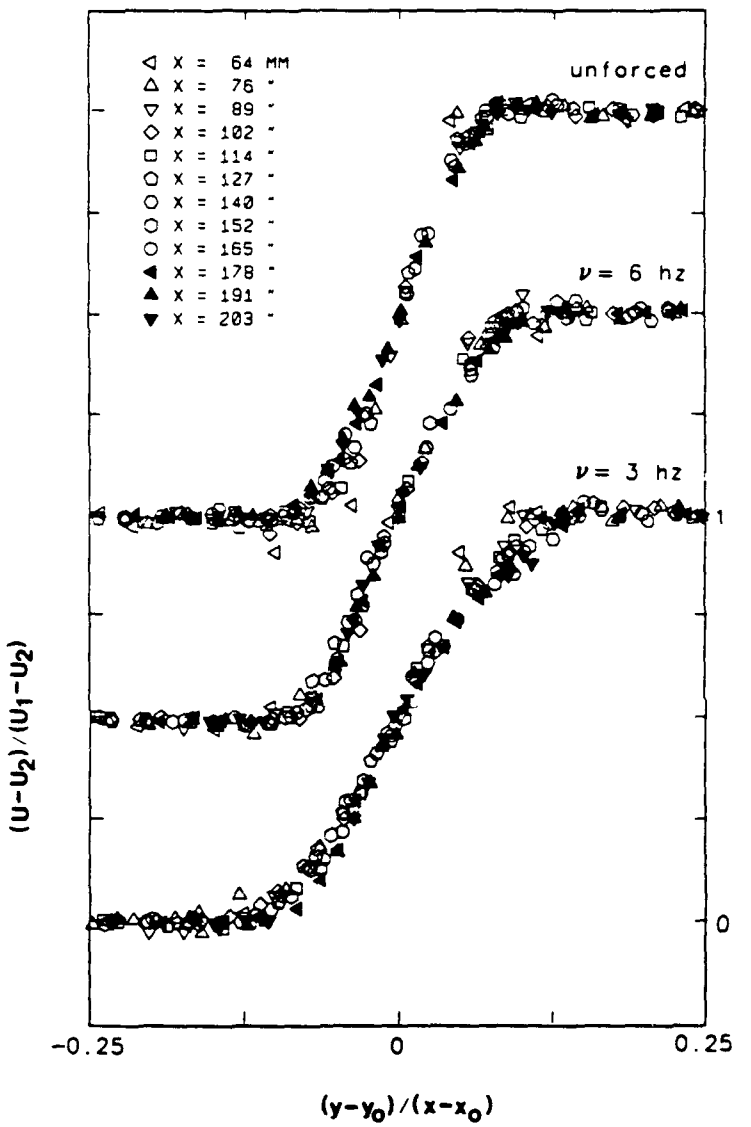
X = 64 MM
X = 76 "
X = 89 "
X = 102 "
X = 114 "
X = 127 "
X = 140 "
X = 152 "
X = 165 "
X = 178 "
X = 191 "
X = 203 "
unforced
ν = 6 hz
ν = 3 hz
1
0
-0.25
0
0.25
(U-U2)/(U1-U2)
(y-y0)/(x-x0)

Figure 2.4

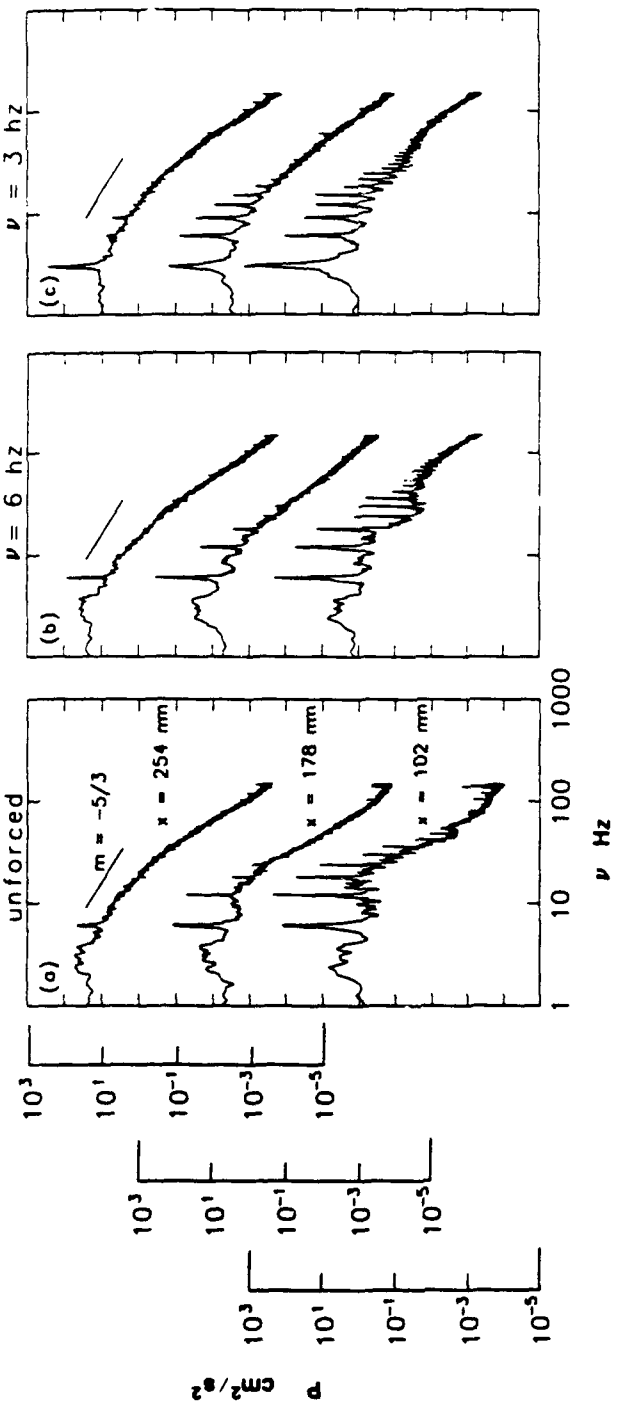
unforced
ν = 6 hz
ν = 3 hz
(a)
(b)
(c)
m = -5/3
x = 254 mm
x = 178 mm
x = 102 mm
1
10
100
1000
ν Hz
P cm²/s²
10³
10¹
10⁻¹
10⁻³
10⁻⁵

Figure 2.5

depend on the existence of an inertial subrange, but rather on the presence of turbulence or fine-scale random vortical structures, which can exist even at relatively low Reynolds numbers. In fact, the characteristic time necessary for establishment of an inertial subrange may lead to its appearance farther downstream from where mixing transition takes place. In the present experiments the inertial subrange at x = 25.4 cm is estimated to be 5 Hz < ν < 32 Hz (cf. Jimenez, Martinez-Val & Rebollo 1979), and the logarithmic slope of the power spectrum within this subrange is approximately -5/3. Ho & Huerre (1984) assert that typical transition Reynolds numbers in liquids fall in the range 750 < Re < 1700.

2.3. *Flow Visualization*

Introduction of a controlled vorticity distribution into the boundary layer of the flow partition by the surface heaters is accompanied by small localized density gradients in the adjacent fluid. The corresponding refractive index gradients are exploited for flow visualization by means of a sensitive double-pass Schlieren system (Fiedler, Nottmeyer, Wegener & Raghu 1985). This technique allows the effect of forcing to be studied nonintrusively in planes parallel and normal to the flow span. The Schlieren view can be thought of as a planar projection of streaklines of slightly heated fluid elements. In the present investigation, the Schlieren view is in the spanwise (x-z) plane of the mixing layer and consists of a 13.2-cm-diameter circle centered in midspan. Because the flow is forced, two Schlieren views photographed at the same phase relative to the excitation waveform and centered 7.6 cm and 15.2 cm downstream of the trailing edge of the flow partition can be combined into a composite showing the flow for 1 cm ≤ x ≤ 21.8 cm.

Photographs of the flow subjected to spanwise-uniform 5-Hz harmonic excitation are shown in figure 2.6. The flow is from left to right. In the cross-stream (x-y) plane (figure 2.6*a*), the flow is visualized by dye injected into the boundary layer of the low-speed side at midspan. In the spanwise (x-z) plane, visualization was accomplished by

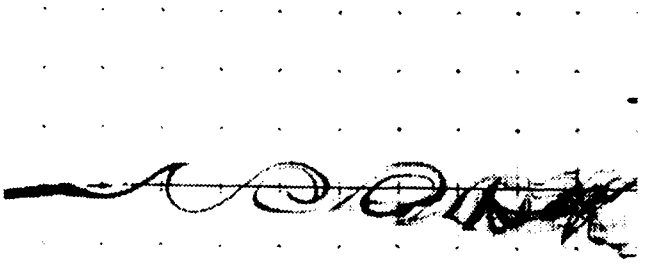

a

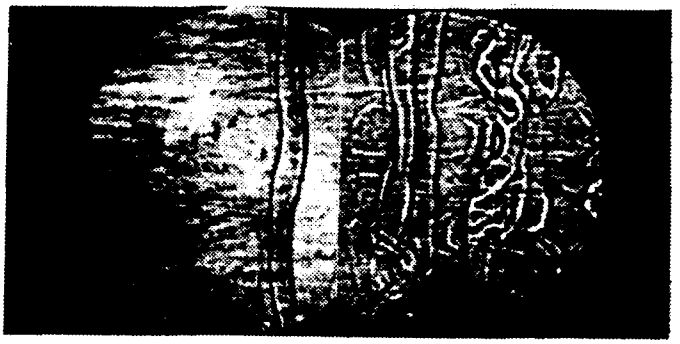

b

Figure 2.6

the Schlieren technique described above. The two views have the same scale, begin (at the left-hand side) 1 cm downstream of the flow partition, and were separately photographed at the same phase relative to the zero crossings of the excitation signal. At this excitation frequency, pairing of the primary vortices does not occur in the streamwise domain shown here.

Although streaklines of colored and heated fluid elements do not necessarily mark the presence of vorticity, they strongly suggest the formation of spanwise-coherent vortices. It is important to recognize that the Schlieren view is a planar projection in the cross-stream direction (i.e., a y-integration) from which depth information has been lost. The Schlieren image of the primary vortex immediately downstream of the first rollup (figure 2.6*b*) is characterized by sharp intensity gradients along its upstream and downstream edges caused by the strong curvature of the thin layer of heated fluid that is rolled into the vortex. The slight spanwise nonuniformity in the instantaneous visualization shown in figure 2.6(*b*) also characterizes the ensemble-averaged flow. Since the excitation waveform corresponding to figure 2.6(*b*) is spanwise uniform, these results also suggest the formation of naturally occurring streamwise vortices in the braid region, as well as the evolution of spanwise nonuniformities in the cores of the primary vortices. The development of small-scale motion within the cores of the spanwise vortices is apparent at the downstream end of the composite Schlieren view.

As noted by Landahl (private communication, 1990), streamwise streaks in transitional flat-plate boundary layers have been identified as regions of high- or low-speed velocity perturbations not necessarily associated with continuous concentrations of streamwise vorticity. Nevertheless, because of the remarkable similarity between the present flow visualization and three-dimensional cross-stream and streamwise vorticity concentrations in the numerical simulations of Rogers & Moser (1989) and Buell & Mansour (1989), we hereinafter refer to streamwise streaks in our Schlieren flow visualization as streamwise vortices. We emphasize that reference to a "streamwise

vortex" in the present work does not refer to a domain containing only streamwise vorticity, nor does it imply that the axis of the vortex is parallel to the streamwise direction.

2.4. *References*

Batchelor, G. K. 1953 *The Theory of Homogeneous Turbulence.* Cambridge University Press.

Buell, J. C. & Mansour, N. N. 1989 Asymmetric effects in three-dimensional spatially developing mixing layers. In *Proc. Seventh Symp. on Turbulent Shear Flows, Stanford University*, pp. 9.2.1-9.2.6.

Champagne, F. H. 1978 The fine-scale structure of the turbulent velocity field. *J. Fluid Mech.* **86**, 67-108.

Fiedler, H. E., Nottmeyer, K., Wegener, P. P. & Raghu, S. 1985 Schlieren photography of water flow. *Experiments in Fluids* **3**, 145-151.

Ho, C.-M. & Huang, L.-S. 1982 Subharmonic and vortex merging in mixing layers. *J. Fluid Mech.* **119**, 443-473.

Ho, C.-M. & Huerre, P. 1984 Perturbed free shear layers. *Ann. Rev. Fluid Mech.* **16**, 365-424.

Jimenez, J., Martinez-Val, R. & Rebollo, M. 1979 On the origin and evolution of three-dimensional effects in the mixing layer. *Final Report DA-ERO 79-G-079.* Universidad Politecnica de Madrid. AD-A096007.

Liepmann, H. W., Brown, G. L. & Nosenchuck, D. M. 1982 Control of laminar instability-waves using a new technique. *J. Fluid Mech.* **118**, 187-200.

Rogers, M. M. & Moser, R. D. 1989 The development of three-dimensional temporally evolving mixing layers. In *Proceedings of Seventh Symposium on Turbulent Shear Flows, Stanford University*, pp. 9.3.1-9.3.6.

Schlichting, H. 1968 *Boundary Layer Theory.* McGraw-Hill.

3. Evolution of Streamwise Vortices and Generation of Small-Scale Motion

3.1. *Technical Background*

The rate at which a reaction product is formed in the mixing layer between two reacting streams can increase by an order of magnitude through a mixing transition downstream of the flow partition (Roshko 1981). The small-scale three-dimensional motion necessary for such mixing enhancement has been connected by Roshko to the appearance of streamwise counter-rotating vortex pairs first observed by Miksad (1972) and Brown & Roshko (1974). The streamwise vortices and the mechanisms by which they lead to the generation of small-scale motion are the subjects of the present experimental investigation.

Flow visualization of a chemically reacting liquid shear layer with a visible reaction product reveals the evolution of spanwise nonuniformities along the primary (spanwise) vortices (Breidenthal 1981). This nonuniformity (dubbed "wiggle") may be described as being nominally sinuous, with considerable variation in spanwise wavelength. As the sinuous structure is convected downstream, its amplitude grows rapidly (apparently as a result of stretching by consecutive primary vortices), with no appreciable change in spanwise wavelength. While there is no evidence that the "wiggle" is associated with a spanwise instability of the primary vortex core, there is no doubt that its appearance marks the formation of streamwise vortical structures. In plan-view time-exposure photographs, these streamwise vortices appear as continuous streaks, starting at approximately the streamwise onset of the wiggle, and have spanwise spacings corresponding to the wiggle's undulations. Farther downstream, the streaks are obscured by a marked increase in the (visible) reaction product.

Time-exposure photographs were also obtained by Konrad (1976) and Bernal & Roshko (1986) over a large range of Reynolds number (Re) in a non-reactive gas mixing layer facility. These authors found that the mean onset Re of the streaks increases with the shear layer velocity ratio, and although they are not necessarily equally spaced

over a considerable distance downstream of the flow partition, their mean spanwise spacing scales with the vorticity thickness at the streamwise location where they first become visible. Similar observations were reported by Miksad (1972). Contour plots of time-averaged streamwise velocity in a plan view at a fixed cross-stream elevation (Jimenez 1983) closely resemble the streamwise streaks in the time-exposure photographs. An important feature common to these observations is the preservation of spatial coherence and spanwise spacings of the streaks, despite concomitant pairing of the primary vortices.

Based on flow visualization and high-speed cinematography, Bernal (1981) and Bernal & Roshko (1986) suggested that the counter-rotating streamwise vortex pairs in the plane mixing layer are part of a vortex that continuously loops back and forth in the braid region between adjacent spanwise vortices. The mean spanwise spacing of the streamwise vortices appears to increase somewhat as the vortices are convected downstream, although at a much smaller rate than the rate of change in the cross-stream (or streamwise) dimension of the primary vortices. A somewhat different view concerning the structure of the streamwise vortices was proposed by Hussain (1983). Unlike the model of Bernal & Roshko, Hussain's model emphasizes that the braid region is comprised of slender *discrete* vortices (dubbed "ribs") randomly displaced with respect to each other in directions normal to their axes.

A number of numerical and analytical studies have shown that the streamwise vortical structures can result from nonuniformities of the spanwise vorticity in the braid region between the primary vortices. Lin & Corcos (1984) showed that a weak spanwise-periodic variation of streamwise vorticity in a uniform straining flow (as between two consecutive spanwise vortices) can evolve into concentrated round streamwise vortices. These findings were further confirmed by Ashurst & Meiburg (1988) via simulations based on inviscid vortex dynamics. The direct Navier-Stokes simulations of Metcalfe, Orszag, Brachet, Menon & Riley (1987) show that spanwise

instability modes triggered by upstream nonuniformities in the spanwise vorticity are convected with the flow, grow at rates similar to those of the two-dimensional modes, and lead to the formation of pairs of counter-rotating streamwise vortices in the braid region. Metcalfe *et al.* also remark that pairing of the primary vortices may inhibit the three-dimensional instability, while suppression of pairing may drive the three-dimensional modes to turbulent-like states.

Experimental evidence suggests that the streamwise vortices tend to lock onto small geometric details (imperfections in the flow partition, orientation of screens, etc.) in the experimental apparatus (Bernal 1981, Jimenez 1983). Lasheras, Cho & Maxworthy (1986) showed that small vortex-generating elements mounted on the flow partition could move the origin of these vortices considerably upstream; in the absence of these devices and by careful removal of flow disturbances, the origin could be displaced significantly downstream. In related flow visualization experiments, Lasheras & Choi (1988) studied the evolution of a spanwise-periodic pattern of streamwise vortices produced by flow partitions with corrugated and indented trailing edges. Recent experiments in a plane mixing layer excited by a spanwise array of surface film heaters conclusively demonstrate the ease with which a *nearly arbitrary spanwise distribution* of streamwise vortices can be generated (Nygaard 1987; Fiedler, Glezer & Wygnanski 1988).

An important feature of the time-exposure photographs of Bernal & Roshko (1986) is the gradual disappearance of the streamwise streaks downstream of where they exhibit remarkable spanwise coherence. Spanwise plots of time-averaged streamwise velocity at a number of streamwise stations show a slow streamwise increase of the characteristic spanwise spacing, indicating either loss of spanwise coherence or disappearance of streamwise structures (Huang & Ho 1990). Bernal & Roshko further report that, in the region where time-exposure photographs no longer show the presence of streaks, single snapshots show streamwise vortices having mean spanwise spacing nominally larger than that of the upstream streaks. Furthermore, the spanwise locations

of these streamwise vortices vary with downstream distance in a manner clearly unrelated to (fixed) structural features of the experimental apparatus.

It is clear that time-invariant spanwise vorticity nonuniformities due to irregularities of the experimental apparatus upstream of the trailing edge of the flow partition continuously influence the vortex sheet, which subsequently becomes part of the spanwise vortices and the braid region. Although spanwise vorticity nonuniformities within the braid region lead to the formation of streamwise vortices, experimental and numerical evidence suggests that under some conditions the same disturbances cause little or no distortion of the primary vortices. In the vortex simulations of Ashurst & Meiburg (1988), an initial spanwise-periodic perturbation leads to the formation of streamwise vortices in the braid region but has little effect on the primary vortices themselves. An out-of-phase waviness of the cores of the primary vortices, observed in the early stages of the numerical simulations of Ashurst & Meiburg, is also observed downstream in the experiments of Lasheras & Choi (1988). In both of these investigations, the waviness of the primary vortices seems to decay downstream due to the continuous rotation of their cores. We further note that in the experiments of Lasheras & Choi, streamwise-continuous vortex pairs appear immediately downstream of a flow partition with an indented trailing edge, considerably upstream of the first rollup of the primary vortices. These findings suggest that formation of streamwise vortices in close proximity to the flow partition is mainly the result of upstream nonuniformities in either the experimental apparatus or the flow partition's boundary layers. On the other hand, the observations of Bernal & Roshko (1986) regarding the appearance of streamwise vortices uninfluenced by upstream conditions indicate that, far enough downstream of the flow partition, streamwise vortices may result from an instability of the primary vortices. A spanwise core instability of the primary vortices is a viable mechanism because it is accompanied by distortion of the strain field in the braid region.

Pierrehumbert & Widnall (1982) identified two spanwise instability modes of the primary vortices in their analysis of a shear layer modeled by an array of Stuart vortices. The first mode, referred to as "translative instability," is spanwise and streamwise periodic. The streamwise wavelength is that of the two-dimensional flow. The most unstable translative disturbance has a spanwise wavelength equal to two-thirds the spacing of the undisturbed vortices, although disturbances amplify within a broad band of wavelengths. The authors suggest that the translative instability leads to the formation of streamwise vortices observed in the experiments of Breidenthal (1981). Corcos & Lin (1984) assert that rollup of spanwise vorticity into a streamwise-periodic array of vortices gives rise to a translative core instability that allows spanwise perturbations to grow in such a way that the spanwise vortices are identically distorted. Pierrehumbert (1986) later showed that elliptic two-dimensional vortices are unstable to three-dimensional perturbations, with spanwise wavelengths much smaller than the characteristic vortex core dimension. Pierrehumbert proposed this short-wave instability as a mechanism for the direct transfer of energy from the spanwise vortices into fine-scale turbulence. The second instability mode discussed by Pierrehumbert & Widnall corresponds to spanwise-localized pairing of the primary vortices. This instability mode has a streamwise wavelength twice that of the two-dimensional base flow and, in contrast to the translative instability, has a short spanwise wavelength cutoff. Experimental evidence that the primary vortices are subject to a core instability having a spanwise wavelength longer than the streamwise (Kelvin-Helmholtz) wavelength is also found in the work of Chandrsuda, Mehta, Weir & Bradshaw (1978) and Browand & Troutt (1980, 1985). Some aspects of the core instability have been studied recently by Nygaard & Glezer (1990, 1992).

This section of the present report focuses on the evolution of streamwise vortical structures resulting from spanwise-periodic time-harmonic disturbances upstream of the trailing edge of the flow partition. Although the findings of Breidenthal (1981) and

Bernal & Roshko (1986) indicate that these streamwise vortices play a crucial role in the mixing transition of the plane shear layer, the mechanism by which small-scale motions necessary for such transition are generated has not been studied. The present investigation is also concerned with unanswered questions regarding details of the formation process of the streamwise vortices, their spanwise spacings, their effect on the two-dimensional base flow, and their interaction with the spanwise vortices.

3.2. *Formation of the Streamwise Vortices*

Several experimental investigations of plane mixing layers have demonstrated that streamwise vortices in the braid region can be triggered by spanwise-nonuniform excitation using either passive (e.g., Lasheras & Choi 1988 and Bell & Mehta 1989) or active (Nygaard & Glezer 1989) devices mounted on the flow partition. Because evolution of the streamwise vortical structures appears to be phase-locked to the two-dimensional instability of the base flow, an important attribute of active devices such as our surface heaters is that they allow for streamwise and spanwise instability modes to be excited relatively independently. Spanwise-uniform time-harmonic excitation provides a powerful tool for the manipulation of some streamwise instability modes, with dramatic global effects on the flow. In particular, forcing at the natural (most unstable) frequency produces a region downstream of the flow partition in which the passage frequency of the primary vortices is equal to the forcing frequency and pairing is inhibited (e.g., Roberts 1985). Thus, the evolution of the streamwise vortices can be studied phase-locked to the excitation waveform and in the absence of interactions between the primary vortices.

In a previous investigation, which was supported by AFOSR Grant 86-0324, we studied the effect of spanwise-nonuniform harmonic excitation,

$$E(z,t) = A(z)\sin(\omega_f t) ,$$

on the evolution of the streamwise vortices at relatively low free-stream velocities (18

and 6 cm/sec) (Nygaard 1987; Fiedler *et al.* 1988). The streamwise vortices form at spanwise locations corresponding to minima of A(z) and, at least close to the flow partition, resemble lambda vortices in transitional flat-plate boundary layers (e.g., Saric & Thomas 1983). Within the spanwise resolution of the heating mosaic, the shape of the streamwise vortices was almost invariant with respect to different spanwise-periodic waveforms, A(z), having the same spanwise wavelength, λ_z.

In this subsection we discuss the early stages in the formation of the streamwise vortices. The interaction between the streamwise and spanwise vortices and the subsequent generation of small-scale motion necessary for mixing transition are described in §§3.3-3.5. In both experiments, pairing of the spanwise vortices is inhibited by choosing ν_f to be approximately equal to the natural frequency of the mixing layer. Measurements of the streamwise velocity component are obtained using the hot-wire rake described in §2.1. The length of the velocity time series at each measurement point corresponds to 400 cycles of the harmonic excitation. The data are sampled at 128 ν_f.

The evolution of a spanwise-isolated streamwise vortex was studied by using heating Mosaic I to synthesize a steady 16-element discretization of $E_0(z) = 1 - \cos(2\pi z/\lambda_z)$, where λ_z is equal to the width of 10 heating elements. Because phase jitter in the passage frequency of the spanwise vortices at the measurement station decreases with U_c, the velocities of the two streams are reduced to 25 and 9 cm/sec and the corresponding excitation frequency is $\nu_f = 3.7$ Hz. During excitation of the spanwise-uniform wave train, the flow is illuminated in the x-z plane by a strobe triggered at a phase delay relative to the zero crossings of E(z,t), and photographed using the Schlieren technique described in §2.3. The flow in the y-z plane was visualized by means of dye injection on the low-speed side and was photographed separately at the same phase relative to the zero crossings of E(z,t). Figure 3.1 is a composite of eight pairs of side (x-y) and span (x-z) views taken at equal time intervals

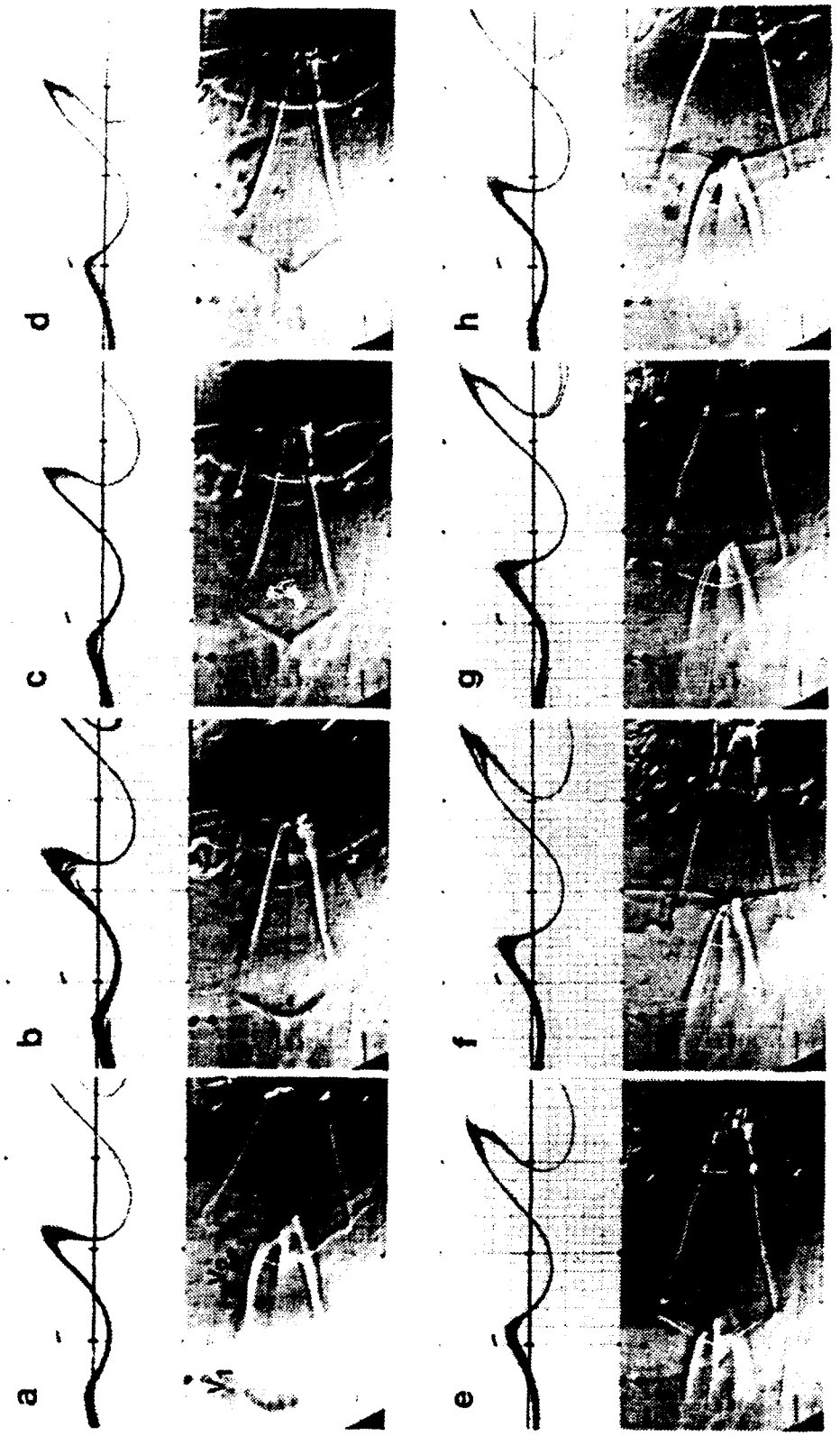

Figure 3.1

during the excitation period. The field of view is between 2.5 and 12.4 cm downstream of the flow partition.

Figure 3.1(*c*) suggests that spanwise-nonuniform vorticity concentrations [at the upstream (left) end of the (x-y) view in figure 3.1*a*], referred to below as V_1, first appear on the crest of the two-dimensional wave *prior* to rollup of the vortex sheet into a primary vortex. Owing to the spanwise-nonuniform excitation, V_1 develops an upstream bend about its middle as it is advected downstream. The streamwise vortices formed during previous cycles of the excitation wave train are observed at the center and downstream end of the Schlieren view in figure 3.1(*a*) (referred to below as V_2 and V_3, respectively). In figures 3.1(*b-d*), the legs of V_2 appear to be connected to V_1 and form a nearly quadrilateral vortex structure embedded in the deformed vortex sheet, marked by dye in the corresponding side view. The downstream edge of the quadrilateral structure lies on the high-speed side of a spanwise vortex, while the upstream edge is deformed and stretched by rollup of the following spanwise vortex.

As a result of the stretching of V_1 and rollup of the spanwise vortex sheet, a new hairpin eddy-like structure forms near the region of maximum curvature of the upstream bend (figure 3.1*e*). Previous experimental work on the formation of streamwise vortices in the braid region emphasizes that streamwise vortices begin to form near a stagnation point (in a reference frame moving with U_c) between two adjacent spanwise vortices and are subsequently stretched continuously in the upstream and downstream directions (Lasheras *et al.* 1986; Lasheras & Choi 1988). Figure 3.1 suggests that variations in the streamwise strain field due to the Kelvin-Helmholtz instability lead to formation of streamwise vortices even before rollup of the primary vortices is completed. Streamwise vortices appear near the high-speed edge of a primary vortex during its rollup, and are then continuously stretched in the upstream direction toward the subsequent spanwise vortex. Consistent with the numerical simulations of Buell & Mansour (1989), we note that, at least within the streamwise domain shown here, neither the heads nor legs of the hairpin eddies appear to be ingested into the spanwise vortices.

The streamwise location at which streamwise vortices first appear is probably related to the amplitude of the upstream disturbances leading to their formation. The appearance of streamwise vortices before rollup of the primary vortices is reported by Huang & Ho (1990), for an unforced plane mixing layer at relatively high Reynolds number, and is also evident in the experiments of Lasheras & Choi (1988), where streamwise counter-rotating vortex pairs appear immediately downstream of a flow partition with an indented trailing edge. While the Lin-Corcos mechanism for the formation of streamwise vortices (Lin & Corcos 1984) may be valid upstream of the rollup of primary vortices, we note that streamwise vorticity can also develop in a spanwise- and streamwise-uniform base flow. An example is the formation of Langmuir circulations in the surface layers of natural waters (Leibovich 1983). These counter-rotating vortex pairs form when the wind blows over water; their axes are nearly parallel to the wind and their crosswind (i.e., spanwise) spacing scales with the vorticity thickness.

While there is no question that spanwise-nonuniform excitation alters the nominally two-dimensional base flow, the extraction of a three-dimensional vortical structure from data of a single velocity component is not a trivial matter. Nevertheless, such a three-dimensional structure would be invaluable as a first step in understanding the dynamics of the flow. Such a vortical structure could be distinguished from the rest of the flow by the high intensity of the rms velocity fluctuations, $u'(x,t)$. A scheme by which $u'(x,t)$ is computed *relative to each individual realization* and then ensemble-averaged ($\langle u'_t(x,t)\rangle$) has been implemented (Glezer, Katz & Wygnanski 1989). Unlike the conventional $\langle u'\rangle$, the ensemble-averaged ("true") rms velocity fluctuations, $\langle u'_t\rangle$, are not prone to spurious contributions from low-frequency variations of the flow relative to its mean (e.g., velocity fluctuations outside the mixing layer induced by passage of spanwise vortices).

The "true" rms velocity fluctuations, phase-averaged over the excitation period, are computed from detailed measurements of the streamwise velocity in y-z planes.

The data shown in figure 3.2 are measured at x = 15 cm, where $Re_{\theta(x)}$ = 570 for the harmonically excited flow. The domain of measurements is rectangular (6 cm × 5.2 cm in the y- and z-directions, respectively), and the measurement points are equally spaced (2mm apart) in each coordinate. The surface, $\langle u'_t \rangle$ = 0.085 cm/sec in y-z-t coordinates, is shown during two periods of the spanwise-uniform and spanwise-nonuniform excitation waveforms. *Note that in this figure, as in all phase-locked plots below, time increases to the left in order to facilitate comparison with the Schlieren and dye views in which the vortical structures are advected to the right.* Although these are not surfaces of constant vorticity, they seem to effectively capture three-dimensional features of the streamwise vortices that are similar to the numerical results of Metcalfe *et al.* (1987) and Buell & Mansour (1989). Our data demonstrate that the streamwise vortex resulting from spanwise-nonuniform excitation induces substantial spanwise variations of $\langle u'_t \rangle$ within the primary vortex and in the braid region. Of particular note is the expansion of turbulent interfaces, probably corresponding to small-scale motion on the high-speed edge of the primary vortex (figure 3.2*b*). These modifications of the nominally two-dimensional base flow are further discussed in §3.4.

3.3. *The Effect of Spanwise Wavelength*

In figure 3.3, we show the effect of λ_z on the ensuing streamwise vortices at higher free-stream velocities (30 and 10 cm/sec) and excitation frequency (ν_f = 5 Hz) than discussed in §3.2. The amplitude of the excitation waveform, A(z), is piecewise-continuous and spanwise-periodic with wavelength, λ_z. To define the waveform, we let $z = z_0 + \lambda_z s$, where z_0 is an arbitrary reference and $0 \le s \le 1$. Then in each wavelength, A(z) is given by $A(z) = A_H$ for $0 \le s \le s_1$, $A(z) = A_L$ for $s_1 \le s \le s_2$, and $A(z) = A_H$ for $s_2 \le s \le 1$. In the present experiments, λ_z is taken as the widths of 2, 4, 8, and 16 elements of Mosaic II (figures 3.3*a,b,c,d*, respectively), $(s_2 - s_1)\lambda_z$ is equal to the width of one heating element, and $A_L = 0.3\ A_H$. Because of its deep minima, this

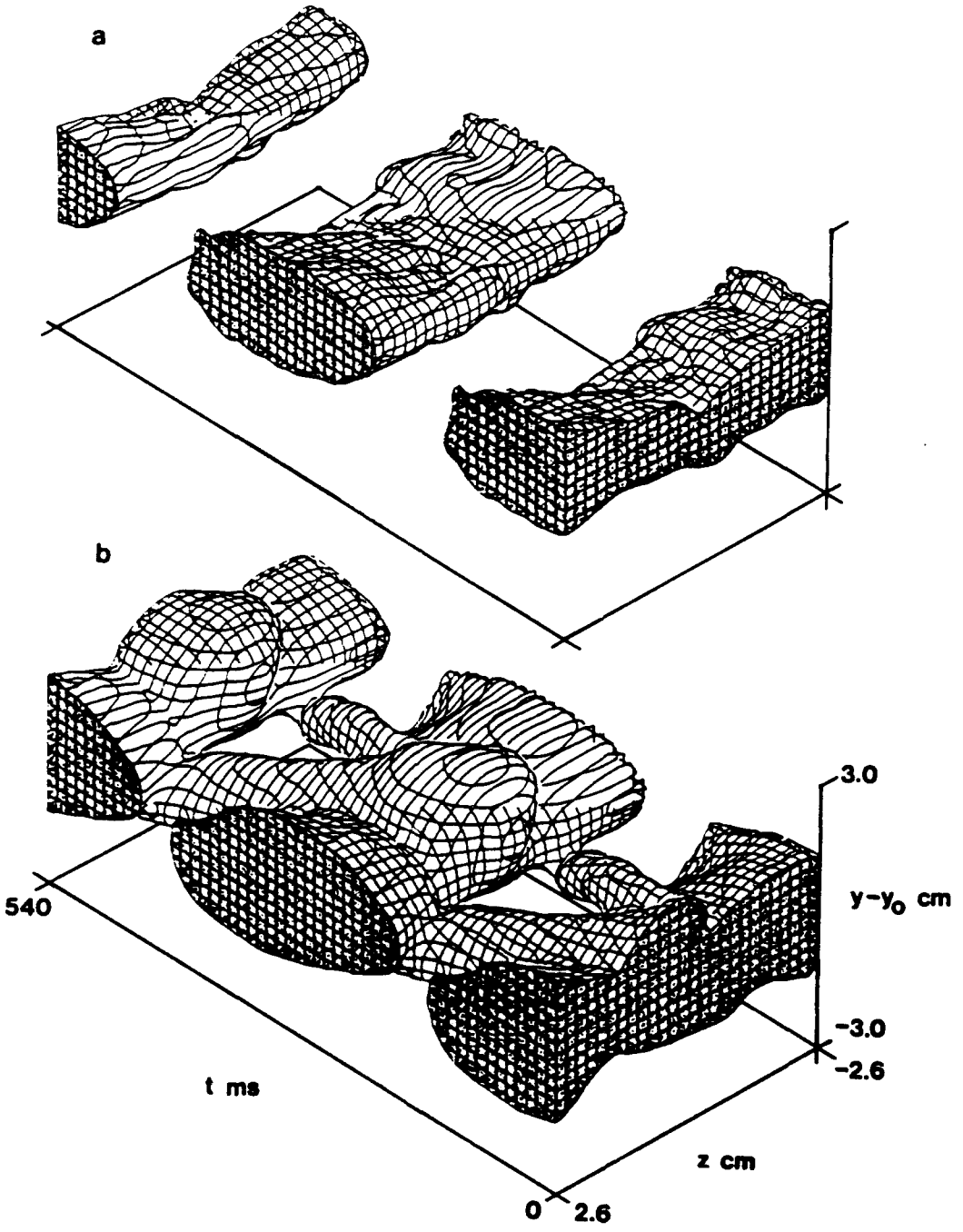

Figure 3.2

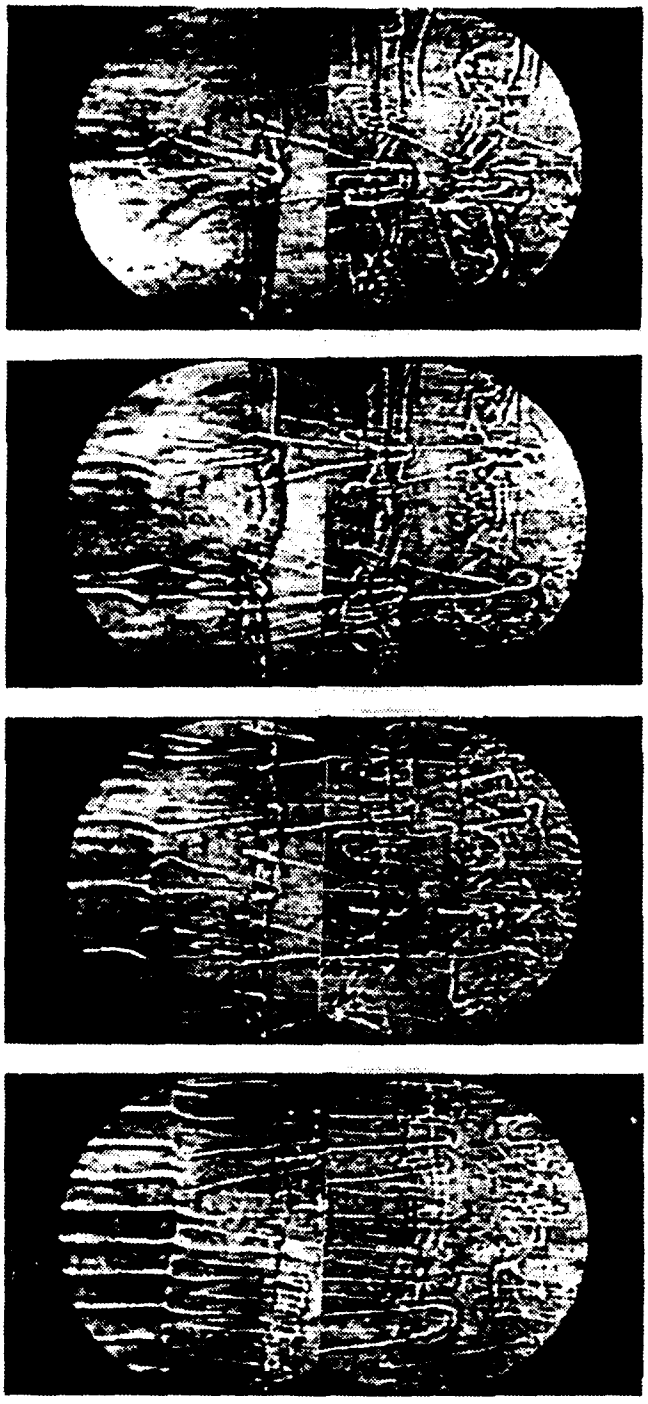

Figure 3.3

waveform is effective in minimizing spanwise jitter in the locations of the ensuing streamwise vortices. All Schlieren views in figure 3.3 were obtained at the same phase relative to the harmonic wave train.

As mentioned above, the forced streamwise vortical structures bear considerable resemblance to lambda vortices in a transitional flat-plate boundary layer. In the present experiments, the included angle Λ between the legs of the streamwise vortices decreases with decreasing λ_z. For relatively long λ_z (e.g., figure 3.3*b*), Λ is unchanged because spanwise interaction among streamwise vortices is reduced. The existence of spanwise-isolated streamwise vortices for $\lambda_z > \lambda_{KH}$ (figure 3.3*a*) indicates that these structures are not part of a single vortex that continuously loops back and forth between adjacent spanwise vortices, as conjectured by Bernal & Roshko (1986). Figure 3.3 further suggests that, for a given excitation frequency, virtually any spanwise wavelength synthesizable by the heating mosaic can be excited and can lead to the formation of streamwise vortical structures. This is supported by the flow visualization study of Lasheras & Choi (1988), where the average spanwise spacing of the streamwise vortices (their figure 25*a*) appears to be much smaller than the spanwise wavelength of their corrugated flow partition.

An important aspect of spanwise-nonuniform excitation at long λ_z (typically longer than λ_{KH}) is shown in figures 3.3(*a*,*b*). In figure 3.3(*a*), the central spanwise vortex deforms at midspan and develops an upstream bend. As shown in the experiments of Lasheras & Choi (1988), the three-dimensional alignment of the approximately streamwise vortices in the braid region is determined by the orientation of the strain field induced by the primary vortices. The spanwise undulations of the primary vortices modify the strain field in the braid region and consequently induce a significant increase in Λ. Farther downstream, the upstream bend in the spanwise vortex (on the right) is increased, and smaller-scale vortical tubes appear to be formed near the head of the streamwise vortex. When λ_z is reduced (figure 3.3*b*), the first

spanwise vortex downstream of the flow partition (on the left) develops spanwise undulations having the wavelength of the excitation. As in figure 3.3(*a*), the forced streamwise vortices are located at the upstream bends of these undulations, and Λ increases with downstream distance.

Of particular note are additional vortex tubes that appear along the legs of the streamwise vortex in the braid region between the spanwise vortices in the center and left of figure 3.3(*b*). These vortex tubes are probably associated with rollup of the streamwise vortices. Such a mechanism is discussed by Pullin & Jacobs (1986) in their numerical study of the nonlinear evolution of an array of inviscid counter-rotating vortex pairs subjected to an applied stretching strain field. This leads to rollup of multiple "secondary" streamwise vortices near each of the legs of a "primary" streamwise vortex. All secondary streamwise vortices associated with a given primary leg have the same sense of rotation. Lasheras *et al.* (1986) studied a streamwise vortex forced by a small hemisphere mounted on the flow partition of a plane mixing layer and proposed an induction mechanism for its spanwise spreading. The appearance of additional vortical tubes in the experiments of Lasheras *et al.* is clearly connected with undulation of the spanwise vortex. This deformation significantly modifies the vorticity and strain distributions in the braid region and, hence, may trigger the secondary instability of Pullin & Jacobs. In fact, forced streamwise vortices show little spanwise spreading when the spanwise vorticity remains approximately two dimensional (figures 3.3*c*,*d*). An upstream bend of the spanwise vortex is also apparent in the photographs of Lasheras *et al.* (their figure 15, corresponding to figure 3.3*b* here).

The undulations of the spanwise vortices result from an instability of their cores. Some preliminary results regarding this core instability have been obtained by Nygaard & Glezer (1990). It appears that, as a result of this instability, the primary vortices undergo spanwise deformation, the wavelength of which typically exceeds λ_{KH}, and induce secondary vortical structures through deformation of the strain field in the braid

region. Although the core instability is apparent in a number of previous experiments (e.g., Chandrsuda *et al.* 1978, Browand & Troutt 1985, and Lasheras & Choi 1988), no previous investigation has established its connection to the formation of streamwise vortices in the braid region.

3.4. *Modification of the Two-Dimensional Base Flow by the Streamwise Vortices*

The response of the flow to spanwise-nonuniform excitation may be evaluated from ensemble-averaged [phase-locked to E(z,t)] time series of the streamwise velocity perturbation,

$$\langle u_{pert}(x,t)\rangle = \langle u(x,t)\rangle - U(x) ,$$

where U(x) is the mean flow velocity computed from the ensemble-averaged data,

$$U(x) = \frac{1}{T_f}\int_0^{T_f} \langle u(x,t)\rangle dt ,$$

and

$$T_f = 1/\nu_f$$

is the temporal period of E(z,t).

In what follows, we study the effect of spanwise-nonuniform excitation on the nominally two-dimensional base flow. The spanwise wavelength of the excitation waveform E(z,t) is synthesized by four-element groups of Mosaic II (λ_z = 2.54 cm). An instantaneous Schlieren visualization of the forced flow is shown in figure 3.3(*c*).

The response of the mixing layer to spanwise-uniform and spanwise-nonuniform excitation close to the trailing edge of the flow partition is shown in figures 3.4(*a*) and 3.4(*b*), respectively, using contour plots of $\langle u_{pert}(z,t)\rangle$ measured at x = 5.1 cm and $y = y_0(x)$. The duration of the ensemble-averaged time series is $4T_f$, and the data are taken equidistantly (2.5 mm apart) along the span. Shaded regions (indicated by dots) correspond to $\langle u_{pert}(z,t)\rangle < 0$. [Despite some spanwise nonuniformity (see also figure

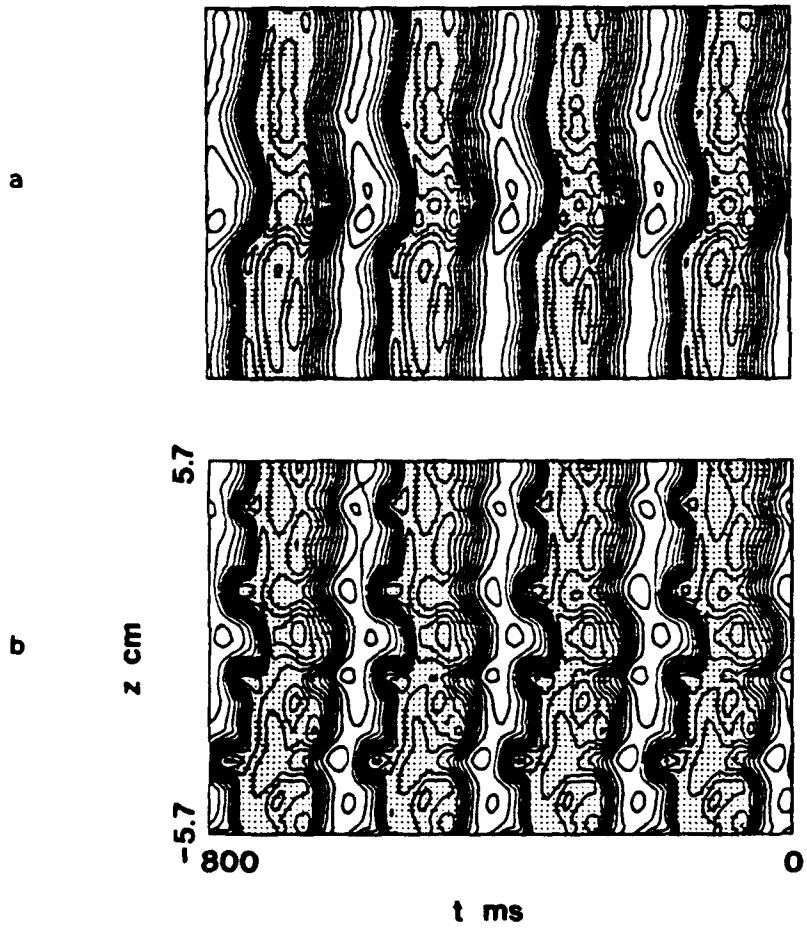

Figure 3.4

2.6*b*), the base flow is quite two-dimensional.] Even though the contour plots in figure 3.4 are planar cross sections of a three-dimensional flow at a fixed cross-stream elevation, they contain useful structural information. The dark spanwise bands in figure 3.4(*a*) represent times of most rapid velocity increase (or decrease) and can be associated with phase fronts of the (excited) Kelvin-Helmholtz instability. Note that the y-elevation of the probe is such that $\langle u_{pert}(z,t)\rangle < 0$ during passage of the (high-speed) crest of the two-dimensional instability wave.

At this streamwise station, the primary vortex rollup has just begun (figure 2.6*a*), and the vortical structure excited by spanwise-nonuniform heating already has an upstream bend about its middle as it is advected downstream (e.g., figure 3.1*c*). The induced velocity fluctuations, $\langle u_{pert}(z,t)\rangle$, in figure 3.4(*b*) are consistent with these observations. As discussed in §3.3, the upstream bend of the streamwise vortical structure first appears on the (high-speed) crest of the two-dimensional wave lying above the cross-stream elevation of the probe at $y = y_0(x)$ (i.e., for $\langle u_{pert}(z,t)\rangle < 0$ in figure 3.4*a*). Because the streamwise vortex is advected in a shearing flow, its induced velocity field acts to move fluid down (or up) from higher (or lower) cross-stream elevations. Hence, the streamwise velocity at a given y-elevation may be higher or lower than it would be in the absence of spanwise-nonuniform excitation, and the presence of the streamwise vortices is marked by local minima or maxima of $\langle u_{pert}(z,t)\rangle$. For example, higher-momentum fluid from the high-speed side is moved down between the counter-rotating legs of a streamwise vortex and, similarly, lower-momentum fluid from the low-speed side is moved up between the legs of adjacent streamwise vortices. This results in alternating local maxima and minima of velocity perturbations within the negative (shaded) regions. The strength of velocity perturbations induced by the streamwise vortices is time-periodic because these vortices, inclined in the streamwise direction as they are advected past the measurement station, are themselves time-periodic.

Even though spanwise-nonuniform excitation has a marked effect on the phase-averaged data close to the flow partition (cf. figure 3.4*b*), its effect on the approximately two-dimensional mean base flow is felt only farther downstream, as can be deduced from cross-stream profiles of the temporal mean of the streamwise velocity. These profiles are shown in figure 3.5(*a*) for spanwise-uniform excitation and figures 3.5(*b,c*) for spanwise-nonuniform excitation. The velocity profiles in figures 3.5(*b*) and 3.5(*c*) are measured at spanwise stations corresponding to passage of the head of a streamwise vortex (i.e., its downstream tip) and halfway ($\lambda_z/2$) between heads of two adjacent streamwise vortices (hereinafter referred to as the "tail"), respectively. The velocity profiles in figure 3.5(*a*) are similar to those found in other investigations of mixing layers subjected to harmonic forcing by other means (e.g., Weisbrot 1984). Of particular note is the development of a slight velocity overshoot (exceeding U_1) at the high-speed side, reported earlier by Gaster, Kit & Wygnanski (1985) for a mechanically forced flow. In addition to a velocity overshoot at the high-speed side, the measurements of Weisbrot reveal a velocity undershoot at the low-speed side.

To the extent that streamwise derivatives of the time-averaged cross-stream velocity component in a two-dimensional mixing layer are small compared to $\partial U/\partial y$ (e.g., Townsend 1980), the mean spanwise vorticity, Ω_z, of the flow will be dominated by the latter. Hence, the velocity overshoot evident in figure 3.5(*a*) may mark the appearance of (small) *negative* values of Ω_z on the high- and low-speed edges of the mixing layer. Although negative spanwise vorticity may also be present in the unforced flow, its mean magnitude is likely to be considerably smaller owing to substantial variation among the cross-stream widths of the primary vortices. The phase-averaged measurements of Weisbrot (1984) indicate the existence of small vorticity peaks at the high- and low-speed edges of the primary vortices; however, it is not clear that these peaks are negative. On the other hand, careful measurements of spanwise vorticity in an unforced mixing layer reveal negative concentrations of

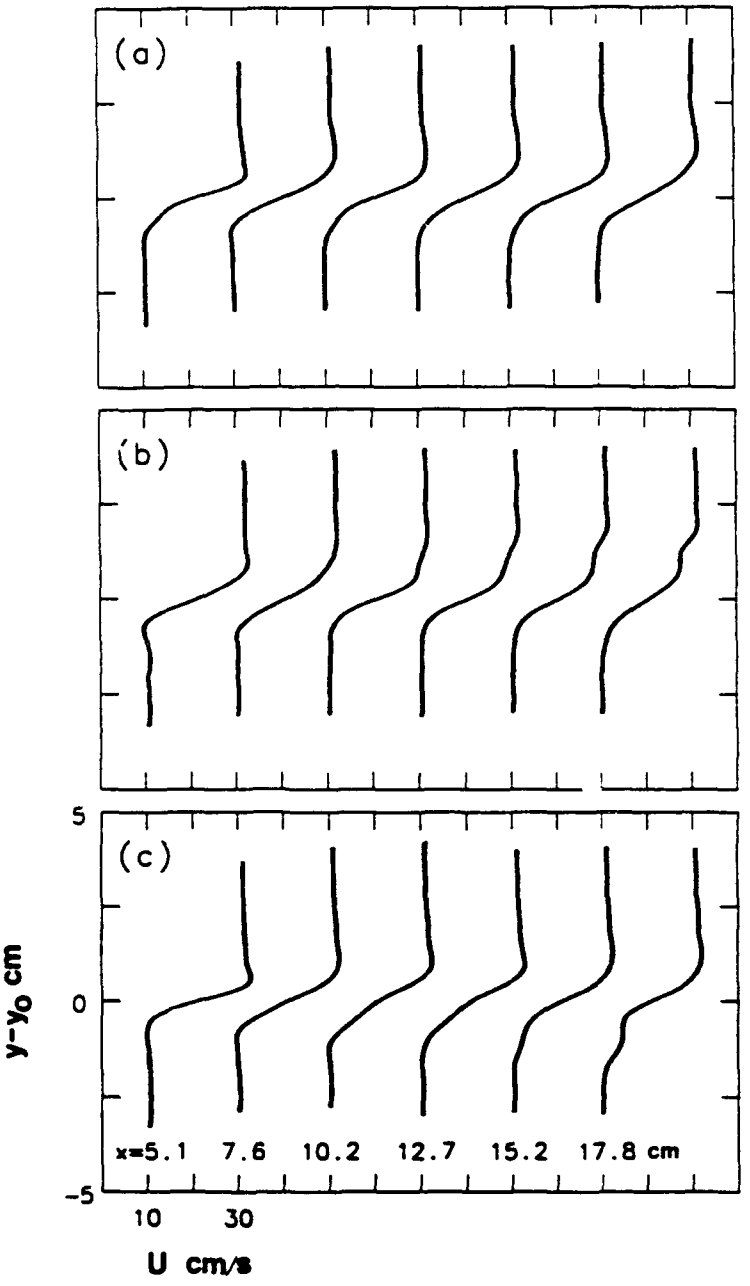

Figure 3.5

spanwise vorticity apparently originating from the boundary layer of the low-speed stream on the flow partition (Lang 1985). We also note that streamwise velocity overshoot (or undershoot) on the high-speed (or low-speed) edge of the mixing layer may lead to a significant diminution in the momentum thickness, even though the width of the mixing layer (as measured by the presence of vorticity) does not necessarily decrease.

When the excitation waveform is spanwise-nonuniform, the mean velocity profiles significantly distort downstream. Because the approximately streamwise vortices in the braid region are inclined in the x-y plane, the profiles in figures 3.5(*b*,*c*) are most strongly affected near their high- and low-speed edges, respectively. Furthermore, since the streamwise vortical structures have their origin in hairpin eddies that form on the high-speed side of the spanwise vortices (figure 3.1*f*), the mean profiles are first distorted near the high-speed edge. Because "localized" inflection points of the distorted mean velocity profiles mark regions of large shear, their appearance has important consequences from the standpoint of mixing transition. These regions are associated with thin internal shear layers, in which the growth rate of small disturbances is proportional to the local rate of strain and inversely proportional to the shear layer thickness (Landahl & Mollo-Christensen 1986). The rapid amplification of these small-scale disturbances is similar to the inviscid instability observed by Klebanoff, Tidstrom & Sargent (1962) in a transitional boundary layer.

Distortion of the streamwise velocity profiles due to spanwise-nonuniform excitation is not restricted to the cross-stream (x-y) plane. Surfaces of mean streamwise velocity are also deformed in the y-z plane (figure 3.6 for x = 10.2 cm, and figure 3.7 for x = 17.8 cm). Spanwise-uniform excitation results in a reasonably two-dimensional distribution of the mean streamwise velocity at x = 10.2 cm, while at x = 17.8 cm, some nonuniformity associated with "natural" evolution of three-dimensional flow structures is developed. The disturbances leading to these flow structures are most likely

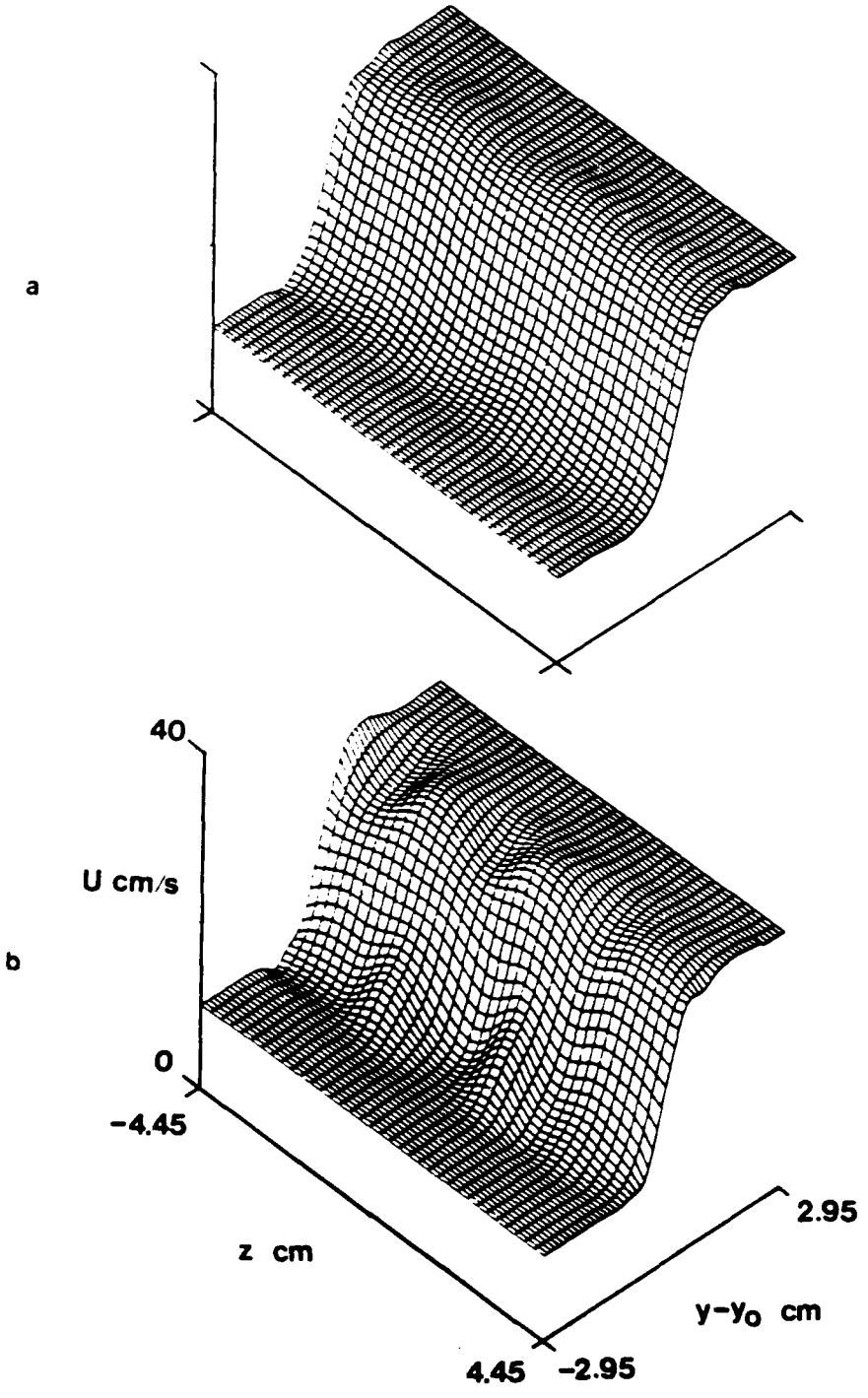

Figure 3.6

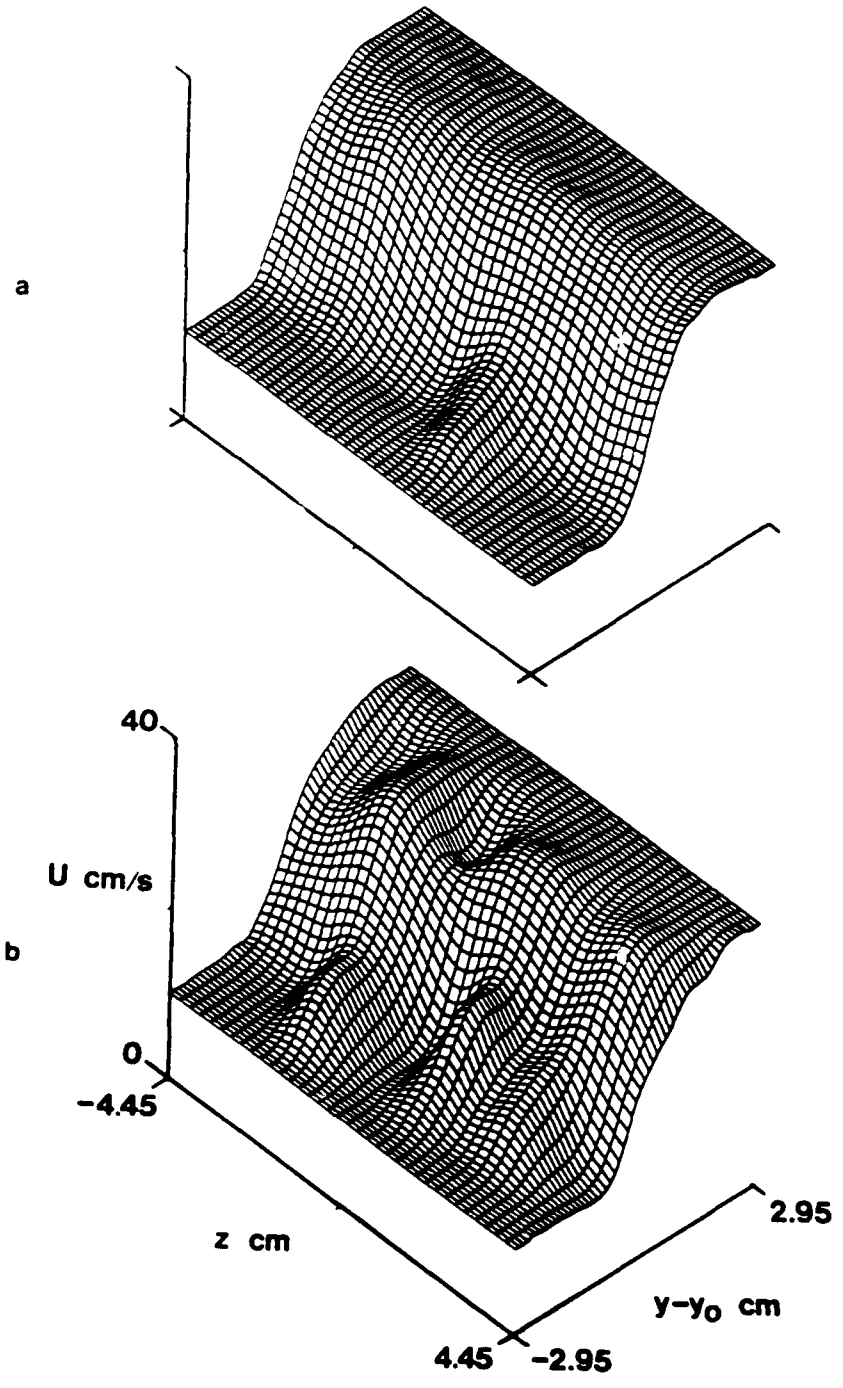

Figure 3.7

associated with imperfections in the experimental apparatus. The respective Reynolds numbers based on the spanwise-averaged momentum thickness, $\Theta(x)$, are 340 and 570. When the excitation waveform is spanwise nonuniform, the temporal mean streamwise velocity distribution develops trough- and ridge-like distortions aligned in the y-direction and alternating in the z-direction with the spanwise wavelength of the excitation waveform. Distortion of the mean streamwise velocity distribution results in a substantial increase in $\Theta(x)$ at these two streamwise locations and, consequently, in an increase in the respective values of $Re_{\Theta(x)}$ (490 and 950). Although this distortion is strongest along the high- and low-speed edges of the mixing layer (i.e., at the heads and tails of the streamwise vortices), it is evident throughout the entire velocity surface and is accompanied by approximately spanwise-periodic inflection points in spanwise profiles of the mean streamwise velocity at fixed y-elevations. As does the distortion of the cross-stream profiles, these inflection points suggest the formation of local maxima of spanwise strain rate and rapid amplification of small disturbances. The breakdown of these rapidly amplifying structures leads to the generation of small-scale turbulence. The formation of localized shear layers by interaction among the streamwise and primary vortices is also suggested by Corcos (1988). Such shear layers may be formed by the wrapping of spanwise vortex lines around cores of streamwise vortices.

The role of streamwise vortices in the formation of spanwise concentrations of small-scale flow structures is demonstrated in spanwise contour plots of velocity power spectra, $P(z,\nu)$, (figure 3.8 at x = 10.2 cm, and figure 3.9 at x = 17.8 cm). These data are plotted at y-elevations of the inflection points on the high- and low-speed edges of the mean cross-stream velocity profiles that result from spanwise-nonuniform excitation (cf. figures 3.5*b,c*). Corresponding spectra for spanwise-uniform harmonic excitation are shown for comparison in figures 3.8(*a,c*) and 3.9(*a,c*). The spanwise profile of the mean streamwise velocity at the y-elevation of each contour plot is shown to the left.

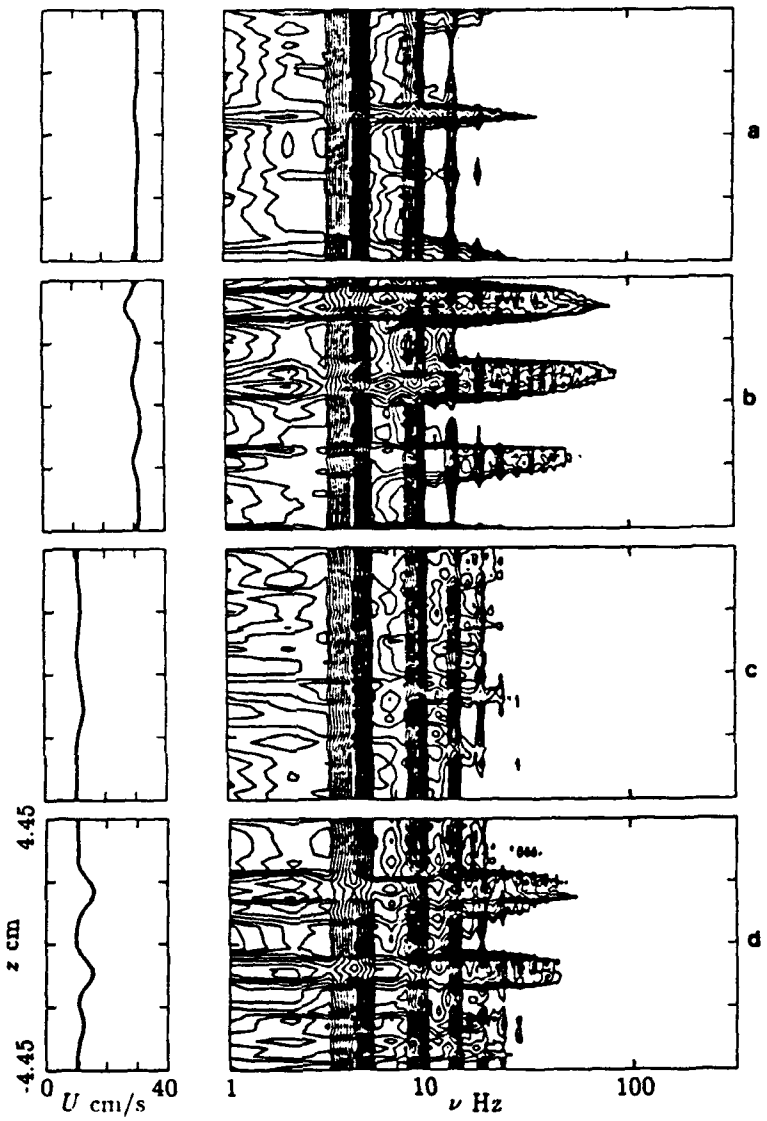

Figure 3.8

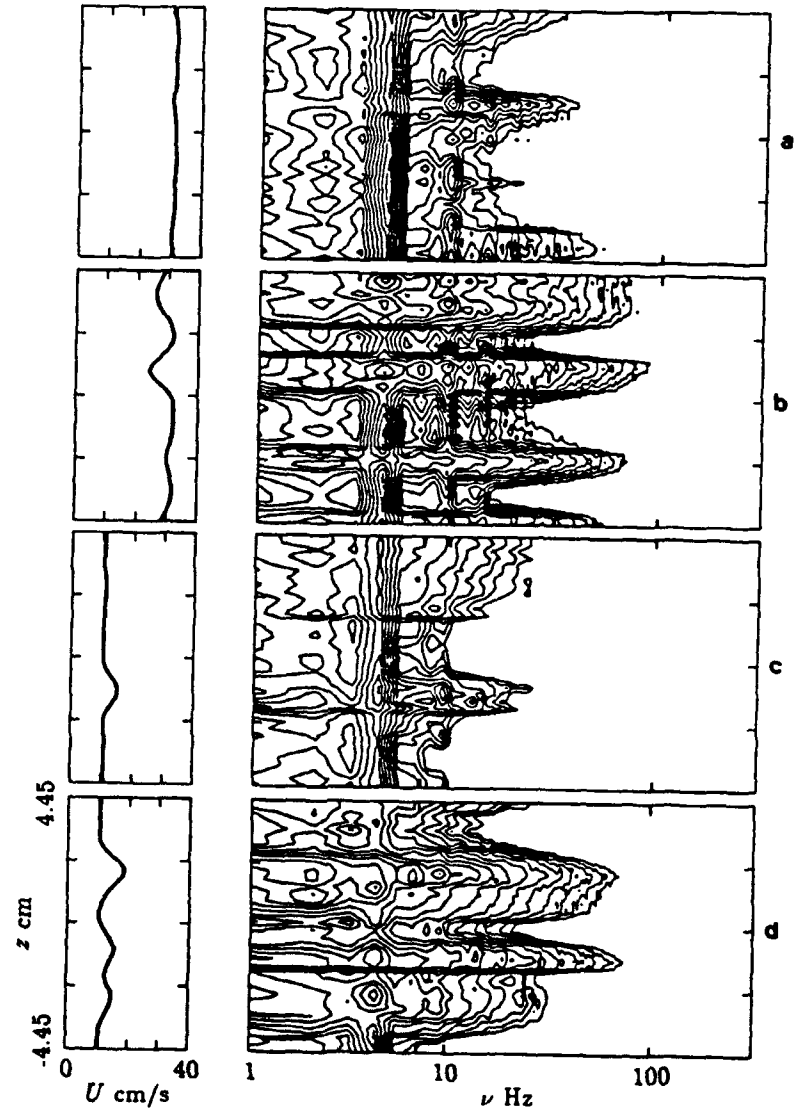

Figure 3.9

Bands of high-frequency spectral components that are approximately spanwise periodic form when the flow is subjected to spanwise-nonuniform excitation. These bands are centered around spanwise extrema of U, and the sharp spanwise gradients along their edges approximately coincide with spanwise inflection points of U (figures 3.8*b,d* and 3.9*b,d*). Note that the spanwise positions of the bands near the high- and low-speed edges of the mixing layer are offset by $\lambda_z/2$, as are the heads and tails of the streamwise vortices. The formation of these bands near the inflection points suggests that the inflection points play an important role in the generation of high-frequency small-scale motion. Furthermore, at the spanwise locations of the bands, the amplitude of the spectral components at the excitation frequency ν_f and its first harmonic, $2\nu_f$, undergo considerable attenuation between x = 10.2 cm and 17.8 cm, indicating (spanwise-nonuniform) energy transfer from low to high frequencies. This process is accompanied by a substantial reduction in the amplitude of higher harmonics of the excitation frequency. A similar trend is apparent in the streamwise variation of the power spectra of streamwise velocity in an unforced mixing layer undergoing small-scale transition (Huang & Ho 1990).

Cross-stream integrated amplitudes of the spectral components of $\langle u_{pert}(x,t)\rangle$ at the forcing frequency and its first harmonic, denoted by A_1 and A_2, respectively, are shown in figure 3.10 for spanwise-uniform and spanwise-nonuniform excitation (cf. figures 3.5*a-c*). To the extent that the local slope of each curve is a measure of local streamwise amplification rate (cf. e.g., Gaster *et al.* 1985), the value of x at which the slope vanishes is the location of zero spatial amplification. When the flow is excited by a spanwise-uniform wave train, A_1 increases somewhat between x = 5.1 cm and 7.6 cm, and then remains almost unchanged until x = 15.2 cm, where it begins to decay (except possibly at the head location). The second harmonic content of $\langle u_{pert}(x,t)\rangle$ for the case of spanwise-uniform excitation is indicative of nonlinear behavior of two-dimensional spanwise vortices. It is remarkable that when the flow is subjected to

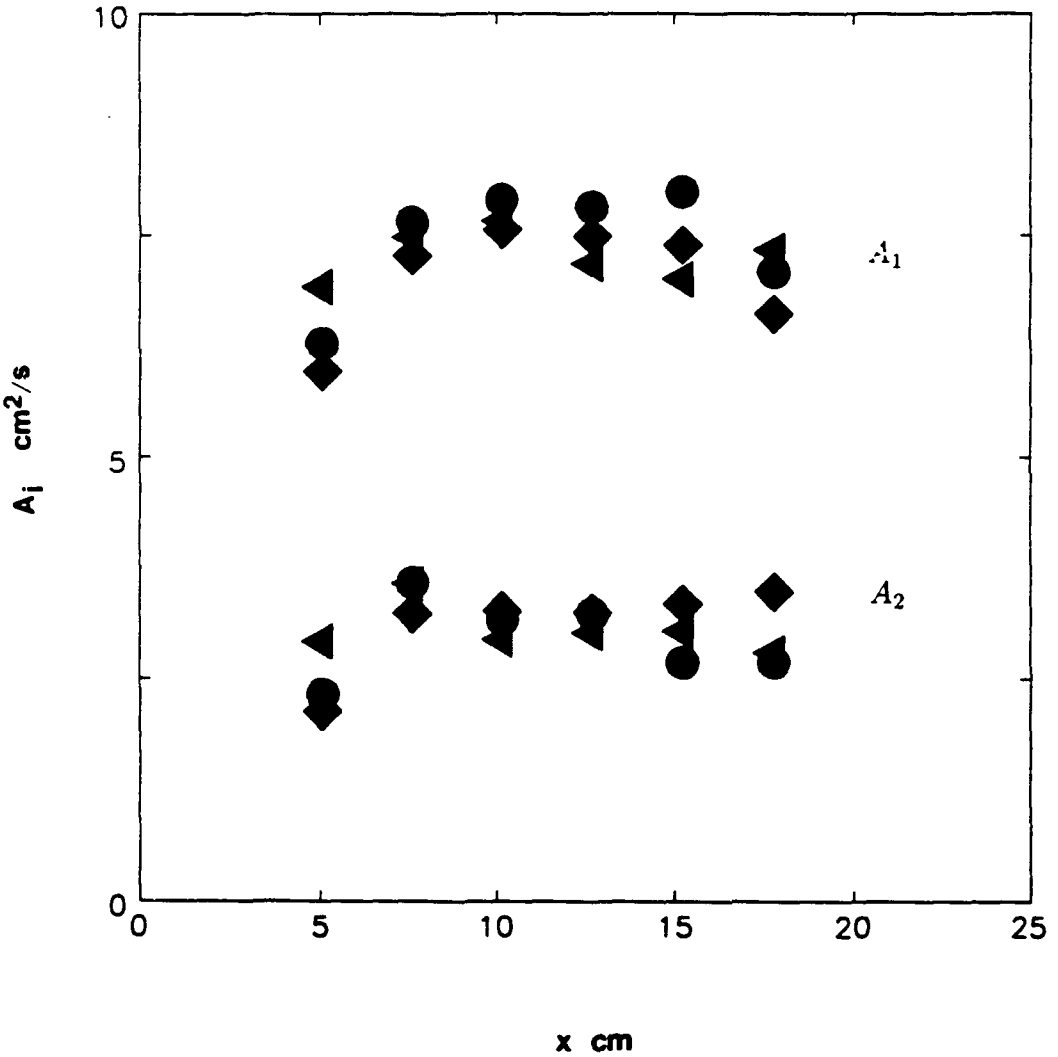

Figure 3.10

spanwise-nonuniform excitation, streamwise distributions of A_1 and A_2 at spanwise locations of the heads and tails of the streamwise vortices are quite similar to corresponding amplitude distributions under spanwise-uniform excitation. This suggests that at least within the streamwise domain considered here, the evolution of the nominally two-dimensional spanwise vortices is almost unaffected by spanwise-nonuniform excitation and the accompanying formation of the streamwise vortices. In view of this finding, we conclude that attenuation of spectral components at the forcing frequency and its higher harmonics is limited to the neighborhood of spanwise inflection points induced by spanwise-nonuniform excitation (figures 3.8 and 3.9). The direct numerical simulations of Riley, Mourad, Moser & Rogers (1988) show that two-dimensional instability modes of the plane mixing layer also appear to be unaffected by three-dimensional disturbances. We note that these conclusions may not be valid if λ_z is long enough to excite the core instability (cf. figures 3.3*a-b*).

3.5. *The Evolution of Small-Scale Motion*

The phase-averaged flow structure resulting from spanwise-nonuniform excitation is studied in detail in constant-x planes at x = 10.2 cm and 17.8 cm. These streamwise locations are chosen because Schlieren visualization and preliminary measurements indicated that the streamwise vortices are fully developed at x = 10.2 cm and, between this station and x = 17.8 cm, three-dimensionality within the spanwise vortices and in the braid region increases substantially. The data are taken on a rectangular grid measuring 8.9 cm and 5.9 cm in the spanwise and cross-stream directions, respectively.

Phase-averaged turbulent fluctuations of the streamwise velocity component, $\langle u'_t(x,t)\rangle$, are calculated from instantaneous velocity records (Glezer *et al.* 1989). This technique uses a (digital) high-pass filter and, as discussed in §3.2, is extremely effective in capturing small-scale streamwise motions associated with passage of large coherent vortical structures at the measurement station. Turbulent structures can also

be identified by an intermittency, $\gamma(\mathbf{x},t)$, defined in terms of the presence or absence of small-scale fluctuations in space or time. In the present experiments, the temporal intermittency is computed pointwise from the streamwise velocity, $u(\mathbf{x},t)$, using the procedure of Glezer & Coles (1990). The local rms deviation, $\epsilon(\mathbf{x},t)$, from a least-squares straight-line fit of three data points in the time series $u(\mathbf{x},t)$ is computed for the middle point and compared with a prescribed threshold. If $\epsilon(\mathbf{x},t)$ exceeds the threshold, the flow is called turbulent and the intermittency is set to unity at the middle point; otherwise, it is set to zero. The result is a time series, $\gamma(\mathbf{x},t)$, of ones and zeros. The ensemble-averaged intermittency, $\langle\gamma(\mathbf{x},t)\rangle$, varies between zero and one and may be thought of as a measure of the probability that the flow is turbulent.

Figures 3.11(*a-b*), at x =10.2 cm, and figures 3.11(*c-d*), at x =17.8 cm, show contour plots of $\langle u'_t\rangle$ and $\langle\gamma\rangle$ in the y-t plane for spanwise-uniform excitation. At the measurement station, passage of the spanwise vortex can be recognized by concentrations of small-scale velocity fluctuations. Whereas at x = 10.2 cm, $\langle u'_t\rangle$ is mostly concentrated in a relatively small region closer to the low-speed edge of the vortex (figure 3.11*a*), at x = 17.8 cm (figure 3.11*c*) the cross-stream distribution of $\langle u'_t\rangle$ within the spanwise vortex is considerably broader and has a lower maximum. The cross-stream intermittency distribution during passage of the spanwise vortex at x = 10.2 cm (figure 3.11*b*) has two maxima, upstream and downstream, which appear to be associated with entrainment of irrotational fluid from the low- and high-speed streams, respectively. Three equally spaced, weak intermittency maxima in the braid region correspond to higher harmonics in the velocity spectra (cf. figure 3.8*a*) and can be connected with a Kelvin-Helmoltz instability of the material interface separating the high- and low-speed fluid. Similar structures are also apparent in the numerical results of Lummer discussed by Fiedler (1988). It is noteworthy that, unlike $\langle f\rangle$, corresponding levels of $\langle u'_t\rangle$ in the braid region are considerably lower than within the spanwise vortices. This is because the intermittency data are sensitive to the presence of

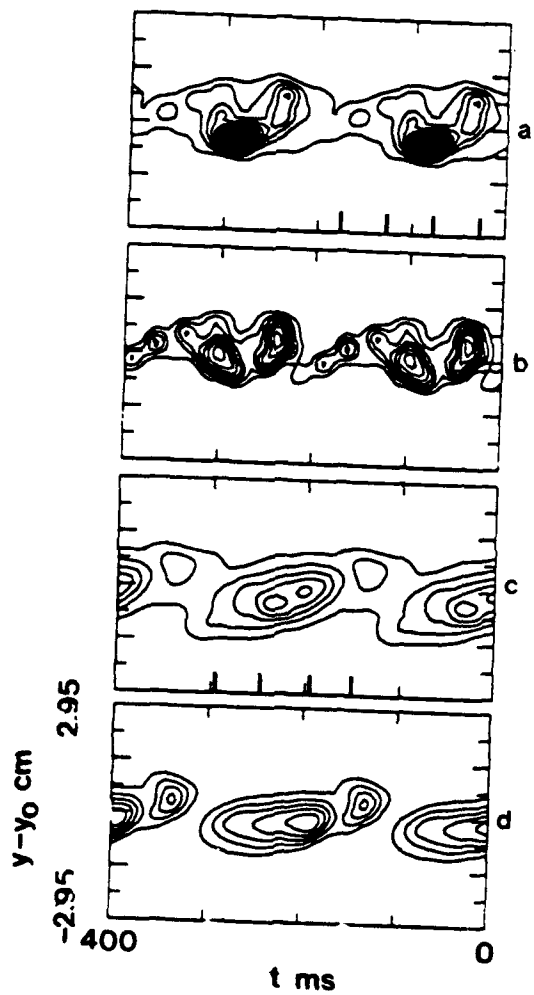

Figure 3.11

turbulent interfaces and are not a measure of turbulence intensity. As with $\langle u'_t \rangle$, the cross-stream distribution of $\langle \gamma \rangle$ at x = 17.8 cm (figure 3.11*d*) is broader and has a single peak (cf. Oster & Wygnanski 1982).

That the phase-averaged structure of the base flow in the y-t plane is substantially modified by spanwise-nonuniform excitation is demonstrated in contour plots of $\langle u'_t \rangle$ and $\langle \gamma \rangle$ at spanwise locations corresponding to heads and tails of the streamwise vortices (figures 3.12 and 3.13, respectively). For x = 10.2 cm, at the spanwise locations of heads of the streamwise vortices, regions of small-scale motion progressively contaminate toward the high-speed side (figures 3.12*a,b*). Farther downstream, the heads of the streamwise vortices do not "wrap" around the spanwise vortices (as suggested, for example, by the sketches of Lasheras & Choi 1988) but protrude in the downstream direction toward the braid region (figures 3.12*c,d*). As observed by Bernal & Roshko (1986), the streamwise vortices tend to move away from the spanwise vortices, i.e., toward the high- and low-speed streams. Hence, the heads (or tails) of the streamwise vortices are advected faster (or slower) than the spanwise vortices and can protrude into the downstream (or upstream) braid regions. Similar behavior is evident in the direct numerical simulation of a temporally developing mixing layer (Rogers & Moser 1989) *after* pairing of the spanwise vortices.

The present results further indicate that the streamwise vortices may form closed toroidal "ribs" around the primary vortices, which become part of "cat's-eye"-like structures (discussed in more detail below). For x = 10.2 cm, at spanwise locations of the tails, regions of small-scale motion are extended upstream near the low-speed edge (figures 3.13*a,b*). Farther downstream (x = 17.8 cm), the tail of the streamwise vortex has clearly moved away from the spanwise vortex and is stretched in the upstream direction (figures 3.13*c-d*). While the global features, such as general orientation and morphology of the members of a spanwise group of streamwise vortices, are preserved during passage through the streamwise domain considered here, the detailed structure of

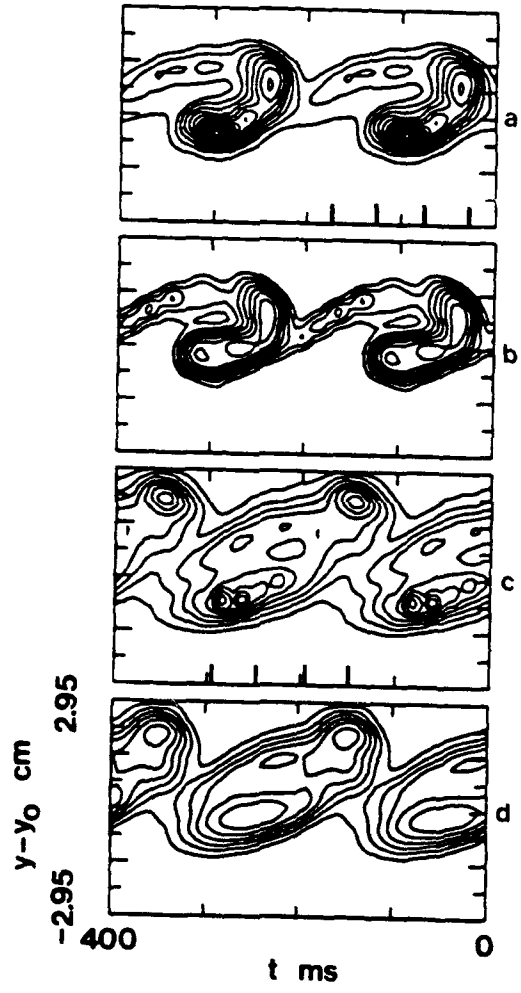

Figure 3.12

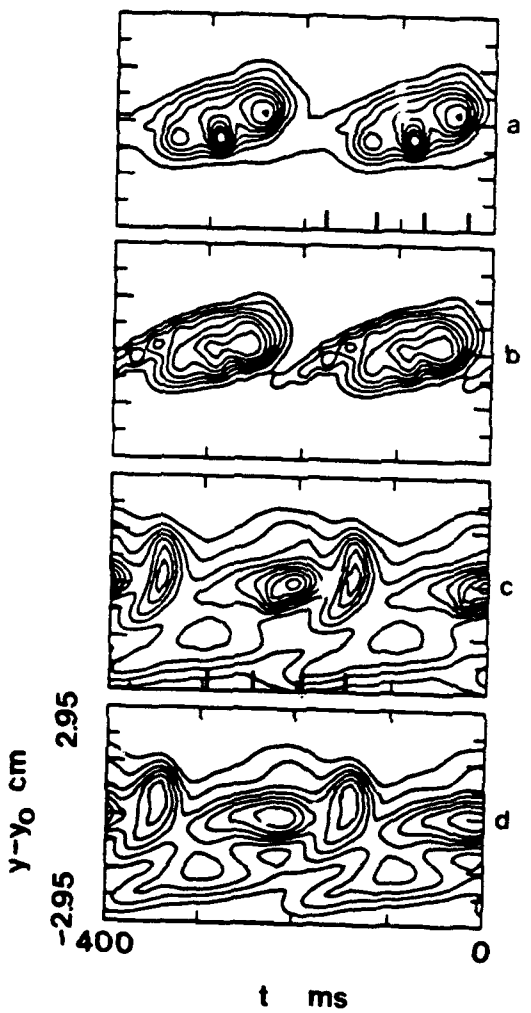

Figure 3.13

individual vortices within that group may evolve and become dissimilar as the vortices are advected downstream. This can be inferred from projections of three-dimensional contours of $\langle u'_{za} \rangle$ (shown in figures 3.17-3.19 and discussed below). Structural differences between streamwise vortices of a given spanwise group can be related to the onset of core instability of the primary vortices (cf. figures 3.3*a*,*b*).

Structural details of interfaces (or boundaries) separating turbulent and nonturbulent fluid in shear flows can be studied by using zone-averaged turbulent intensity (e.g., Glezer *et al.* 1989),

$$\langle u'_{za}(\mathbf{x},t) \rangle = \frac{\langle u'(\mathbf{x},t)\gamma(\mathbf{x},t) \rangle}{\langle \gamma(\mathbf{x},t) \rangle} .$$

Zone-averaged flow quantities are normally biased toward (and hence emphasize) flow features near turbulent boundaries characterized by low values of $\langle \gamma \rangle$. The values of the zone-averaged u', where $\langle \gamma \rangle \cong 1$, are approximately equal to $\langle u'_t \rangle$. Although u' and γ vanish outside turbulent regions, in the present manuscript $\langle u'_{za} \rangle$ is calculated only for $\langle \gamma \rangle \geq 0.005$.

Contours of $\langle u'_{za} \rangle$ in the y-t plane are shown in figure 3.14(*a*) for spanwise-uniform excitation and figure 3.14(*b-e*) for spanwise-nonuniform excitation. Figures 3.14(*b-e*) show cross sections of a streamwise vortex at four equally spaced spanwise locations between the head and tail of the vortex. The head of the streamwise vortex (figure 3.14*b*) appears to be separated from the spanwise vortex at the latter's upstream edge, as may be inferred from a narrow region of lower turbulence intensity between them. A cross section through a leg of the streamwise vortex (figure 3.14*c*) shows a considerable increase in turbulence intensity in the braid region. The local peak in turbulence intensity within the leg is due to its intersection with the y-t plane at a small angle. The interaction between the tail of the streamwise vortex and the spanwise vortex is shown in figures 3.14(*d-e*) and is accompanied by reduction in turbulence intensity within the core of the primary vortex. This reduction occurs at

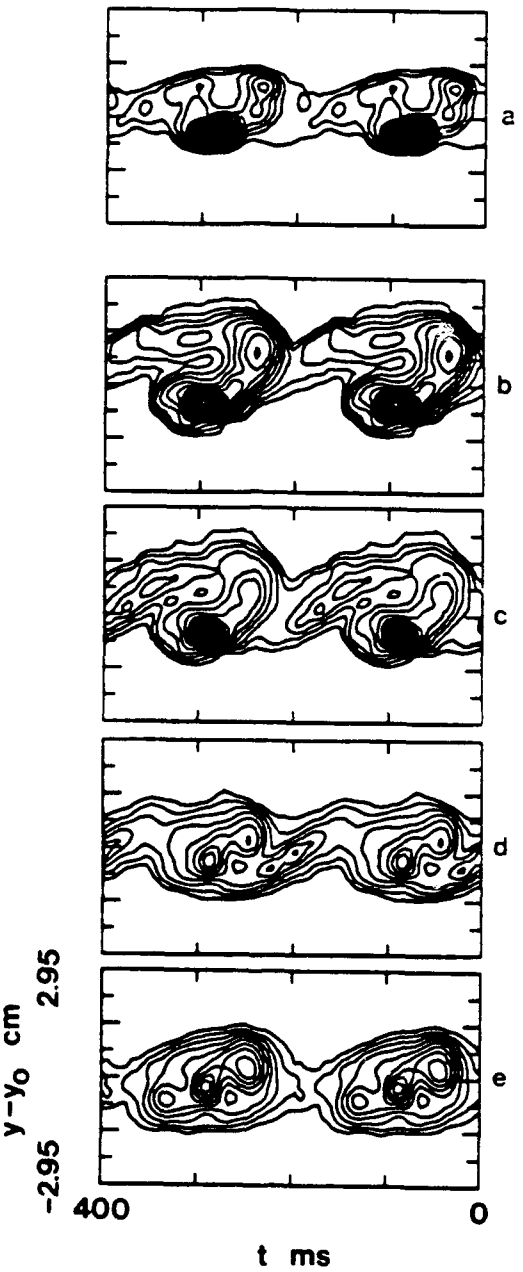

Figure 3.14

spanwise locations that approximately coincide with legs of the streamwise vortices at the low-speed edge of the primary vortex (see also figure 3.15*g* below). Note also the upstream extension (toward the braid region) of the low-speed edge of the primary vortex (figure 3.14*e*).

The phase-averaged flow structure was also studied in y-z planes at different phase delays relative to the zero crossings of the time-harmonic excitation, E(z,t). In each of figures 3.15(*a-h*), for x = 10.2 cm, and figures 3.16(*a-h*), for x = 17.8 cm, we show four pairs of contour plots of $\langle u'_{za} \rangle$ taken at equal time intervals during the excitation period. These times are referred to below as t_1, t_2, t_3, and t_4, and are chosen so that t_1 and t_3 correspond approximately to passage of the centers of the braid region and the core of the spanwise vortex (as measured by the peak of $\langle u'_{za} \rangle$), respectively. The contour plots (*a-d*) of each figure are for spanwise-uniform excitation. Because cross sections in the y-z plane are extremely sensitive to spanwise undulations of the primary vortices, the data in figures 3.15 and 3.16 are actually plotted along lines of constant spanwise phase of the two-dimensional base flow. The necessary phase information is obtained from a (discrete) Fast Fourier Transform of the velocity time series measured at a y-elevation outside the mixing layer on the high-speed side (the largest spanwise phase variation is 27°).

Spanwise concentrations of zone-averaged turbulence intensity in the braid region are clearly associated with the legs of the streamwise vortices (figure 3.15*e*), in agreement with the observations of Breidenthal (1981). In the absence of the streamwise vortices (figure 3.15*a*), there is very little turbulent activity in the braid region. The y-z plane at $t = t_2$ is closer to the downstream spanwise vortex and, hence, the streamwise vortices are at higher y-elevations than at $t = t_1$. Furthermore, at $t = t_2$ (counter-rotating) pairs of streamwise vortices are closer to each other, indicating that the heads begin to form. We note that tails of streamwise vortices from the downstream braid region appear at the low-speed side. The heads and tails of the streamwise vortices are also apparent at the downstream edge of the spanwise vortex ($t = t_4$, figure 3.15*h*).

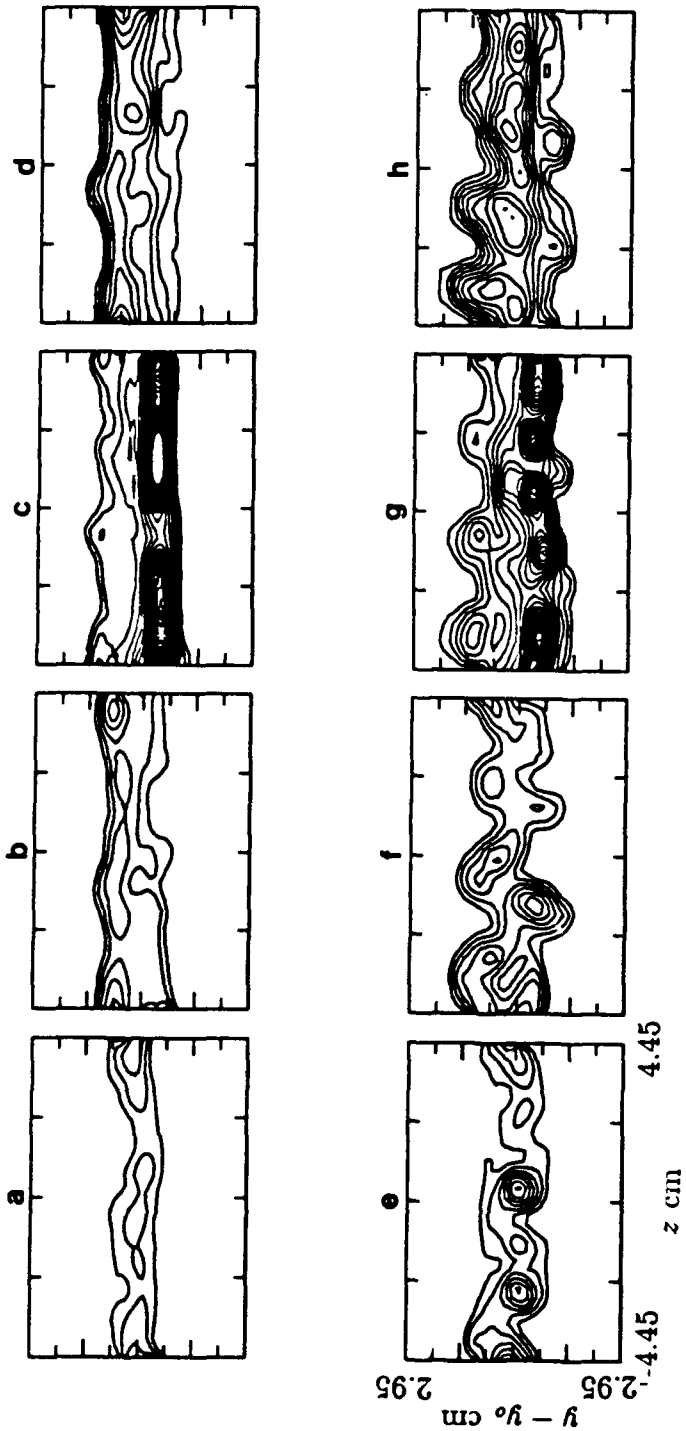

Figure 3.15

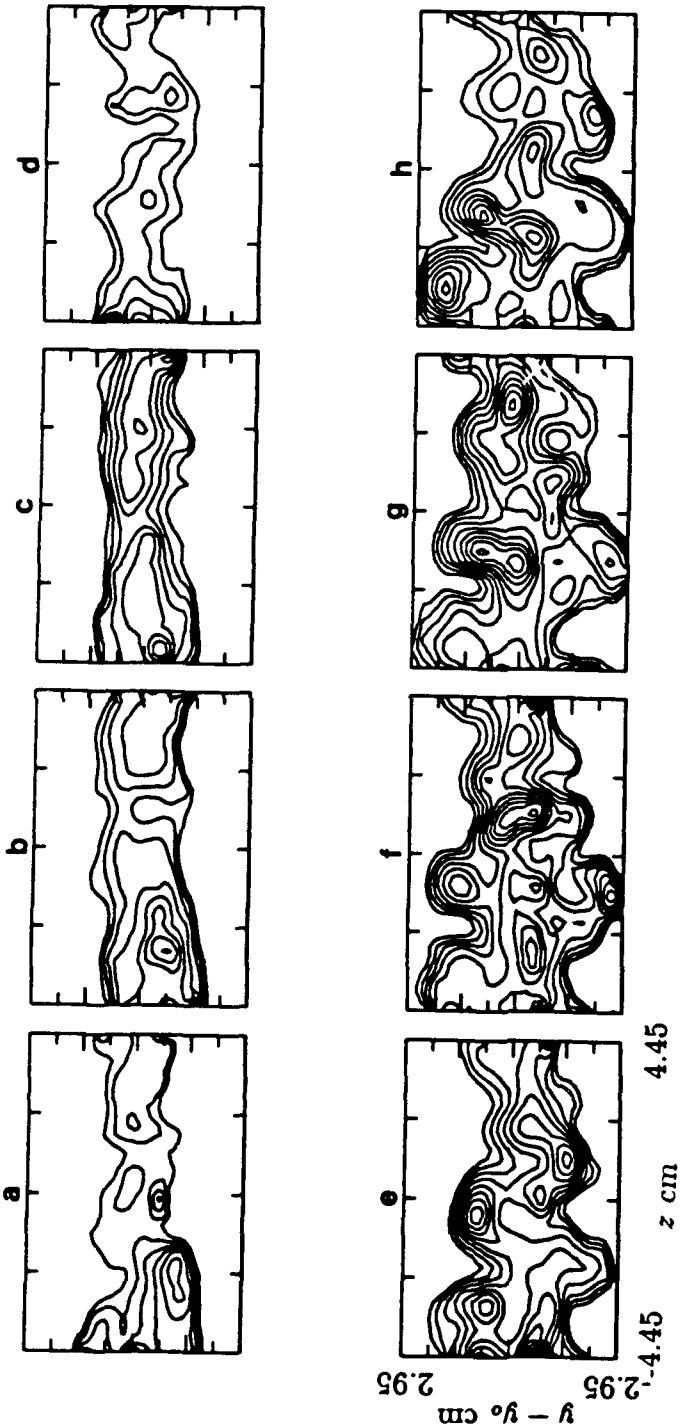

Figure 3.16

The contour plots at $t = t_3$ (figures 3.15*c,g*) represent cross sections through the center of the core of the spanwise vortex (as may be measured by a maximum of the turbulence intensity). Modification of the structure of the primary vortex by spanwise-nonuniform excitation is evident in the appearance of concentrations of turbulent intensity at spanwise locations of the heads of the streamwise vortices and from breakdown of the primary vortex core into spanwise-periodic concentrations of small-scale motion having a spanwise wavelength of approximately $\lambda_z/2$. The spanwise locations of these turbulence concentrations also coincide with inflection points of the mean spanwise profile of streamwise velocity (e.g., figure 3.8). Furthermore, as discussed in §3.5 below, breakdown of the core is connected with the formation of approximately spanwise-periodic concentrations of all three vorticity components within the spanwise vortex as a result of its interaction with the streamwise vortices. We believe that this breakdown is a precursor to the rapid spreading of three-dimensional small-scale motion within the core of the spanwise vortex, which is necessary for mixing transition. Figures 3.16(*e-h*) show that at $x = 17.8$ cm the flow is clearly dominated by the streamwise vortices. Of particular note is the reduction in the spanwise periodicity of the concentrations of small-scale motion within the core of the primary vortex (compare figure 3.16*g* to 3.15*g*), which suggests spanwise mixing. This evolution is accompanied by a significant increase in the cross-stream width of the mixing layer. The corresponding data for spanwise-uniform excitation (figures 3.16*a-d*) show less cross-stream spreading and significantly less spanwise nonuniformity within the primary vortex and the braid region.

As noted in §3.2, iso-surfaces of zone-averaged rms streamwise velocity fluctuations may be useful in studying the three-dimensional structure of the flow. Figures 3.17 and 3.18 show the surface $\langle u'_{za}(y,z,t)\rangle/\Delta U = 0.03$ at $x = 10.2$ cm and 17.8 cm, respectively, during two periods of the excitation waveform. These and the following iso-surface plots (figures 3.19 and 3.22 below) begin at $t = t_1 - T_f/8$, i.e., at a

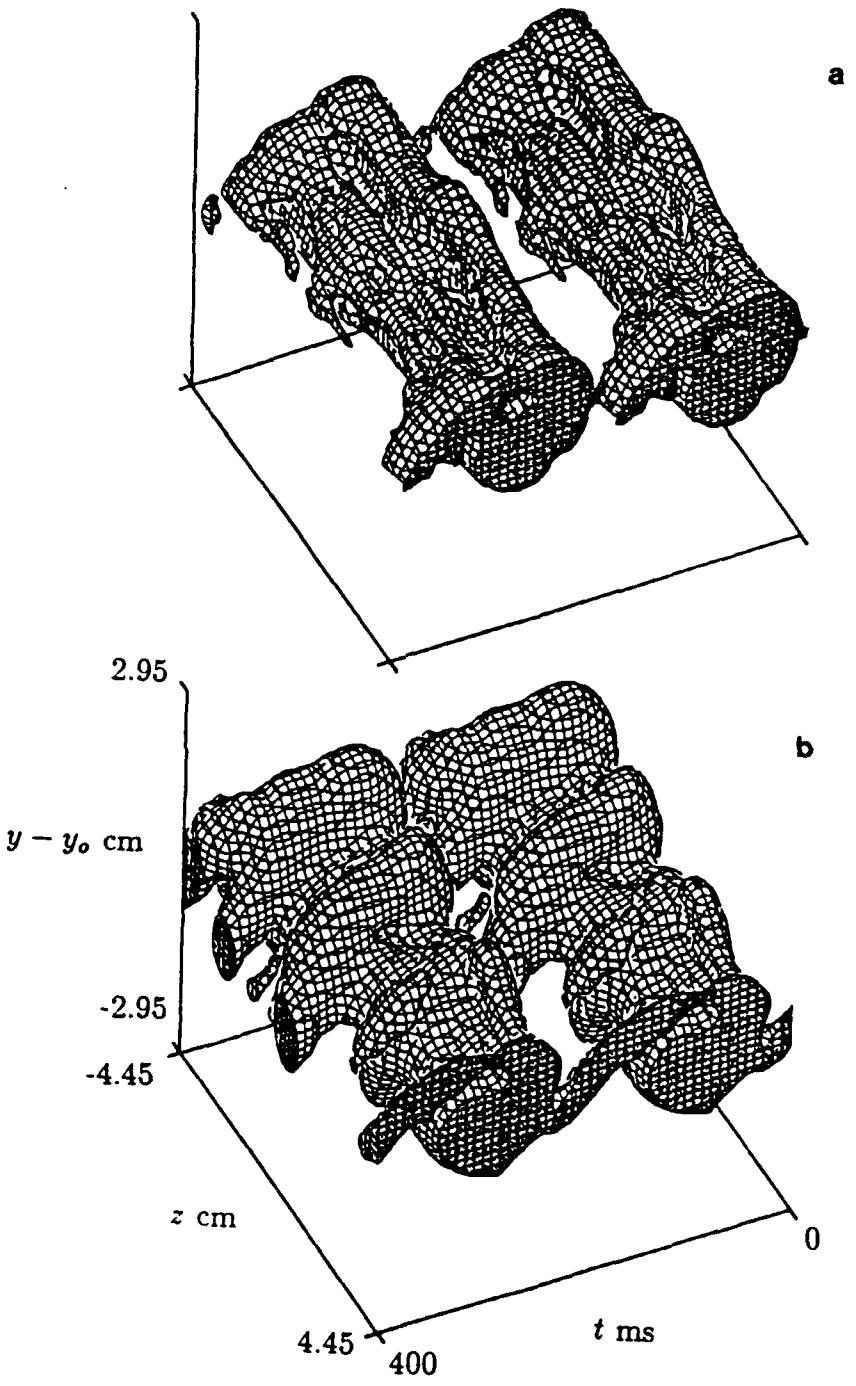

Figure 3.17

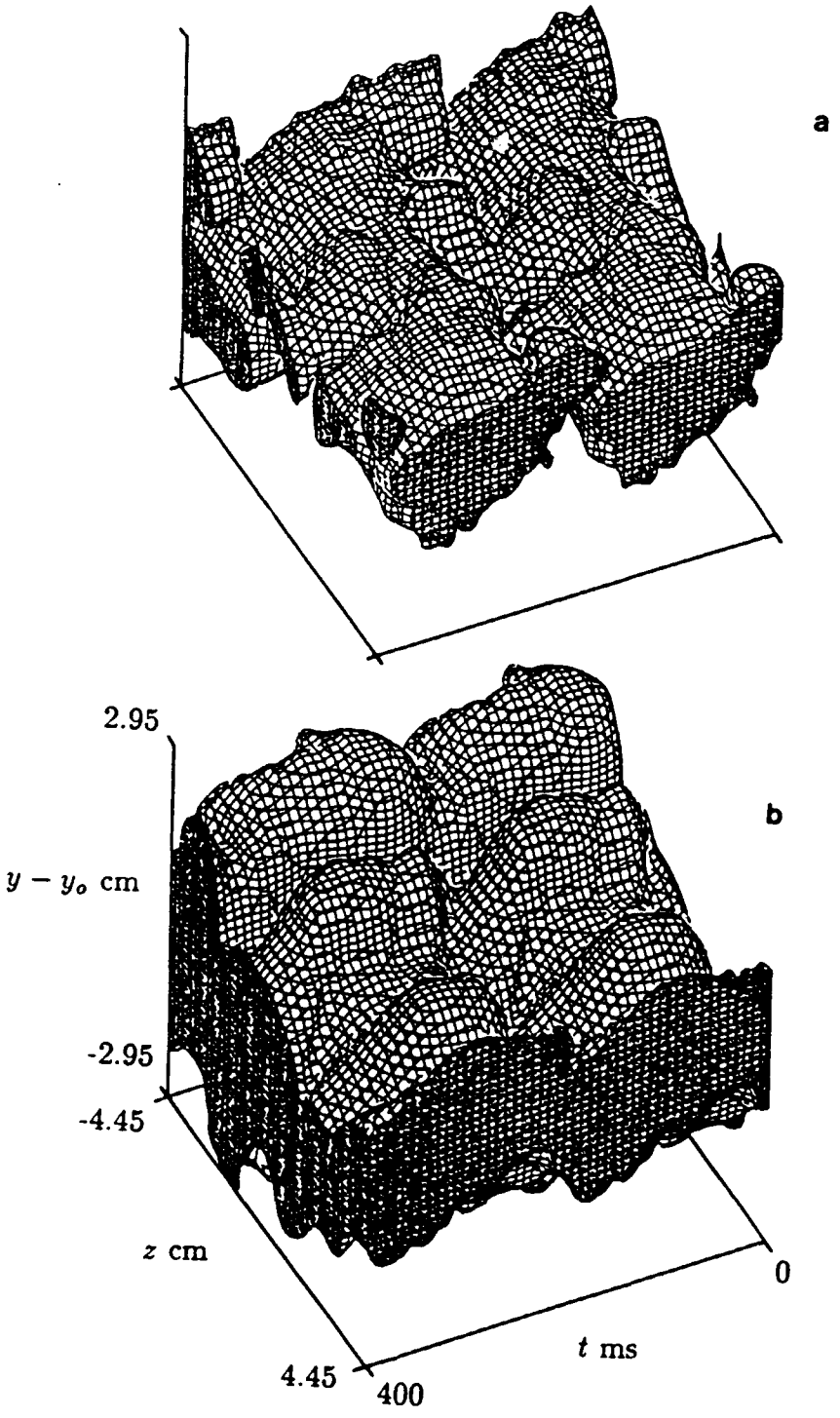

Figure 3.18

cross section in the y-z plane close to the center of the braid region (cf. figures 3.15*a,e*). When the excitation is spanwise-uniform, the spanwise vortices and the braid region are approximately two dimensional. The spanwise trough along each primary vortex separates upstream and downstream regions of concentrated velocity fluctuations, apparently connected with entrainment of high- and low-speed fluid, respectively, into the spanwise vortex. Spanwise-nonuniform excitation leads to formation of structures with substantial spanwise nonuniformity. The heads of the streamwise vortices appear on the high-speed side of the primary vortex, with spanwise spacings approximately equal to the excitation wavelength, λ_z. The legs of streamwise vortices in the braid region are not all of equal strength, presumably due to spanwise variations in the strain field, which is in turn affected by the primary vortices. (As shown in figure 3.3, spanwise undulations of the primary vortices have a substantial effect on the evolution of the streamwise vortices.) Figure 3.17(*b*) further suggests that appearance of the streamwise vortices results in substantial enlargement of turbulent interfaces into the free streams.

For spanwise-uniform excitation, figure 3.18(*a*) shows that, farther downstream, the primary vortices have developed spanwise irregularities. These appear to be associated with formation of unforced streamwise vortices. Note the decrease in the inclination relative to the x-direction of the major axis of the nominally oval cross section of these vortices. Because the fundamental instability mode becomes neutral where the major axis is oriented normal to the streamwise direction (roughly at x = 10.2 cm in our experiments) and decays thereafter, this change has been connected by Weisbrot (1984) with spatial amplification of harmonically excited waves. For spanwise-nonuniform excitation, figure 3.18(*b*) shows a substantial increase in the cross-stream width of the mixing layer (as may be defined by spreading of turbulent interfaces), although this surface does not show details of the streamwise structures. For x = 17.8 cm, the surface $\langle u'_{za}(y,z,t)\rangle/\Delta U = 0.055$ (figure 3.19) indicates that the

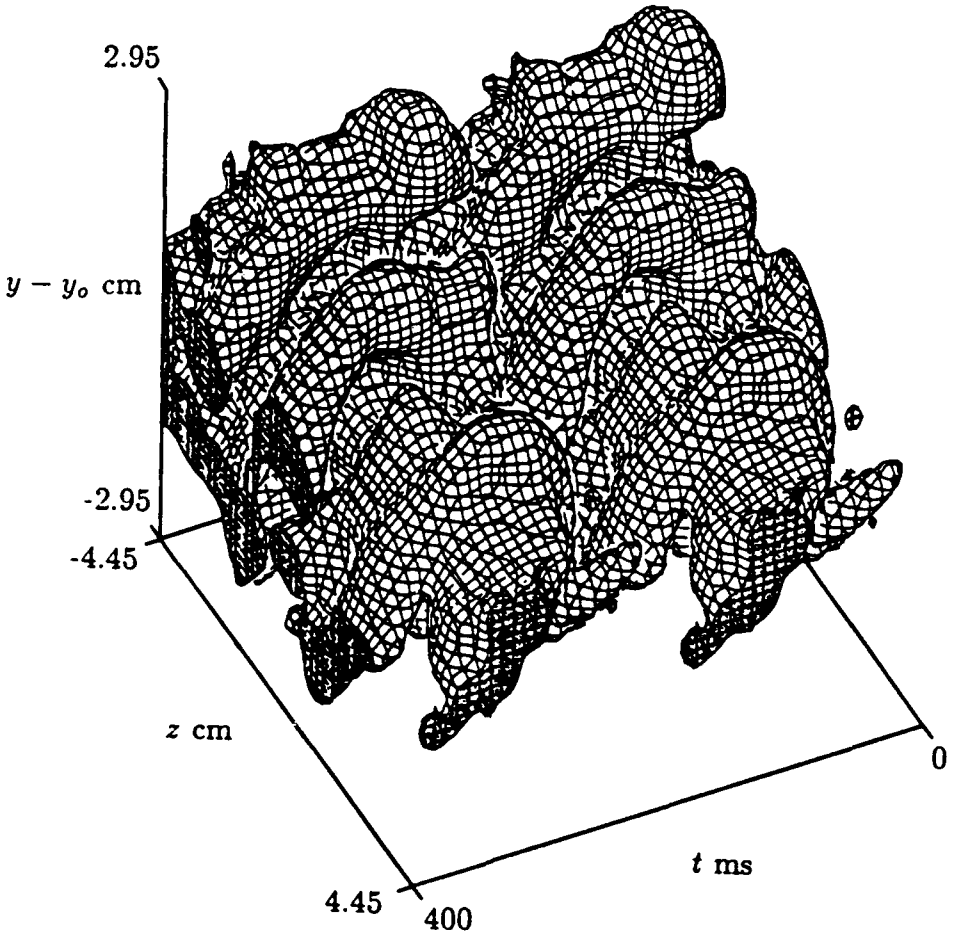

Figure 3.19

heads and tails of the streamwise vortices protrude into the downstream and upstream braid regions, respectively. As discussed above, this protrusion is possible because the heads and tails are advected at higher and lower velocities than the high-speed and low-speed edges of the primary vortices, respectively. Figure 3.19 also suggests the formation of approximately toroidal regions of $\langle u'_{za} \rangle$ around the primary vortices due to the upstream and downstream protrusion of the streamwise vortices (see also figure 3.3*d*).

3.6. *An Approximation to Cross-Stream Vorticity*

We next focus attention on the phase-averaged cross-stream component of vorticity, $\langle \Omega_y \rangle = \partial\langle u \rangle/\partial z - \partial\langle w \rangle/\partial x$. Owing to phase averaging, characteristic length scales in the spanwise direction are smaller than those in the streamwise direction. Hence, the ensemble-averaged cross-stream vorticity components may be *approximated* by $\langle \tilde{\Omega}_y \rangle = \partial\langle u(x,t) \rangle/\partial z$. Although it is clear that this approximation makes it impossible to distinguish between vortical and irrotational distortions of the streamwise velocity profile, its use in what follows enables us to develop a three-dimensional structure of the streamwise vortices. Contours of $\langle \tilde{\Omega}_y \rangle$ are shown in figures 3.20, for $x = 10.2$ cm, and figures 3.21, for $x = 17.8$ cm, at $t = t_1$, t_2, t_3, and t_4 (cf. figures 3.15 and 3.16). In most of the braid region, the vorticity within the streamwise vortices is likely to have two approximately equal components in the x- and y-directions (Ω_x and Ω_y). Thus, streamwise vortices in the y-z plane at $t = t_1$ (figure 3.20*e*) may be recognized by alternating concentrations of positive and negative $\langle \tilde{\Omega}_y \rangle$, coinciding with concentrations of $\langle u'_{za} \rangle$ in figure 3.15(*e*). It should be noted that the level of $\langle \tilde{\Omega}_y \rangle$ is quite low for spanwise-uniform excitation (figure 3.20*a*). A notable feature of the results for spanwise-nonuniform excitation (figures 3.20*e-h* and 3.21*e-h*) is the downstream preservation of spanwise (and streamwise) coherence of the phase-averaged flow features. In contrast, contour plots of $\langle u'_{za} \rangle$ have less spanwise coherence at $x = 17.8$ cm (figures 3.16*e-h*) than at $x = 10.2$ cm (figures 3.15*e-h*).

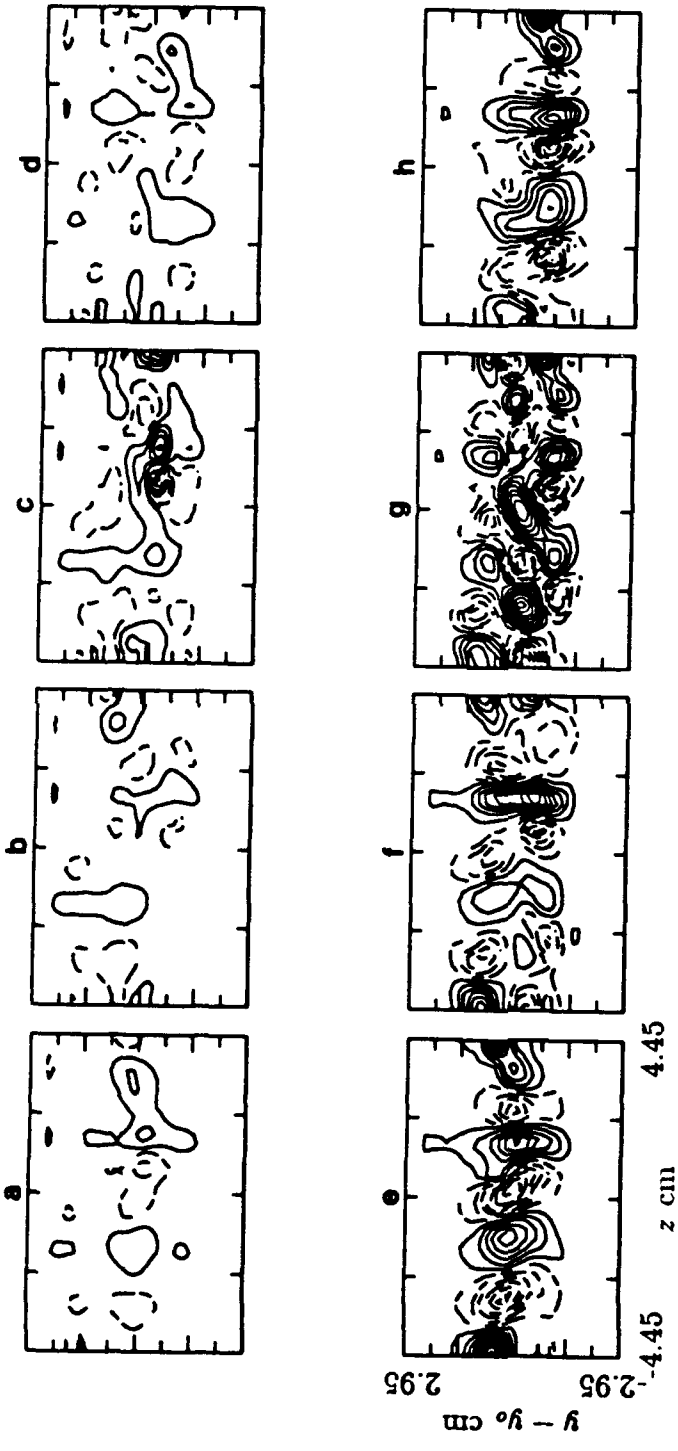

Figure 3.20

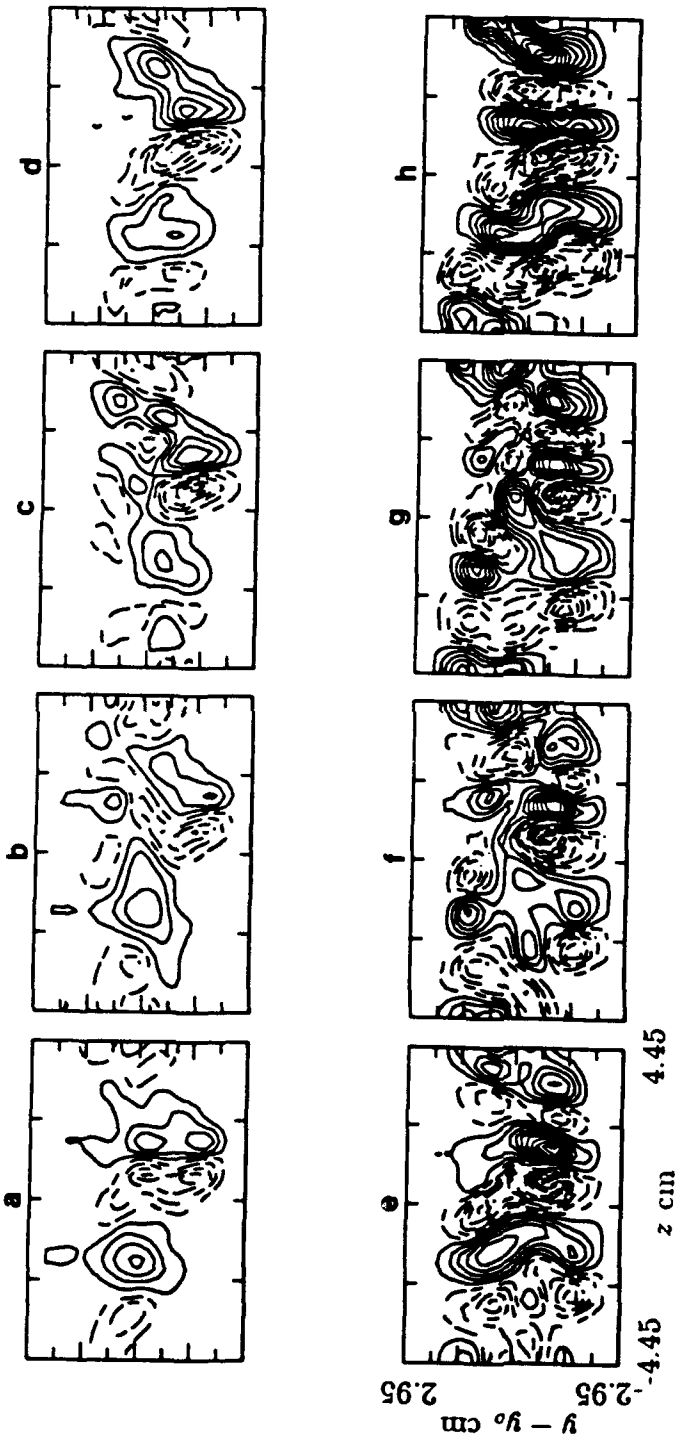

Figure 3.21

Of particular interest is the distribution of $\langle\tilde{\Omega}_y\rangle$ within the primary vortex core when the mixing layer is subjected to spanwise-nonuniform excitation. [Note for comparison the corresponding distributions for spanwise-uniform excitation in figure 3.20(*c*) for x = 10.2 cm and figure 3.21(*c*) for x = 17.8 cm.] The distribution of $\langle\tilde{\Omega}_y\rangle$ in the y-z plane at $t = t_3$ (figures 3.20*g* and 3.21*g*) is comprised of three approximately regular spanwise rows, each consisting of approximately spanwise-periodic concentrations of $\langle\tilde{\Omega}_y\rangle$ of alternating signs having a wavelength $\lambda_z/2$. Concentrations of $\langle\tilde{\Omega}_y\rangle$ of the same sign in the top and bottom rows occur at approximately the same z-coordinate and appear to be associated with streamwise vortices in the upstream and downstream braid regions, respectively. The middle row (within the core of the spanwise vortex) is offset in the z-direction relative to the upper and lower rows by $\lambda_z/2$.

A strikingly similar distribution of the streamwise vorticity, Ω_x, is found in direct numerical simulations of a mixing layer (Buell & Mansour 1989) that allow for streamwise growth. The spanwise distribution of Ω_x leads to spanwise-periodic intensification and weakening of the spanwise vorticity, Ω_z, and the formation of cup-shaped concentrations. The cups form at the center of quadrupoles comprised of four adjacent concentrations of Ω_x (two in the middle row), which produce positive spanwise strain (i.e., stretching of spanwise vorticity). The spanwise locations of the resulting cups alternate above and below the middle row much like the heads and tails of the streamwise vortices. The distribution of cross-stream vorticity, Ω_y, also has a quadrupolar structure very similar to that of figures 3.20(*g*) and 3.21(*g*) (Buell, private communication, 1990). These distributions of Ω_x and Ω_y within the cores of the primary vortices may result from vortex lines looping between cups. In connection with the spanwise-periodic concentrations of $\langle u'_{za}\rangle$ in figure 3.15(*g*), we note that the upper and lower cups in the results of Buell & Mansour appear at similar spanwise locations and, hence, are likely related to the spreading of small-scale motion within the core of the primary vortex.

The existence of spanwise concentrations of $\langle\tilde{\Omega}_y\rangle$ in the upper and lower rows of figures 3.20(*g*) and 3.21(*g*) may be jointly due to tilting of spanwise vortices by streamwise vortices and to the transport of cross-stream vorticity along the legs of the streamwise vortices in the upstream and downstream directions. It should be noted that axial flow along the legs of the streamwise vortices (associated with vorticity transport) can also contribute to mixing (or at least stirring) of fluid from both streams. The apparent "tagging" of the streamwise vortices by $\langle\tilde{\Omega}_y\rangle$ allows for study of their protrusion into the upstream and downstream braid regions (figure 3.19). Contour plots of $\langle\tilde{\Omega}_y\rangle$ at $t = t_1$ and t_4 (figures 3.21*e,h*) show vertical stacks of concentrations (pairs and triplets) of the same sign, representing cross sections of streamwise vortices from the upstream and downstream braid regions. As mentioned in §3.4, the numerical results of Rogers & Moser (1989) show that (after pairing of two primary vortices is completed) streamwise vortices are stretched beyond the upstream and downstream spanwise vortices and toward the respective upstream and downstream braid regions. Contours of $\partial\langle v\rangle/\partial z$ in the braid region (approximating $\langle\Omega_x\rangle$) measured by Huang & Ho (1990) show the appearance of cross-stream (vertical) pairs of concentrations of Ω_x. Those data were obtained downstream of the first rollup of the primary vortices, and the authors remarked that the formation of streamwise vortices began immediately downstream of the flow partition.

Given the qualitative agreement between our measurements and the numerical results of Buell & Mansour (1989) and Rogers & Moser (1989), we believe that, even though $\langle\tilde{\Omega}_y\rangle$ is only an approximation for the cross-stream vorticity component, it is nevertheless useful in marking the streamwise vortices. Figures 3.22(*a,b*) show plots of the surface $\langle\tilde{\Omega}_y(y,z,t)\rangle = 4$ sec^{-1} at $x = 10.2$ and 17.8 cm, respectively (cf. figures 3.17*b* and 18*b*). At $x = 10.2$ cm, the legs of the streamwise vortices in the braid region are unmistakable. Although the primary vortices are not immediately visible here, they can be identified by the curvature of the nearby streamwise vortices and by spanwise

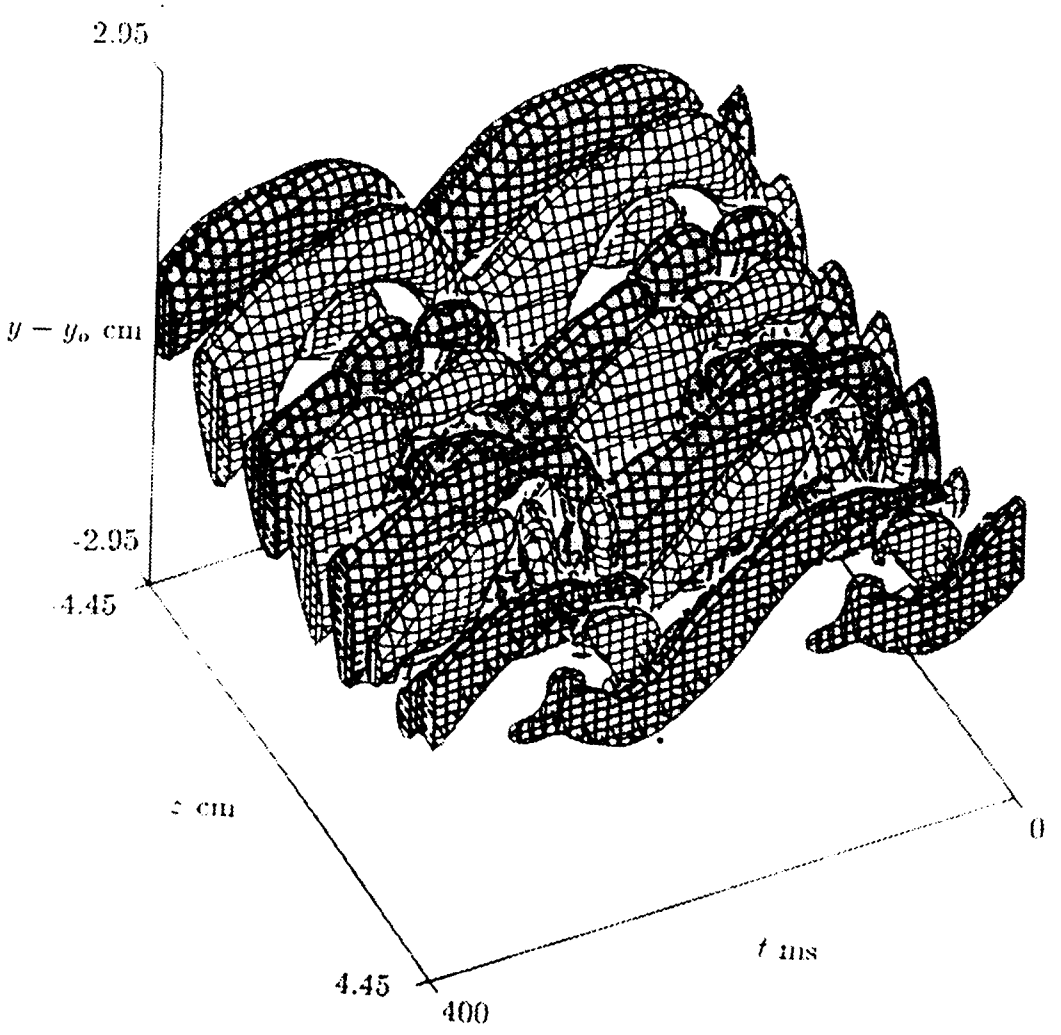

Figure 3.22(*a*)

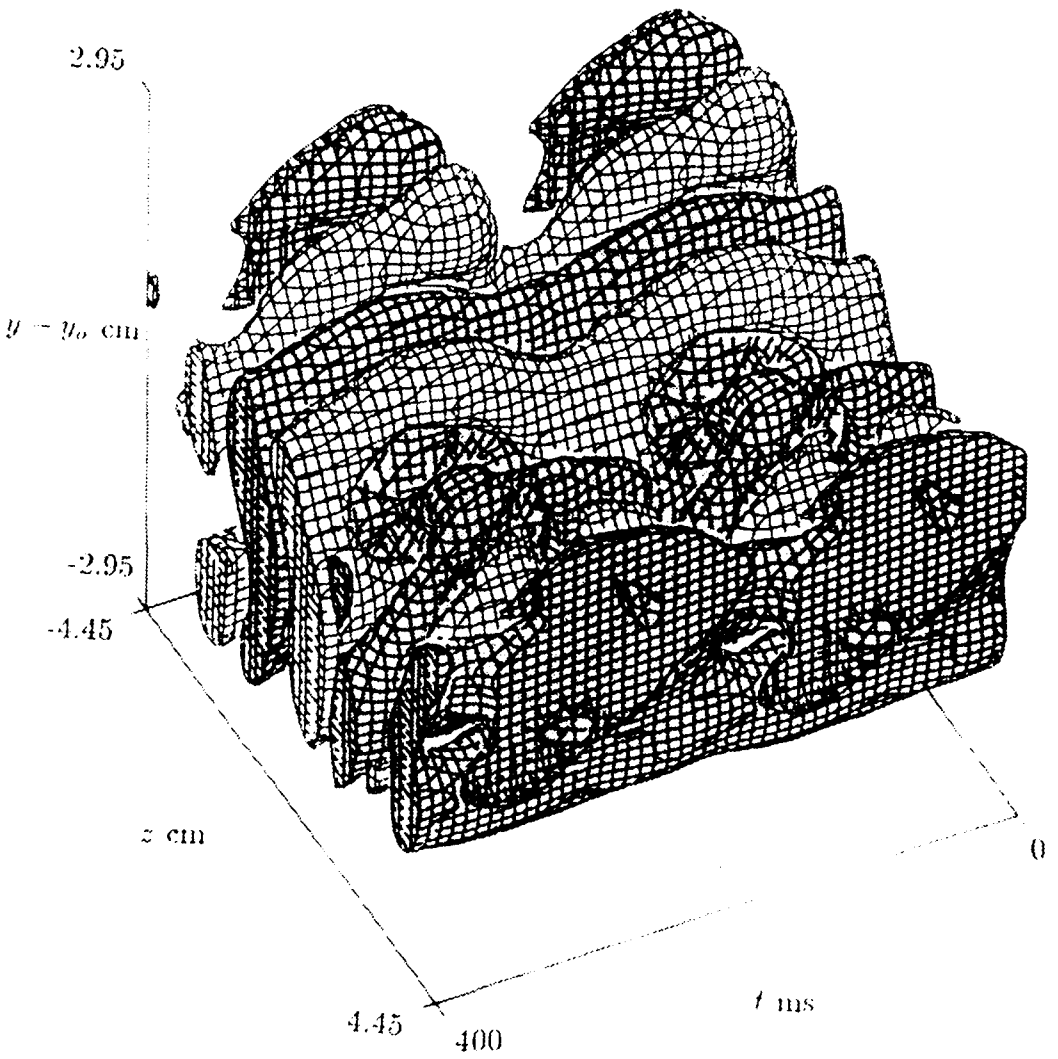

Figure 3.22(*b*)

concentrations of $\langle\tilde{\Omega}_y\rangle$ (figure 3.20*g*). At x = 17.8 cm, the protrusion of streamwise vortices at some spanwise locations gives the appearance of a "cat's-eye"-like surface around the primary vortex. In the braid region, this surface is comprised of the "local" streamwise vortex, as well as streamwise vortices from the upstream and downstream braid regions. A cross section of this structure in the y-t plane (at x = 17.8 cm, z = -1.3 cm) is shown in figure 3.23. At this spanwise location, the "cat's-eye" structure is already apparent at the high-speed edge, while the leg of the streamwise vortex at the low-speed edge is stretched in the upstream direction. A vertical stack of three streamwise vortices in the braid region can also be identified at some spanwise locations in contour plots of $\langle\tilde{\Omega}_y(y,z,t)\rangle$ (figure 3.21*e*) and, as mentioned above, is also evident in the numerical results of Rogers & Moser.

3.7. *Conclusions*

Previous investigations have demonstrated that an unforced plane mixing layer is extremely receptive to small perturbations originating upstream of the flow partition. These perturbations result in spanwise concentrations of streamwise and cross-stream vorticity downstream of the flow partition and, subsequently, in the formation of streamwise vortices bearing considerable resemblance to lambda vortices in a transitional boundary layer. In the present investigation, streamwise vortices are induced by a time-harmonic heat input, which has a spanwise-periodic amplitude distribution, using a mosaic of surface film heaters flush-mounted on the flow partition. The streamwise vortices form downstream of the flow partition, but *upstream* of the first rollup of the primary vortices, presumably due to streamwise strain induced by the primary vortices (Lin & Corcos 1984). Following the next rollup, the streamwise vortices reside in the braid region between consecutive primary vortices.

We have found that, for a given excitation frequency, virtually any spanwise wavelength, λ_z, synthesizable by the heating mosaic can be excited and can lead to the

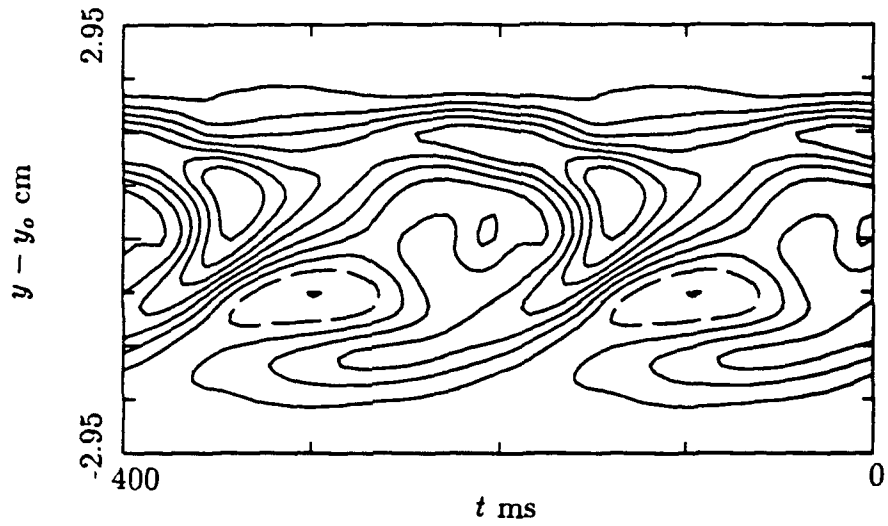

Figure 3.23

formation of streamwise vortices. When the excitation wavelength is smaller than the initial wavelength of the Kelvin-Helmholtz instability, λ_{KH}, the streamwise vortices become narrower with decreasing λ_z due to spanwise interactions. At longer excitation wavelengths, the streamwise vortices become nearly isolated in the spanwise direction, and their shape appears to be wavelength independent. In connection with these results, it is important to recognize that, in all laboratory facilities, spanwise-nonuniform vorticity distributions are transported through boundary layers on the flow partition and may undergo amplification or decay. Hence, the receptivity of these boundary layers is inherently coupled to that of the ensuing shear layer. Furthermore, the sensitivity of the plane mixing layer (and the upstream boundary layers) to spanwise-isolated disturbances suggests that the streamwise growth of streamwise vortices is the result of a localized, rather than a global, spanwise instability mechanism.

The spanwise excitation wavelength has a profound effect on the primary vortices. When λ_z exceeds λ_{KH}, the primary vortices develop spanwise undulations, persisting throughout the streamwise domain of the present observations. These undulations appear to be associated with a (translative) core instability of the primary vortices. Because the strain field within the braid region is dominated by the adjacent spanwise vortices, these undulations are accompanied by an increase in the spread angle of the streamwise vortices, and the appearance of additional vortex tubes along their legs. When $\lambda_z < \lambda_{KH}$, the spanwise vortices appear to be stable (as may be judged by the absence of spanwise undulations) to upstream disturbances that lead to the formation of streamwise vortices. Because of subsequent interaction among the streamwise and spanwise vortices, the direct effect of these disturbances on the vorticity distribution within the spanwise vortices cannot be assessed.

An important objective of the present experiments has been the identification of a mechanism which, following the appearance of streamwise vortices, leads to the generation of small-scale motion and possibly to mixing transition. We have found the

appearance of streamwise vortices to be accompanied by significant distortions in distributions of mean streamwise velocity. These distortions have the shape of troughs and ridges aligned in the cross-stream direction, alternate at the excitation wavelength λ_z, and are strongest at the high- and low-speed edges of the mixing layer (i.e., at the heads and tails of the streamwise vortices). These distortions result in spanwise-periodic inflection points not present in corresponding velocity distributions of the unforced flow. Inflection points of the mean velocity distribution indicate the formation of locally unstable regions of large shear in which broadband perturbations already present in the base flow undergo rapid amplification and breakdown to small-scale motion. Velocity spectra at cross-stream elevations of the inflection points develop spanwise-periodic bands of high-frequency spectral components centered around the heads and tails of the streamwise vortices.

As a result of interaction with the streamwise vortices, the primary vortices develop spanwise-periodic concentrations of small-scale motion having a spanwise wavelength of approximately $\lambda_z/2$ within their cores. We believe that this breakdown of the cores of the primary vortices is a precursor to mixing transition because farther downstream corresponding distributions of small-scale motion have less spanwise coherence. We note that this loss of coherence does not affect other phase-averaged quantities, such as velocity perturbations. The establishment of spanwise-periodic concentrations of small-scale motion is probably associated with the inflectional instability of the mean streamwise velocity distribution discussed above, because such instability at the low- and high-speed edges of the mixing layer leads to spanwise-periodic entrainment variations. Furthermore, these inflection points are presumably related to spanwise-periodic concentrations of all three vorticity components within the spanwise vortices. The evolution of these vorticity concentrations has been discovered by direct numerical simulation (e.g., Buell & Mansour 1989), and their presence in the flow can also be deduced from the present data. The numerical simulations predict the

formation of cup-shaped concentrations of spanwise vorticity, the spanwise locations of which almost coincide with concentrations of small-scale motion in the present data. The apparent connection between spanwise concentrations of small-scale motion and the changes in the vorticity field is indicative of the mechanisms that precede the onset of mixing transition.

Finally, the research described here utilizes a nominally two-dimensional base flow in which pairing of the primary vortices is inhibited by means of spanwise-uniform harmonic excitation. Experimental results in an unforced mixing layer suggest that small-scale transition occurs only *after* the first pairing of the spanwise vortices (e.g., Huang & Ho 1990). Because our findings indicate that mixing transition in a plane shear layer *subjected to spanwise-nonuniform excitation* may be possible in the absence of pairing, we have recently begun to investigate the effect on the generation of small-scale motion of the pairing of primary vortices accomplished by periodic excitation at the natural frequency and its first subharmonic. The evolution of small-scale motion is being studied in the presence and absence of streamwise vortices.

3.8. *References*

Ashurst, W. T. & Meiburg, E. 1988 Three-dimensional shear layers via vortex dynamics. *J. Fluid Mech.* **189**, 87-116.

Bell, J. H. & Mehta, R. D. 1989 Three-dimensional structure of plane mixing layers. *Joint Institute of Aeronautics and Acoustics Rep. TR-90.* NASA Ames Research Center.

Bernal, L. P. 1981 The coherent structure of turbulent mixing layers. I. Similarity of the primary vortex structure. II. Secondary streamwise vortex structure. Ph.D. thesis, California Institute of Technology.

Bernal, L. P. & Roshko, A. 1986 Streamwise vortex structure in plane mixing layers. *J. Fluid Mech.* **170**, 499-525.

Breidenthal, R. E. 1981 Structure in turbulent mixing layers and wakes using a chemical reaction. *J. Fluid Mech.* **109**, 1-24.

Browand, F. K. & Troutt, T. R. 1980 A note on spanwise structure in the two-dimensional mixing layer. *J. Fluid Mech.* **97**, 771-781.

Browand, F. K. & Troutt, T. R. 1985 The turbulent mixing layer: geometry of large vortices. *J. Fluid Mech.* **158**, 489-509.

Brown, G. L. & Roshko, A. 1974 On density effects and large structure in turbulent mixing layers. *J. Fluid Mech.* **64**, 775-816.

Buell, J. C. & Mansour, N. N. 1989 Asymmetric effects in three-dimensional spatially developing mixing layers. In *Proc. Seventh Symp. on Turbulent Shear Flows, Stanford University*, pp. 9.2.1-9.2.6.

Chandrsuda, C., Mehta, R. D., Weir, A.D. & Bradshaw, P. 1978 Effect of free-stream turbulence on large structures in turbulent mixing layers. *J. Fluid Mech.* **85**, 693-704.

Corcos, G. M. 1988 The role of cartoons in turbulence. In *Perspectives in Fluid Mechanics, Lecture Notes in Physics* (ed. D. E. Coles), vol. 320, pp. 48-65. Springer.

Corcos, G. M. & Lin, S. J. 1984 The mixing layer: deterministic models of a turbulent flow. Part 2. The origin of the three-dimensional motion. *J. Fluid Mech.* **139**, 67-95.

Fiedler, H. E. 1988 Coherent structures in turbulent flows. *Prog. Aerospace Sci.* **25**, 231-269.

Fiedler, H. E., Glezer, A. & Wygnanski, I. J. 1988 Control of the plane mixing layer: some novel experiments. In *Current Trends in Turbulence Research* (ed. H. Branover, M. Mond & Y. Unger), vol. 112, pp. 30-64, AIAA, Washington, D.C.

Gaster, M., Kit, E. & Wygnanski, I. J. 1985 Large scale structures in a forced turbulent mixing layer. *J. Fluid Mech.* **150**, 23-47.

Glezer, A. & Coles, D. E. 1990 An experimental investigation of a turbulent vortex ring. *J. Fluid Mech.* **211**, 243-283.

Glezer, A., Katz, Y. & Wygnanski, I. J. 1989 On the breakdown of the wave packet trailing a turbulent spot in a laminar boundary layer. *J. Fluid Mech.* **198**, 1-26.

Huang, L.-S. & Ho, C.-M. 1990 Small scale transition in a plane mixing layer. *J. Fluid Mech.* **210**, 475-500.

Hussain, A. K. M. F. 1983 Coherent structures and incoherent turbulence. In *Turbulence and Chaotic Phenomena in Fluids: Proceedings of the International Symposium on Turbulence and Chaotic Phenomena in Fluids, Kyoto, Japan* (ed. T. Tatsumi), Elsevier.

Jimenez, J. 1983 A spanwise structure in the plane shear layer. *J. Fluid Mech.* **132**, 319-336.

Klebanoff, P. S., Tidstrom, K. D. & Sargent, L. M. 1962 The three-dimensional nature of boundary layer instability. *J. Fluid Mech.* **12**, 1-41.

Konrad, J. H. 1976 An experimental investigation of mixing in two-dimensional turbulent shear flows with applications to diffusion limited chemical reactions. Ph.D. thesis, California Institute of Technology.

Landahl, M. T. & Mollo-Christensen, E. 1986 *Turbulence and Random Processes in Fluid Mechanics.* Cambridge University Press.

Lang, D. B. 1985 Laser Doppler velocity and vorticity measurements in a turbulent shear layer. Ph.D. thesis, California Institute of Technology.

Lasheras, J. S. & Choi, H. 1988 Three dimensional instability of a plane free shear layer: an experimental study of the formation and evolution of streamwise vortices. *J. Fluid Mech.* **189**, 53-86.

Lasheras, J. C., Cho, J. S. & Maxworthy, T. 1986 On the origin and evolution of streamwise vortical structures in a plane, free shear layer. *J. Fluid Mech.* **172**, 231-258.

Leibovich, S. 1983 The form and dynamics of Langmuir circulations. *Ann. Rev. Fluid Mech.* **15**, 391-427.

Lin, S. J. & Corcos, G. M. 1984 The mixing layer: deterministic model of a turbulent flow. Part III. The effect of plane strain on the dynamics of streamwise vortices. *J. Fluid Mech.* **141**, 139-178.

Metcalfe, R. W., Orszag, S. A., Brachet, M. E., Menon, S. & Riley, J.J. 1987 Secondary instability of a temporally growing mixing layer. *J. Fluid Mech.* **184**, 207-243.

Miksad, R. W. 1972 Experiments on the nonlinear stages of free-shear-layer transition. *J. Fluid Mech.* **56**, 695-719.

Nygaard, K. J. 1987 Construction, instrumentation, and testing of a spanwise forced plane mixing layer facility. M.S. report, The University of Arizona.

Nygaard, K. J. & Glezer, A. 1989 On the spanwise structure of a plane mixing layer. In *Advances in Turbulence 2* (ed. H.-H. Fernholtz & H. E. Fiedler), pp. 461-466. Springer.

Nygaard, K. J. & Glezer, A. 1990 Core instability of the spanwise vortices in a plane mixing layer. *Phys. Fluids A* **2**, 461-464.

Nygaard, K. J. & Glezer, A. 1992 Phase excitation of a plane mixing layer. *J. Fluid Mech.* (to be submitted).

Oster, D. & Wygnanski, I. 1982 The forced mixing layer between parallel streams. *J. Fluid Mech.* **123**, 91-130.

Pierrehumbert, R. T. 1986 Universal short-wave instability of two-dimensional eddies in an inviscid fluid. *Phys. Rev. Lett.* **57**, 2157-2159.

Pierrehumbert, R. T. & Widnall, S. E. 1982 The two- and three-dimensional instabilities of a spatially periodic shear layer. *J. Fluid Mech.* **114**, 59-82.

Pullin, D. I. & Jacobs, P. A. 1986 Inviscid evolution of stretched vortex arrays. *J. Fluid Mech.* **171**, 377-406.

Riley, J. J., Mourad, P. D., Moser, R. D. & Rogers, M. M. 1988 Sensitivity of mixing layers to three-dimensional forcing. In *Center for Turbulence Research: Proceedings of Summer Program 1988*, pp. 91-116. Center for Turbulence Research, NASA Ames.

Roberts, F. A. 1985 Effects of a periodic disturbance on structure and mixing in turbulent shear layers and wakes. Ph.D. thesis, California Institute of Technology.

Rogers, M. M. & Moser, R. D. 1989 The development of three-dimensional temporally evolving mixing layers. In *Proceedings of Seventh Symposium on Turbulent Shear Flows, Stanford University*, pp. 9.3.1-9.3.6.

Roshko, A. 1981 "The plane mixing layer: flow visualization results and three-dimensional effects. In *The Role of Coherent Structures in Modelling Turbulence and Mixing, Lecture Notes in Physics* (ed. J. Jimenez), vol. 136, pp. 208-217. Springer.

Saric, W. S. & Thomas, A. S. W. 1983 Experiments on the subharmonic routes to turbulence in boundary layers. In *Turbulence and Chaotic Phenomena in Fluids: Proceedings of the International Symposium on Turbulence and Chaotic Phenomena in Fluids, Kyoto, Japan* (ed. T. Tatsumi), Elsevier.

Townsend, A. A. 1980 *The Structure of Turbulent Shear Flows*, 2nd ed. Cambridge University Press.

Weisbrot, I. 1984 A highly excited turbulent mixing layer. M.S. thesis, Tel Aviv University.

4. Phase Excitation of a Plane Shear Layer

4.1. *Introduction*

Experimental investigations of nominally *two-dimensional* plane shear layers suggest that substantial spanwise deformations of the primary vortices can result from relatively small disturbances in the free streams. Of particular note are the flow visualization photographs of Chandrsuda, Mehta, Weir & Bradshaw (1978), which show that spatially nonuniform entrainment into a single stream mixing layer can lead to spanwise-nonuniform pairing and branching of the primary vortices. Browand & Troutt (1980, 1985) used time series of instantaneous spanwise profiles of the streamwise velocity in a two-stream mixing layer to detect irregular spanwise patterns, which the authors described as vortex "terminations" or "branches." These patterns were attributed in a later paper (Browand & Ho 1987) to spanwise-nonuniform pairing interactions between adjacent primary vortices due to slight spanwise variations in the free-stream velocities. This and other experimental evidence (e.g., Keller, Ellzey, Pitz, Shephard & Daily, 1988; Delville, Bellin, Garem & Bonnet 1988) indicate that the characteristic spanwise wavelength of the deformations of the primary vortices is typically larger than the streamwise wavelength of the Kelvin-Helmholtz instability λ_{KH} of the base flow.

The evolution of the primary (spanwise) vortices in a plane mixing layer has been connected with the propagation and amplification of two-dimensional instability waves (e.g., Ho & Huerre 1984). The Strouhal number of the most-amplified wave corresponds to the natural frequency of the mixing layer, and the associated phase velocity is equal to the average velocity, U_c, of the two streams. This implies that even small spanwise variations in U_c can lead to significant spanwise phase distortions of the unstable wave train, and, as a result, to spanwise-nonuniform rollup and deformations of the ensuing primary vortices. Such deformations are clearly apparent in the flow visualization photographs of Lasheras & Choi (1988), which were taken in a shear layer having spanwise-nonuniform free-stream velocity distributions.

Core deformations of the primary vortices can apparently be effected by the introduction of time-dependent spanwise phase perturbations at the trailing edge of the flow partition. Browand & Prost-Domasky (1990) and Dallard & Browand (1992) used a spanwise array of speakers to excite two adjacent spanwise segments of a two-stream mixing layer with time-harmonic wave trains having slightly different frequencies. This excitation leads to the appearance of spanwise defects in time series of instantaneous spanwise profiles of the streamwise velocity that are similar to the unforced patterns previously observed by Browand & Troutt (1980, 1985). The defects first appear at spanwise positions corresponding to frequency discontinuities and are a precursor to the appearance of additional spanwise defects farther downstream. Because the two frequencies are very close ($f_2 = 1.1f_1$), the two spanwise segments of the excitation waveform may be thought of as two almost identical wave trains undergoing a slow time-periodic phase shift at their beat frequency ($0.1f_1$). Hence, it may be argued that defects appear (at the beat frequency) at spanwise positions of phase discontinuities of the excitation waveform.

It is important to recognize that the measurements of Browand and his co-workers were taken at a fixed cross-stream elevation near the outer edge of the mixing layer (Browand & Troutt 1980, 1985; Browand & Prost-Domasky 1990). Hence, ostensibly the defects are the footprints of three-dimensional vortical structures within the shear layer. Such structures were observed by Nygaard & Glezer (1990) in a preliminary investigation of the effect of spanwise-nonuniform phase excitation on the evolution of a two-stream shear layer. The excitation waveform was a time-harmonic wave train having a piecewise continuous spanwise-periodic phase distribution with a constant phase difference, $\Delta\Phi$. It was found that the primary vortices undergo spanwise deformation, the wavelength of which typically exceeds λ_{KH}, and induce secondary vortical structures, the shape and strength of which vary with $\Delta\Phi$. In particular, when $\Delta\Phi = 180^o$, the primary vortices and the induced secondary vortices appear to be of

comparable strength and diamond-shape vortex cells appear in the spanwise (x,z) plane of the mixing layer.

Spanwise instability modes of the shear layer that can lead to core deformations of the primary vortices have been studied analytically and numerically. In an analysis of a shear layer modeled by an array of Stuart vortices, Pierrehumbert & Widnall (1982) identified two such instability modes resulting from interaction of two oblique time-harmonic wave trains having equal amplitudes and opposite wave angles. The first mode, referred to as "translative instability," is spanwise and streamwise periodic. The authors conjectured that the translative instability can lead to the formation of streamwise vortices, which had been observed in the experiments of Breidenthal (1978). In a related study, Corcos & Lin (1984) showed that the rollup of spanwise vorticity into a streamwise-periodic array of vortices can give rise to a translative core instability, which allows spanwise perturbations to grow in such a way that all spanwise vortices are identically distorted. The second instability mode identified by Pierrehumbert & Widnall is subharmonic, can lead to spanwise-localized pairing of the primary vortices, and has a short spanwise wavelength cutoff, below which three-dimensional disturbances do not amplify. A similar instability was also observed in a numerical study by Meiburg (personal communication, 1990).

In numerical simulations of a temporally evolving mixing layer, Comte & Lesieur (1990) investigated the evolution of the subharmonic instability and the topology of the streamwise vortices. They found that the introduction of small, random three-dimensional isotropic disturbances can lead to spanwise-nonuniform pairing of the primary vortices with a characteristic spanwise wavelength that is four times greater than the streamwise wavelength of the Kelvin-Helmholtz instability. The addition of two-dimensional disturbances leads to suppression of spanwise-nonuniform pairing, an in-phase waviness of the primary vortices, and the formation of streamwise vortices in the braid region.

That deformations of the primary vortices are an important ingredient in the evolution of the flow, even at high speeds, is demonstrated by the direct numerical simulations of a compressible mixing layer by Sandham & Reynolds (1991). Using random noise as the initial condition, the authors found that oblique waves (which lead to the formation of oblique primary vortices) are the most rapidly amplified instabilities for convective Mach numbers $M_c > 0.6$. [While we are unaware of any other previous experiments in which a plane shear layer was forced with a time-harmonic oblique wave train, the low-speed experiments of Roos, Kegelman & Kibens (1989) in a shear layer facility having a flow partition with a swept trailing edge clearly demonstrate the receptivity of the flow to oblique disturbances.] Sandham & Reynolds further propose that the nonlinear development of a single oblique wave and pairs of equal and opposite oblique waves leads to the formation of oblique vortices and pairs of staggered Λ vortices, respectively.

The numerical and analytical investigations cited above clearly suggest that the plane shear layer is receptive to time-harmonic excitation having spanwise nonuniform phase distribution, while experimental evidence suggests that spanwise phase distortion of two-dimensional instability modes can have dramatic effects on the rollup and evolution of the primary vortices. The present work builds on these findings and focuses on the evolution of three-dimensional vortical structures resulting from spanwise phase nonuniformities of the fundamental and subharmonic instabilities of the base flow.

As discussed above, experimental observations suggest that phase distortions of the nominally two-dimensional instability modes in a plane shear layer can lead to significant distortions of the ensuing primary and secondary vortical structures. In most of these investigations, phase distortions resulted from uncontrollable and unknown disturbances in the free streams. Controlled excitation of phase disturbances has been limited to time-periodic phase distortions by means of spanwise variations of the forcing

frequency (Browand & Troutt 1980, 1985; Browand & Prost-Domasky 1990) and to passive excitation of oblique instability modes by means of geometrical alterations in the flow partition (Roos *et al.* 1989). The present investigation focuses on the effect of controlled phase excitation on the evolution of the primary and secondary vortices. In most of the experiments described below, the free-stream velocities are 30 and 10 cm/sec and the excitation frequency is $\nu_f = 5$ Hz.

4.2. *Phase Excitation Using Surface Heaters*

Due to the quadratic dependence of Joulean dissipation on input voltage to the heaters, the spanwise distribution of input excitation power is given by

$$E(z,t) = E_0(z)\{1 + \cos[\omega_f(z)t + \Phi(z)]\} ,$$

where $E_0(z)$ is the mean power, $\nu_f(z) = \omega_f(z)/2\pi$ is the spanwise distribution of excitation frequency, and $\Phi(z)$ is the spanwise phase distribution. The linear heater array described in §2.1 is used to synthesize a 32-element discretization of $E(z,t)$, where $E_0(z)$, $\omega(z)$, and $\Phi(z)$ are, in principle, arbitrary and can be programmed from the laboratory computer. In the experiments of Nygaard & Glezer (1991), $E_0(z)$ was piecewise constant and spanwise periodic, and ν_f and Φ were constant. We note that spanwise-amplitude modulation of the excitation wave train does not distort its spanwise phase. In what follows, time-invariant phase excitation at a fixed ν_f is effected by spanwise-linear and spanwise-periodic piecewise-constant phase distributions $\Phi_l(z)$ and $\Phi_{sp}(z)$, respectively. The spanwise-linear phase distribution $\Phi_l(z) = \beta z$ results in a time-harmonic oblique wave having a spanwise wave number β. In the present experiments, $\beta \leq 0.87$ cm^{-1}, corresponding to phase increments $\Delta\Phi_l \leq 6\pi/32$ between adjacent heaters. Spanwise-linear phase distributions were used by Robey (1987) and Schneider (1989) in experimental investigations of oblique waves in a flat-plate boundary layer.

To define $\Phi_{sp}(z)$, we let $z = z_0+\lambda_z s$, where z_0 is an arbitrary reference, λ_z is the spanwise wavelength, and $0 \le s \le 1$. Then, in each wavelength, $\Phi_{sp}(z)$ is given by $\Phi_{sp} = 0$ for $0 \le s \le s_1$ and $s_2 \le s \le 1$ (where $s_1 < s_2$), and $\Phi_{sp} = \Delta\Phi$ for $s_1 \le s \le s_2$. In the present experiments, λ_z is taken to be the width of 2, 4, 8, and 16 elements of the linear heating array, $s_2-s_1 = 0.5$, and $0 \le \Delta\Phi \le \pi$. With $\Phi(z) = \Phi_{sp}(z)$, $E(z,t)$ can be expanded in Fourier series,

$$E(z,t) = E_0[1 + e(z,t)] ,$$

where

$$e(z,t) = \cos\left[\frac{\Delta\Phi}{2}\right]\cos\left[\omega_f t + \frac{\Delta\Phi}{2}\right] + \sin\left[\frac{\Delta\Phi}{2}\right]\sin\left[\omega_f t + \frac{\Delta\Phi}{2}\right]\sum_{n=1}^{\infty}\left[\frac{4}{2n-1}\right]\sin\frac{2(2n-1)\pi z}{\lambda_z} .$$

Thus, for a given $\Delta\Phi$, $E(z,t)$ is a linear superposition of a time-harmonic spanwise-uniform wave train and pairs of equal and opposite oblique waves having spanwise wave numbers $\beta_n = (2n-1)2\pi/\lambda_z$. The amplitudes of the spanwise-uniform and oblique wave trains are proportional to $\cos(\Delta\Phi/2)$ and $\sin(\Delta\Phi/2)$, respectively (the amplitudes of the oblique waves also decrease like $1/n$). Hence, when $\Delta\Phi = 0$, $E(z,t)$ is a spanwise uniform wave train and, when $\Delta\Phi = \pi$, $E(z,t)$ is a superposition of pairs of equal and opposite oblique waves only.

We note that $\Phi_{sp}(z)$ was chosen because, unlike continuously differentiable waveforms (e.g., a sinusoidal distribution), $E(z,t)$ can be easily discretized by the heater array for any λ_z that is equal to the width of an integer number of heating elements. Furthermore, as shown in §3.3, when $\Delta\Phi = \pi$, there exists a short wavelength cutoff, λ_{crit}, below which $E(z,t)$ is not amplified. Thus, it may be argued that there is a corresponding cutoff spanwise wave number, β_{crit}, such that pairs of equal and opposite oblique waves are attenuated when $\beta_n > \beta_{crit}$. Hence, for small λ_z, $E(z,t)$ is effectively a linear superposition of a two-dimensional wave train and a single pair of oblique waves, all at the same (excitation) frequency.

The response of the flow to phase excitation close to the trailing edge of the flow partition is shown in time plots of ensemble-averaged spanwise distributions of the streamwise velocity perturbation, $\langle u_{pert}(z,t)\rangle$ (figure 4.1). [The ensemble-averaged streamwise velocity, $\langle u(x,t)\rangle$, is phase-locked to E(z,t) and $\langle u_{pert}(x,t)\rangle = \langle u(x,t\rangle - U(x)$, where U(x) is the mean flow velocity.] These data are measured at x = 5.1 cm and $y = y_0$ [y_0 is the cross-stream elevation where $U(x) = U_c = (U_1+U_2)/2$]. In figure 4.1, the origins of successive profiles are equally displaced in time, producing z-t maps that capture spanwise features of the forced flow before the rollup of the primary vortices is completed. The centers of the dark bands correspond to extrema of $\langle u_{pert}(z,t)\rangle$.

When the excitation waveform is spanwise-uniform (figure 4.1*a*), the flow appears to be reasonably two dimensional. It is noted that the dark bands in the z-t maps have been associated by Browand and his coworkers with the passage of the primary vortices (Browand & Troutt 1980, 1985; Browand & Prost-Domasky 1990). In figure 4.1(*b*), $\Phi(z)$ is spanwise-linear, $\Phi_l(z) = \beta z$, where $\beta = 0.571$ rad/cm, and it clearly results in spanwise-oblique phase distribution of $\langle u_{pert}(z,t)\rangle$. Furthermore, the dark bands in the z-t map suggest the rollup of oblique primary vortices. In figure 4.1(*c*), $\Phi(z) = \Phi_{sp}(z)$ and $\lambda_z = 7.62$ cm is the width of 12 heating elements such that $\Delta\Phi = \pi$ at the center 6 elements. As discussed above, this excitation waveform corresponds a family of equal and opposite oblique waves, and it leads to spanwise-periodic phase discontinuities of $\langle u_{pert}(z,t)\rangle$ at the excitation wavelength, λ_z. The z-t maps suggest that the rollup of the primary vortices occurs in spanwise segments of constant phase.

4.3. *Spanwise-Linear Phase Excitation*

The effect of a spanwise-linear phase distribution, $\Phi_l = \beta(z-z_0)$ (where z_0 is an arbitrary reference), is studied using flow visualization. The resulting excitation waveform is a time-harmonic oblique wave train having streamwise and spanwise wave numbers, $\alpha = 2\pi\nu_f/U_c$ and β. In the present experiments, $\alpha \cong 1.57$ cm^{-1}, and the

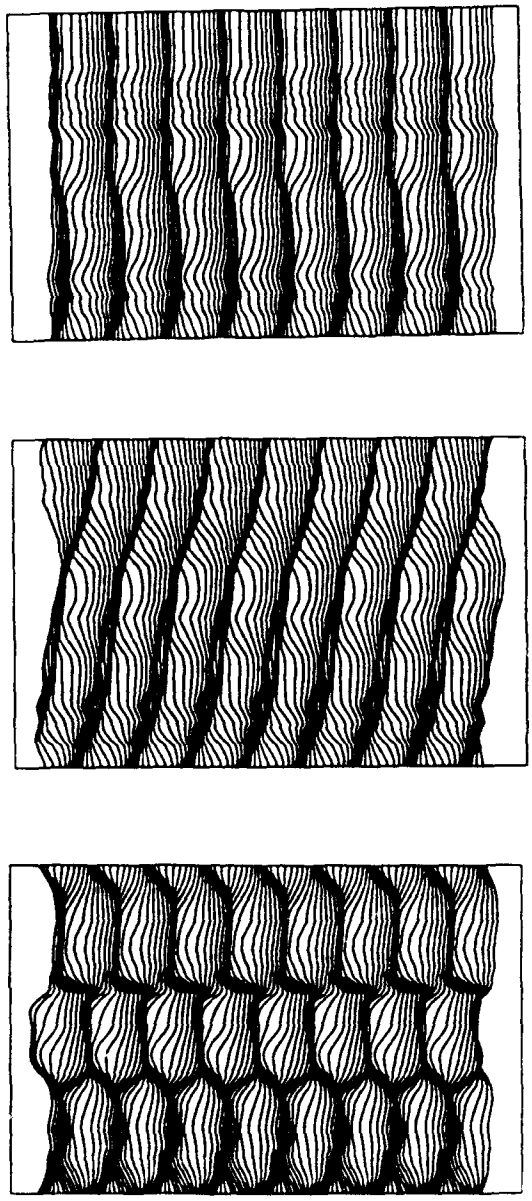

Figure 4.1

response of the flow to excitation with β = 0.29, 0.58, and 0.87 cm^{-1} is shown in figures 4.2(*a*), (*b*), and (*c*), respectively. The corresponding wave angles, ψ = arctg(β/α), between the wave vectors and the streamwise direction are 10°, 20°, and 29°. It is important to recognize that, unlike excitation of two-dimensional waves, the excitation of oblique waves in a flat-plate boundary layer gives rise to a three-dimensional vorticity perturbation field with important consequences for the evolution of the excited flow (Hama, Rist, Konzelman, Laurien & Meyer 1987; Robey 1987).

The most striking feature in figure 4.2 is the formation of primary vortices that are oblique in the spanwise (x,z) plane of the shear layer and are advected in the streamwise direction. The angles between the oblique vortices and the streamwise direction are virtually identical to the corresponding wave angles of the excitation wave trains and remain almost invariant throughout the streamwise domain shown here. (Successive primary vortices downstream from the flow partition are referred to below as V_1, V_2, V_3, etc.) As can be seen on the left-hand side of each photograph, the rollup of V_1 occurs along lines of constant phase of the excitation wave train. The rollup clearly does not occur simultaneously along the axis of each vortex, as for the two-dimensional case, but progresses obliquely (along a line of constant phase) as the vortex is advected downstream.

It is apparent from the present and other flow visualization photographs that the rollup at any position along the axes of V_1 in figure 4.2 starts at the same streamwise station, $x = x_r$. Furthermore, because x_r is approximately the same in each of figures 4.2(*a-c*), it may be concluded that spatial amplification of all oblique waves over the range of spanwise wave numbers considered here is almost identical. When β exceeds 0.87 cm^{-1}, we have observed that the flow is no longer locked to the excitation wave train and a streamwise-regular pattern of oblique vortices no longer exists. This does not necessarily imply that, for $\beta > 0.87$ cm^{-1}, oblique waves are not amplified in the plane shear layer because, in the present experiments, the receptivity of the flow

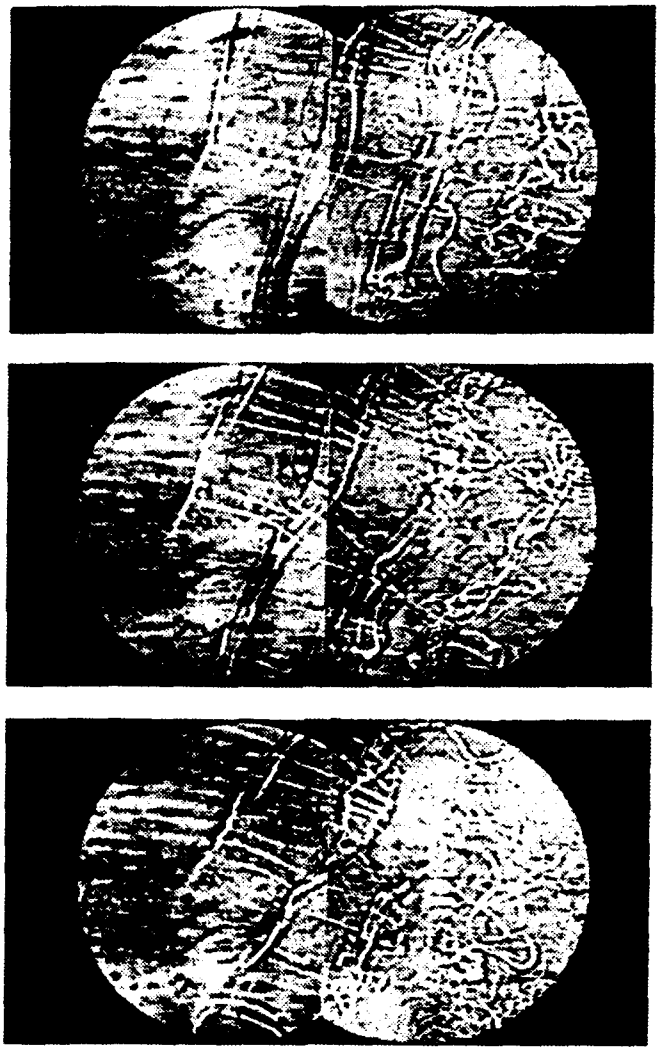

Figure 4.2

partition's boundary layers is inherently coupled to that of the ensuing shear layer. The results of Schneider (1989) indicate that the amplitude of oblique waves in a flat-plate (Blasius) boundary layer measured at a streamwise position corresponding to $Re_{\delta^*} = 1300$ is almost invariant for $\psi < 15°$, and decreases by an order of magnitude for $15° < \psi < 25°$.

The streamwise inclination of the primary vortices is apparently accompanied by a change in the direction of the strain field in the braid region between them, compared to the two-dimensional case. As a result, secondary vortices that are formed in the braid region are approximately aligned with the wave vector of the excitation wave train. High-speed photography has shown that the rotation of these secondary vortices is counter-clockwise when observed in the y-z plane in the downstream direction (we shall comment on that below). We note that, in the absence of phase excitation, virtually no secondary vortices appear in the braid region between V_1 and V_2 (see figure 2.6*b*). However, as β is increased, secondary vortices in the braid region between V_1 and V_2 become more pronounced (cf, for example, figures 4.2*a* and *b*). These vortices are clearly associated with the rollup of V_1 in that they spread in the braid region as the rollup of V_1 progresses. While the amplitude of $E(z,t)$ is spanwise-uniform, spanwise phase discontinuities $\Delta\Phi_1 = 0.68\beta$ having a characteristic length scale equal to the width of one heating element ($\lambda_H = 6.3$ mm) are introduced due to the 32-element discretization of Φ_1. Although the secondary vortices are formed only *after* the rollup of V_1, they are clearly triggered by $\Delta\Phi_1$, as is evident from their spanwise spacings and apparent strength.

The orientation of the secondary vortices is extremely sensitive to deformations along the axes of the primary vortices, as is evident in the braid regions between V_2 and V_3 in figures 4.2(*b*,*c*). The primary vortices appear to be more susceptible to such deformations as β is increased. The characteristic wavelength of these deformations is longer than the streamwise wavelength of the Kelvin-Helmholtz instability. When

$\beta = 0.87$ (figure 4.2*c*), the primary vortex at the downstream edge of the Schlieren view exhibits a bifurcation that is also apparent in the photograph of Chandrsuda *et al.* (their figure 3). Similar bifurcations can be also be inferred from the data of Browand & Prost-Domasky (1990) and were also observed by Nygaard & Glezer (1990) as a result of spanwise-nonuniform phase excitation. As will be shown in the following subsections, such deformations can arise due to interactions between spanwise-uniform and oblique instability waves.

In connection with the appearance of the secondary vortices in the braid region, we consider the temporal evolution of a train of oblique vortices resulting from excitation by an oblique wave train in an unbound, two-stream, two-dimensional shear layer. If $\tilde{y}$ is the cross-stream coordinate, $\tilde{x}$ is parallel to the wave vector of the excitation wave train (which is normal to $\tilde{y}$) and $\tilde{z}$ is normal to the $\tilde{x}$-$\tilde{y}$ plane (i.e., parallel to the axes of the oblique vortices). Then, as shown by Crow (private communication, 1992), the velocity and vorticity components in the $\tilde{z}$-direction, $\tilde{w}$ and $\tilde{\zeta}$, are given by

$$\frac{D\tilde{w}}{Dt} = \frac{\partial \tilde{w}}{\partial t} + \mathbf{u}\cdot\nabla\tilde{w} = \nu\left[\frac{\partial^2 \tilde{w}}{\partial \tilde{x}^2} + \frac{\partial^2 \tilde{w}}{\partial \tilde{y}^2}\right]$$

and

$$\frac{D\tilde{\zeta}}{Dt} = \frac{\partial \tilde{\zeta}}{\partial t} + \mathbf{u}\cdot\nabla\tilde{\zeta} = \nu\left[\frac{\partial^2 \tilde{\zeta}}{\partial \tilde{x}^2} + \frac{\partial^2 \tilde{\zeta}}{\partial \tilde{y}^2}\right],$$

respectively. These equations imply that, in the absence of viscosity, the $\tilde{z}$ velocity and vorticity components of fluid elements within the primary vortices and in the braid region remain unchanged. Because the oblique vortices are advected in a shearing flow, their induced velocity field acts to move high-speed (or low-speed) fluid down (or up) from higher (or lower) cross-stream elevations toward the braid region. The streamwise velocity of the fluid that is moved from the free streams has components in the $\tilde{z}$- and $\tilde{x}$-directions. Figure 4.2 suggests that shear flow in the $\tilde{z}$-direction owing to

the difference in $\tilde{w}$ across the braid region leads to rollup of secondary vortices in the braid region, all of which have the same sense of rotation (counter-clockwise in the $\tilde{y}$-$\tilde{z}$ plane viewed in the positive $\tilde{x}$-direction). These vortices are aligned and stretched by the strain field in the braid region, which is dominated by the velocity components in the $\tilde{x}$-$\tilde{y}$ plane.

4.4. *Time-Periodic Spanwise Phase Excitation*

As discussed in §4.2, when $\Phi = \Phi_{sp}$, $E(z,t)$ is a linear superposition of a time-harmonic spanwise-uniform wave train and pairs of equal and opposite oblique waves having spanwise wave numbers $\beta_n = (2n-1)2\pi/\lambda_z$. Recall that when $\Delta\Phi = 0$, $E(z,t)$ is a spanwise uniform wave train and, when $\Delta\Phi = \pi$, $E(z,t)$ is a superposition of the pairs of oblique waves only. In this subsection, we discuss the effect of the magnitude of $\Delta\Phi$ on the evolution of the flow. The magnitude of $\Delta\Phi$ varies in time when, similarly to $\Phi_{sp}(z)$, the excitation frequency, $\omega_f(z) = 2\pi\nu_f$, is spanwise periodic (with wavelength λ_z) and piecewise constant. If the spanwise frequency variation is $\Delta\omega = \omega_f^2 - \omega_f^1$, where ω_f^1 and ω_f^2 are the two (piecewise-constant) frequencies of adjacent segments of the excitation waveform, then the corresponding phase difference is $\Delta\Phi = (\omega_f^1 - \omega_f^2)t$. When $\Delta\omega$ is small, $\Delta\Phi$ is slowly varying with time between 0 and 2π over the beat period $T_b = 2\pi/\Delta\omega$. In what follows, $\lambda_z = 7.6$ cm ($\beta_1 = 0.82$ cm^{-1}). Schlieren photography and velocity measurements are taken phase-locked to $\Delta\omega$. Phase-locking is accomplished by a conditional trigger derived by a logical "AND" of two pulse trains corresponding to zero-crossings with positive slope of two adjacent segments of the excitation wave trains. The resulting pulse train has a frequency $\Delta\omega$ and can be time-delayed to achieve a desired phase relative to the data-acquisition clock.

The effect of excitation with $\nu_f^1 = 4.9$ Hz and $\nu_f^2 = 5.0$ Hz is shown in figure 4.3, which is a sequence of composite Schlieren photographs taken in the x-z plane at six equal time intervals centered around $t = T_b/2$ that corresponds to $\Delta\Phi = \pi$ (figure 4.3*d*).

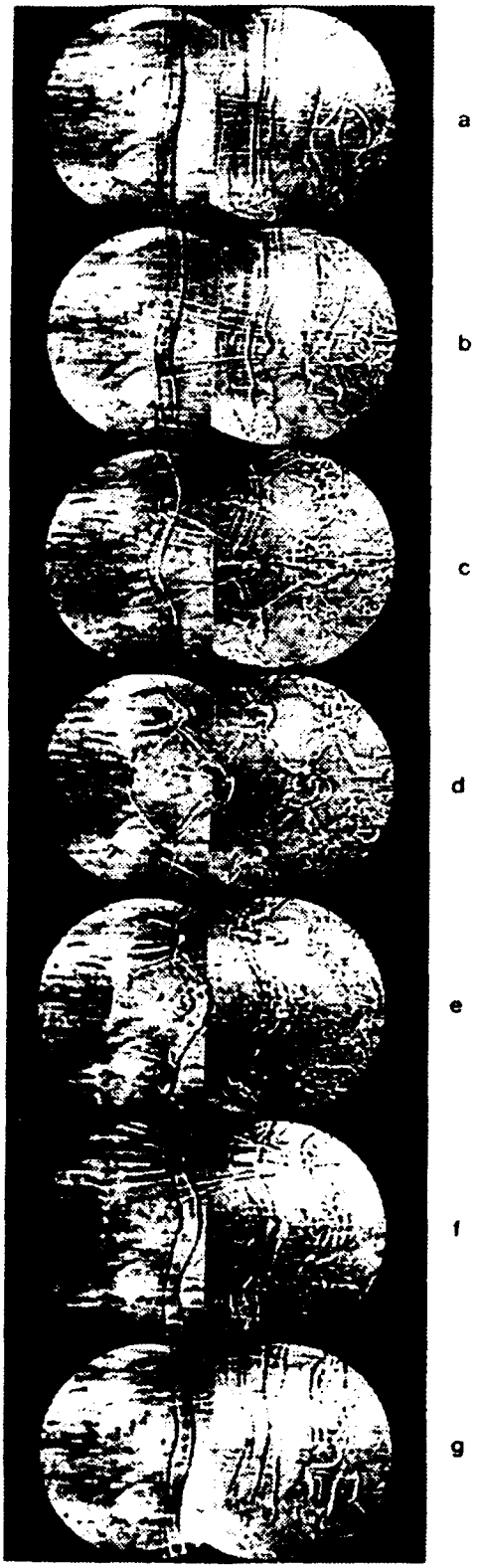

Figure 4.3

The spanwise phase increments, $\Delta\Phi$, of figures 4.3(*a-g*) are 0.16π, 0.44π, 0.72π, π, 1.28π, 1.56π, and 1.84π, respectively. The spanwise field of view is approximately $1.5\lambda_z$, and the frequency of the center segment is 4.9 Hz. At a given time, say $t = t_0$, the wave fronts of all segments of the spanwise excitation waveform are in phase. Because the frequency of the center segment is slightly lower than the frequencies of the outer segments, the excitation waveform at the center segment begins to develop a phase-lag with respect to the excitation waveforms of the outer segments when $t > t_0$. As a result, adjacent spanwise segments of the primary vortices, which are phase-locked to spanwise segments of the excitation waveform having different frequencies, develop spanwise-periodic distortions. These distortions are the result of spanwise-nonuniform rollup of the primary vortices, which (as shown in §3.1) is sensitive to spanwise phase variations in the excitation wave train. We note that, since ν_f^1 and ν_f^2 are very close, it may be assumed that the streamwise amplification of adjacent segments of the excitation wave train are virtually identical.

In figure 4.3(*a*), the spanwise phase increments are relatively small and the primary vortices are almost two dimensional. Deformations of the primary vortices that are symmetric about the midspan are more evident in figure 4.3(*b*). The undulations of the primary vortices persist and even appear to intensify with downstream distance (figure 4.3*c*). Because primary vortices in an unforced plane mixing layer are advected in a nominally two-dimensional strain field and presumably deform in a plane that is aligned with the direction of maximum strain, the amplitude of the deformation can increase with downstream distance. There is a striking similarity between the spanwise vortices in figures 4.3(*b,c*) and the translatively unstable Stuart vortices studied by Pierrehumbert & Widnall (1982). Their results suggest that the most unstable translative disturbance has a spanwise wavelength that is equal to two-thirds of the spacing of the undisturbed vortices, although disturbances having a broad band of spanwise wavelengths can be amplified. Pierrehumbert & Widnall also argued that the

translative instability can lead to the formation of secondary ("streamwise") vortices in the braid region between adjacent primary vortices. Figure 4.3 clearly shows the formation of secondary vortices when the primary vortices distort along their axes.

The secondary streamwise vortices form in the braid region near maxima of the spanwise curvature of the primary vortices. Although these secondary vortices are similar in appearance to streamwise vortices that can be triggered by spanwise-nonuniform amplitude excitation as discussed in §3, there is a considerable difference in the spanwise widths of the secondary vortices that result from the two different excitation waveforms. While the spanwise widths of the former scale with the deformation of the primary vortices, the spanwise widths of the latter (in the absence of core deformations of the primary vortices) are significantly smaller (see figures 3.3*c,d*). It is clear that spanwise deformations of the primary vortices increase with $\Delta\Phi$ (figure 4.3*c*) and the induced streamwise vortices become considerably more pronounced.

When $\Delta\Phi = \pi$ (figure 4.3*d*), the flow is forced by pairs of oblique waves of equal magnitude and opposite angle (without the presence of the two-dimensional excitation wave train), and the structure of the primary vortices as viewed in the x-z plane is drastically altered. The x-z projection of these vortical structures is comprised of a pattern of diamond-shaped cells ("chain-link"-like structure) that repeat in the spanwise and streamwise directions. Similar structures are also apparent in numerical simulations of compressible and incompressible mixing layers that are forced by a pair of oblique waves at the fundamental frequency (Sandham & Reynolds 1991; Collis, Lele, Moser & Roger 1991). As will be shown below, these vortical structures are primary vortices having spanwise-periodic deformations in planes that are tilted around the z-axis relative to the streamwise direction. The spanwise deformations of adjacent primary vortices are 180° out-of-phase along the z-axis, thus forming the diamond-shaped pattern in the x-z view. The deformed primary vortices may undergo pairing at spanwise locations corresponding to streamwise edges of the diamond-shaped cells. Of

particular note is the fact that the number of primary vortices is actually *doubled*, and their passage frequency is equal to *twice* the forcing frequency. The streamwise length of each cell, measured between its streamwise edges, is equal to λ_{KH} of the two-dimensionally forced flow.

As mentioned in §4.1, the second spanwise instability mode identified by Pierrehumbert & Widnall (1982) corresponds to spanwise-localized pairing of the primary vortices. This instability mode has a streamwise wavelength that is *twice* that of the two-dimensional base flow and, in contrast to the translative instability, has a short spanwise wavelength cutoff. There is no question that the core deformation corresponding to $\Delta\Phi = \pi$ is essentially similar to the pairing instability of Pierrehumbert & Widnall, even though the streamwise wavelength in the present experiments is λ_{KH}. Similar to results of Pierrehumbert & Widnall, the next subsection confirms that core deformation of the spanwise vortices can only be excited if the spanwise forcing wavelength exceeds a short wavelength cutoff.

When $\Delta\Phi > \pi$, the secondary vortical structures weaken and become pairs of hairpin-like counter-rotating vortices (figures 4.3*e-f*). Because the wave train in the center segment is now leading in phase relative to its adjacent segments, the center segment of the primary vortex is symmetrically bent around midspan in the downstream direction. The secondary vortices appear near upstream bends corresponding to the outer segments, and they are displaced in the spanwise direction by $\lambda_z/2$ compared to secondary vortices resulting from phase excitation with $\Delta\Phi < \pi$ (cf. figure 4.3*c*). Similar to figures 4.3(*b,c*), this instability of the primary vortices in figures 4.3(*e,f*) appears to be "translative" in the parlance of Pierrehumbert & Widnall (1982). Finally, as $\Delta\Phi$ approaches 2π (figure 4.3*g*), the spanwise vortices become almost two dimensional again.

We note in passing that the evolution of vortical structures in a plane mixing layer is extremely sensitive to the spanwise distribution of $\Phi(z)$. For example, when $\Phi(z)$ is

not spanwise-periodic but has a spanwise hat-shaped phase discontinuity with $\Delta\Phi = \pi$ in the center segment of the excitation waveform, each of the ensuing primary vortices bifurcates into upstream and downstream branches that form a closed diamond-shaped vortical cell (Nygaard & Glezer 1990).

Some features of the phase-averaged three-dimensional vortical structures are obtained from measurements of the streamwise velocity component in the y-z plane at x = 10.2 cm (the domain of measurements is rectangular, measuring 6 cm × 8.9 cm). The free-stream velocities for these measurements are 36 and 12 cm/sec, ν_f^1 = 6.9 Hz, ν_f^2 = 7.0 Hz, and λ_z = 7.6 cm. Time series of the streamwise velocity component are measured phase-locked to the beat frequency $\Delta\nu_b$ = 0.1 Hz, such that each data record includes 4480 measurements equally spaced over the beat period. Ensemble-averaged data are calculated from 40 such data records. The vortical structures are distinguished by concentrations of high-frequency turbulent fluctuations of the streamwise velocity component, $\langle u'_{trms}(\mathbf{x},t)\rangle$, which is calculated following the procedure of Nygaard (1991).

Figure 4.4 shows the surfaces $\langle u'_{trms}\rangle$ = 1.0 cm/sec in the y-z-t coordinates during two consecutive periods of the excitation wave train (ν_f^2 = 7 Hz). The spanwise phase amplitudes, $\Delta\Phi$, at the starting time of each of figures 4.4(*b-d*) are chosen so that these figures correspond approximately to figures 4.3(*c-e*). Note that because time increases to the left, the flow appears to be moving to the right. In figure 4.4(*a*), $\Delta\Phi \cong 0$ and the excitation wave train and the primary vortices are nominally spanwise uniform. Figures 4.4(*b-d*) clearly show the evolution of the secondary vortical structures. Of particular note is what appears to be spanwise-localized pairing of the distorted spanwise vortices when $\Delta\Phi = \pi$. One may also conclude that the spanwise vortices are distorted in planes that are inclined relative to the streamwise direction.

Figure 4.5 is a time series of phase-averaged spanwise profiles of ensemble-averaged spanwise distributions of the streamwise velocity perturbation $\langle u_{pert}(z,t)\rangle$ measured phase-locked to $\Delta\nu_b$ and plotted during one beat period (10 sec) of the two

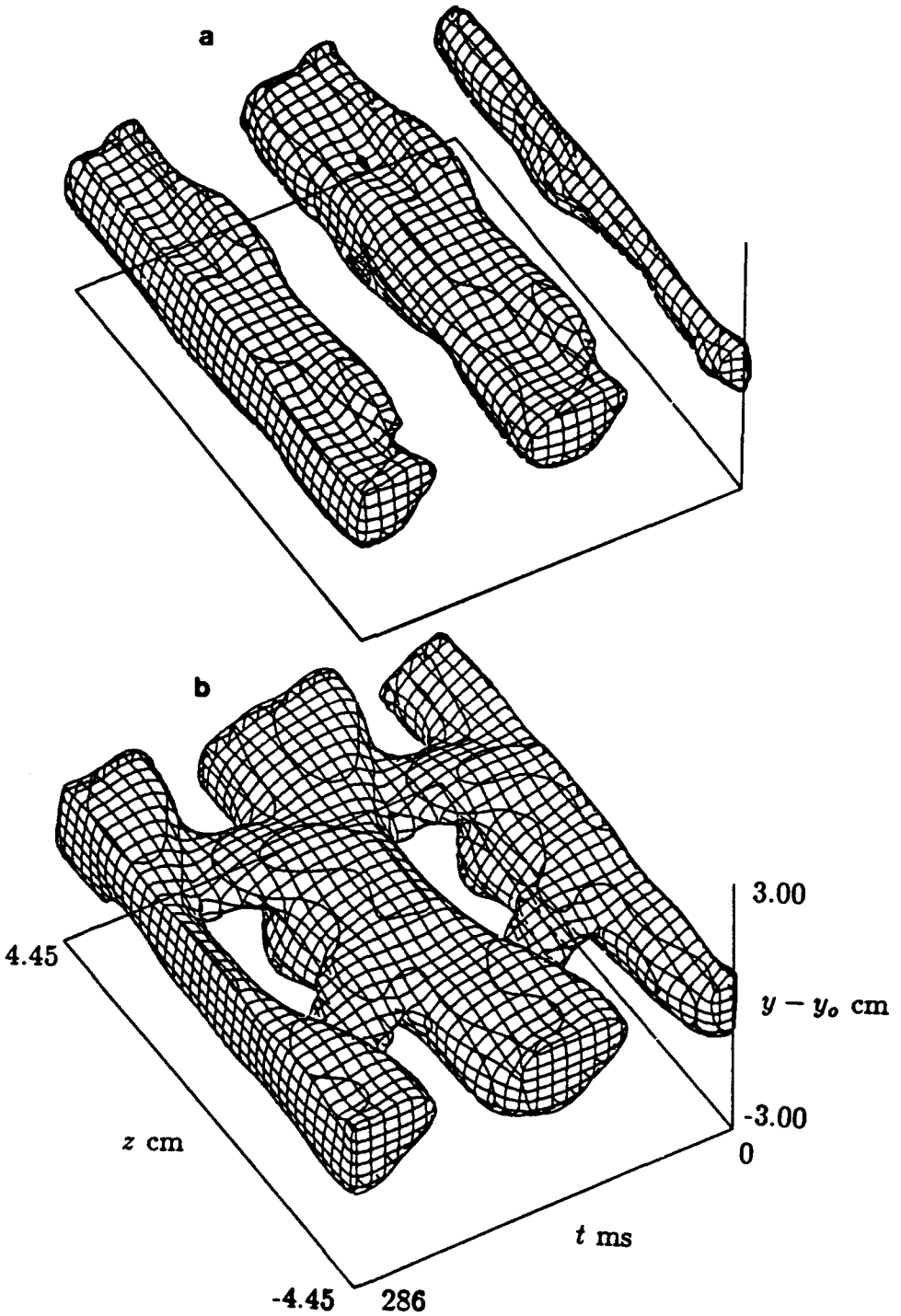

Figure 4.4(*a-b*)

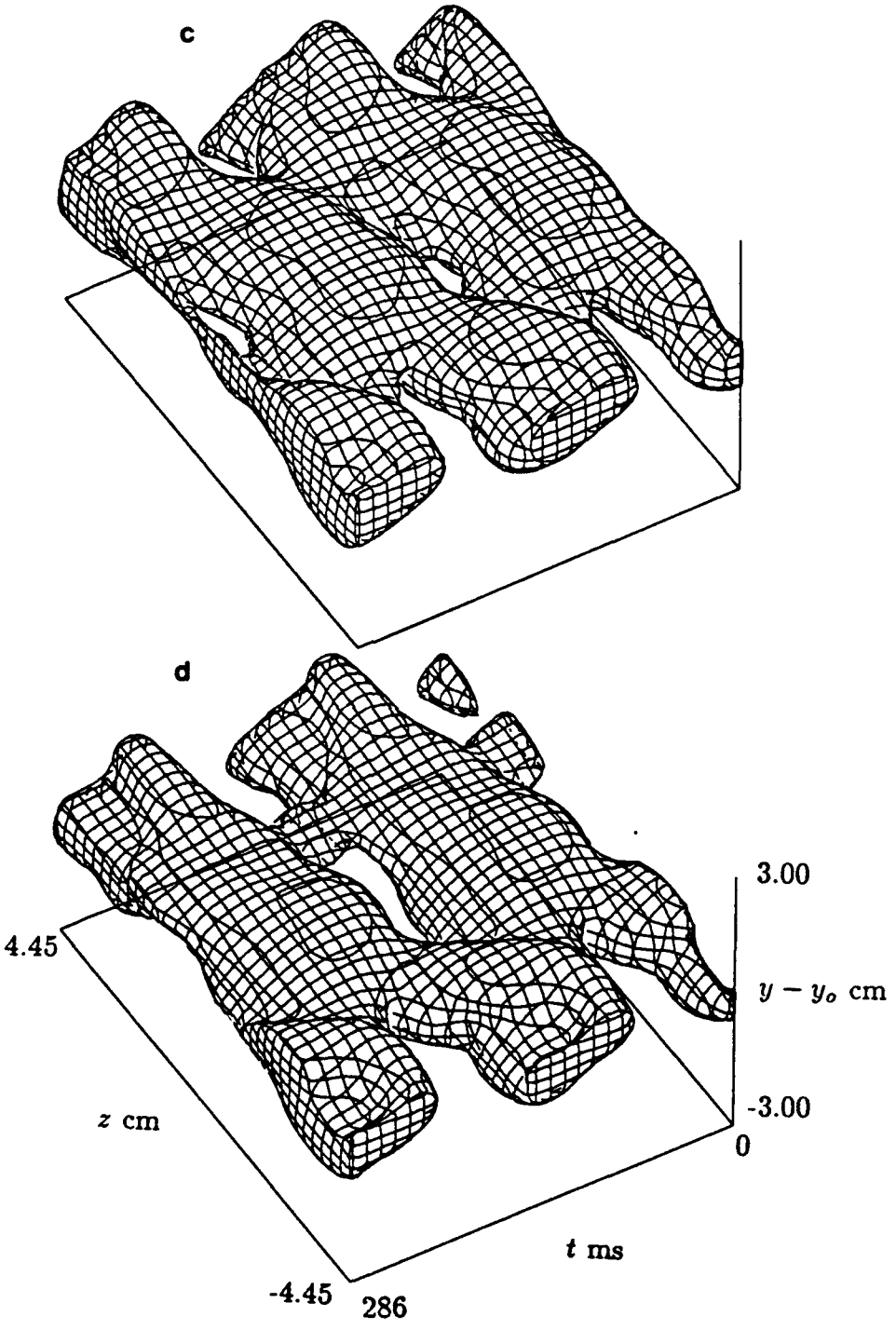

Figure 4.4(*c-d*)

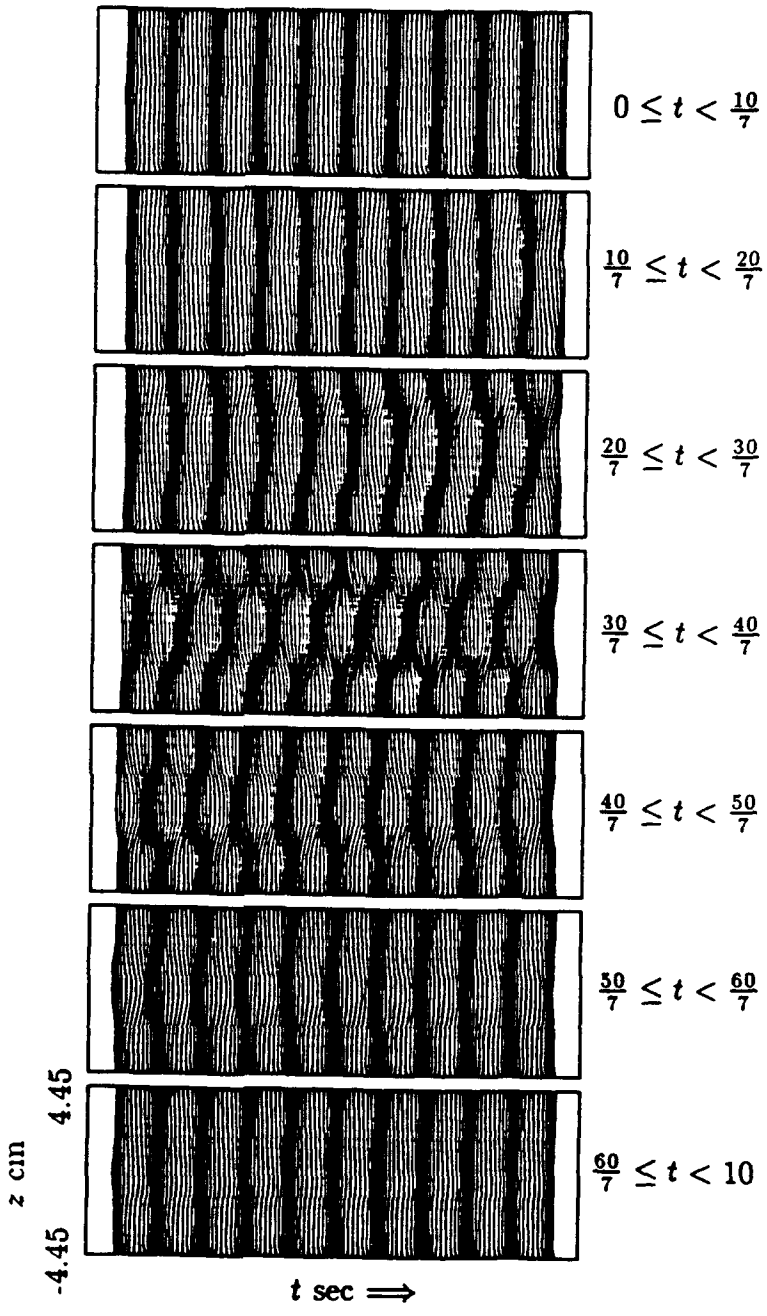
$0 \leq t < \frac{10}{7}$
$\frac{10}{7} \leq t < \frac{20}{7}$
$\frac{20}{7} \leq t < \frac{30}{7}$
$\frac{30}{7} \leq t < \frac{40}{7}$
$\frac{40}{7} \leq t < \frac{50}{7}$
$\frac{50}{7} \leq t < \frac{60}{7}$
$\frac{60}{7} \leq t < 10$
4.45
z cm
-4.45
t sec ⟹

Figure 4.5

excitation wave trains. These data are measured at x = 10.2 cm and at a y-elevation corresponding to a spanwise- and time-averaged streamwise velocity of 30 cm/sec. These types of plots have been used by Browand and his coworkers to capture spanwise features of the primary vortices, which appear as dark bands (Browand & Troutt 1980, 1985; Browand & Prost-Domasky 1990). At $t = t_0$, the flow is nominally two dimensional. As $\Delta\Phi$ increases, the primary vortices begin to develop spanwise undulations of wavelength λ_z. Note that because time increases from left to right, the bend in the center segment of the spanwise vortex points to the right. The effect of the secondary vortices that are apparent in figures 4.3(*b*,*c*) is not felt at this cross-stream elevation until their strength becomes comparable with the primary vortices ($t-t_0 > 3$ sec). When $t-t_0 = 5$ sec ($\Delta\Phi = \pi$), it is not possible to distinguish between the "secondary" and "primary" vortices, and a spanwise-cellular vortex structure emerges. The center segment appears to be "dislocated" ("vortex termination" in the parlance of Browand & Troutt) from the outer segments. It is important to recognize, however, that these data are a cross-section of three-dimensional flow structures at a fixed cross-stream elevation. When $\Delta\Phi > \pi$, the secondary vortical structures weaken (as can be asserted by their induced velocity perturbations) and the spanwise undulations of the primary vortices are essentially out-of-phase with respect to the undulations for $\Delta\Phi < \pi$. Although $\Delta\Phi$ varies linearly in time, the spanwise response of the flow as shown in figure 4.5 is not exactly symmetric in time with respect to the instant when $\Delta\Phi = \pi$. This is probably the result of spanwise phase distortion already present in the nominally two-dimensional base flow (cf. figure 2.6*b*). These data, along with the data of figure 4.4, demonstrate that the "dislocations," observed in figure 4.5 and in the work of Browand and his coworkers, are clearly connected with a three-dimensional flow structure.

4.5. *Receptivity to Excitation Wavelength*

In this subsection, we discuss the effect of the wavelength of Φ_{sp} on the evolution of primary vortices and, in particular, the existence of a short-wavelength cutoff, below which the spanwise vortices appear to be stable to spanwise-periodic phase excitation. Recall that core deformations of the primary vortices in unforced mixing layers appear to be have a characteristic spanwise wavelength, λ_c, which exceeds λ_{KH}. In the present experiments, $\Delta\Phi$ is time-invariant ($\Delta\Phi = \pi$) and λ_z is varied by the equivalent width of two heating elements.

Figures 4.6(*a-i*) are Schlieren photographs in the x-z plane (10 cm < x < 18.0 cm) where $U_1 = 30$ cm/sec, $U_2 = 10$ cm/sec, $\nu_f = 5$ Hz, and $\lambda_{KH} = 4$ cm. The spanwise excitation wavelengths in figures 4.6(*b-i*) decrease from 10.26 cm to 1.27 cm in increments of 1.27 cm. The response to spanwise-uniform excitation is shown for reference in figure 4.6(*a*). When $\lambda_z > 5.08$ cm $> \lambda_{KH}$ (figures 4.6*b-f*), the primary vortices are deformed and diamond-shaped cells appear in the x-z planview. The spanwise width of each cell is approximately equal to λ_z. When $\lambda_z < \lambda_{KH}$ (figures 4.6*g-i*), the primary vortices become almost spanwise-uniform. These results indicate that there is a critical spanwise excitation wavelength, λ_{crit}, below which spanwise phase disturbances that are induced by a family of pairs of equal and opposite oblique waves apparently decay. Figures 4.6(*g,h*) further imply that $\lambda_{crit} \cong \lambda_{KH}$. Because $\lambda_{KH} \cong (U_1+U_2)/2\nu_f$, the corresponding spanwise wave number, $\beta_{crit} \cong 4\pi\nu_f/(U_1+U_2)$, gives a criteria for the decay of the pairs of oblique waves.

Pierrehumbert & Widnall (1982) observed a short wavelength cutoff for a subharmonic instability in which the primary vortices are spanwise undulated out-of-phase with respect to each other. Similar to the arguments put forth by these authors, the short-wave cutoff in the present experiments suggests that λ_{crit} increases like λ_{KH} with downstream distance. Hence, phase disturbances of a given spanwise wavelength gradually decay as they are advected downstream. In the present experiments, the flow

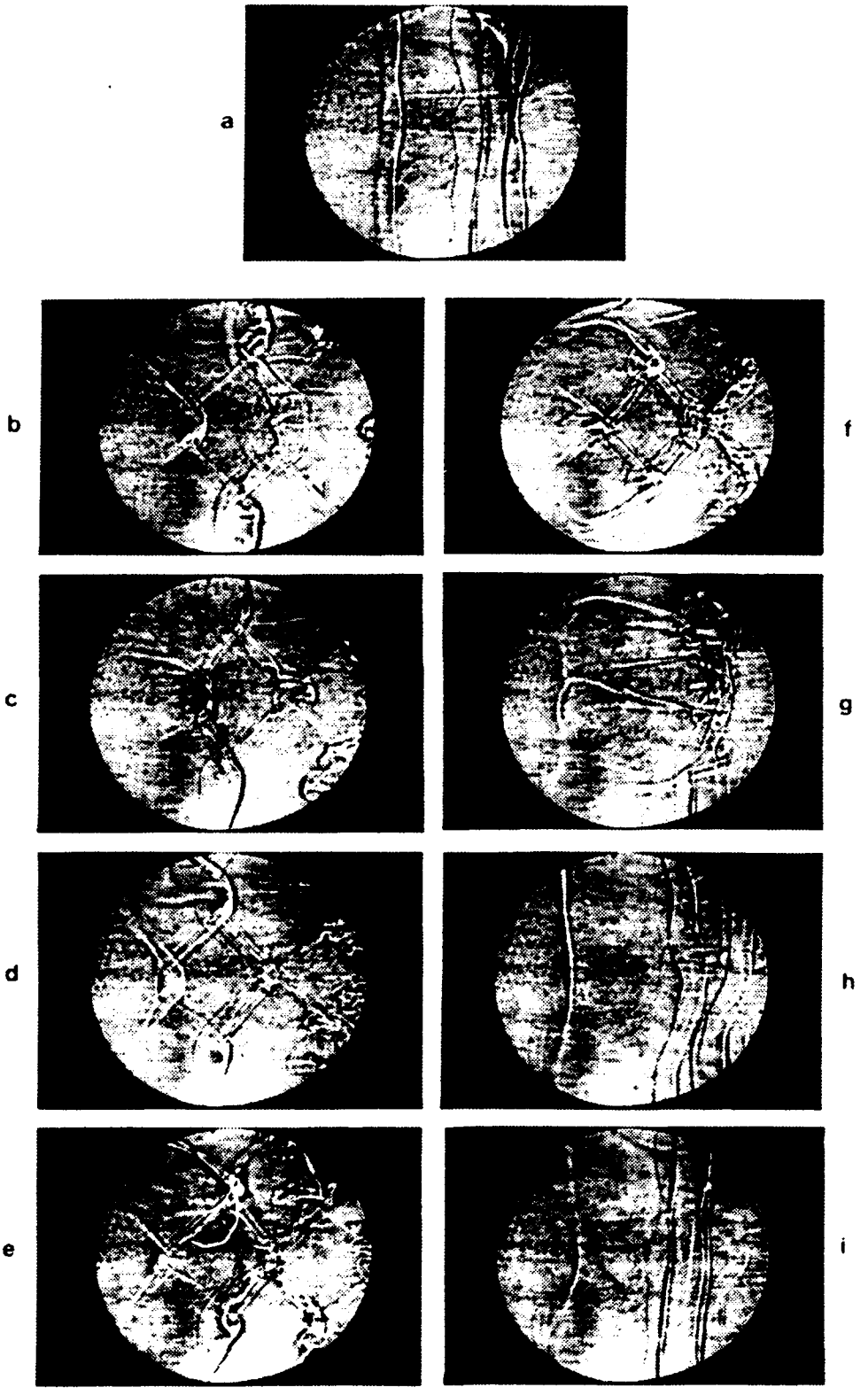

Figure 4.6

is forced. Hence, λ_{KH} is almost unchanged within the streamwise domain shown in figure 4.6 and, consequently, the magnitude of the phase deformations appears to be invariant with x. On the other hand, in an unforced mixing layer, amplification of the three-dimensional instability mode leading to deformations of the primary vortices may be overwhelmed by the amplifying two-dimensional instability modes.

The photographs of figure 4.6 also reveal interesting features concerning the evolution of small-scale flow structures. As the spanwise excitation wavelength is decreased (but is still greater than λ_{crit}), small-scale structures appear within the cores of the primary vortices, ostensibly as a result of mean flow distortion. As will be shown in the next subsection, such phase excitation may result in a higher-order inviscid inflectional instability that amplifies broadband disturbances.

4.6. *Time-Invariant Spanwise Phase Excitation*

The response of the shear layer to spanwise-periodic (λ_z = 5.1 cm, β_1 = 1.23 cm^{-1}), piecewise-constant, and time-invariant phase distribution with ($\Delta\Phi = \pi/2$) and without ($\Delta\Phi = \pi$) the presence of a two-dimensional excitation wave train is shown in figures 4.7(*a*) and (*b*), respectively. We note that, when $\Delta\Phi = \pi/2$, the amplitudes of the two-dimensional wave train is approximately four times lower than the amplitude of the lowest-order pair of oblique waves. Cross-stream distributions of the streamwise velocity are measured at a number of streamwise (x) stations at three equally spaced spanwise locations, $z_1 = 0$, $z_2 = z_1 + \lambda_z/4$, and $z_3 = z_1 + \lambda_z/2$. Because the phase distribution, $\Phi_{sp}(z)$, is taken to be symmetric relative to $z = 0$, $\Delta\Phi = \Phi_{sp}(z_1) - \Phi_{sp}(z_3)$ and a spanwise phase discontinuity occurs at z_2. The spanwise measurement stations are marked in figure 4.7(*a*) for reference.

Perspective contour plots of the phase-averaged turbulent fluctuations $\langle u'_{trms} \rangle$ in the y-t planes at z_1, z_2, and z_3 at x = 15.2 cm during two periods of the excitation wave train are shown in figures 4.8 ($\Delta\Phi = \pi/2$) and 4.9 ($\Delta\Phi = \pi$). A corresponding plot for spanwise-uniform excitation at z_1 is shown for reference in figure 4.10. When

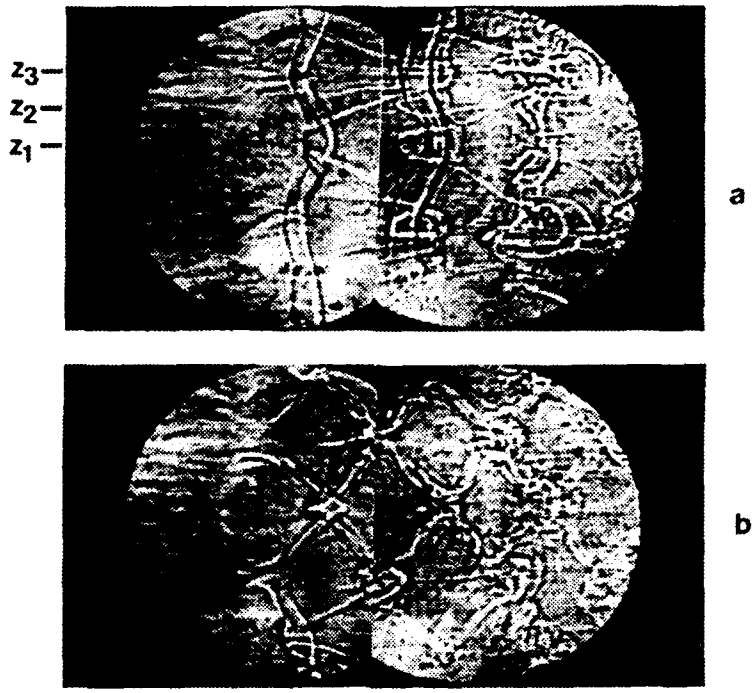

Figure 4.7

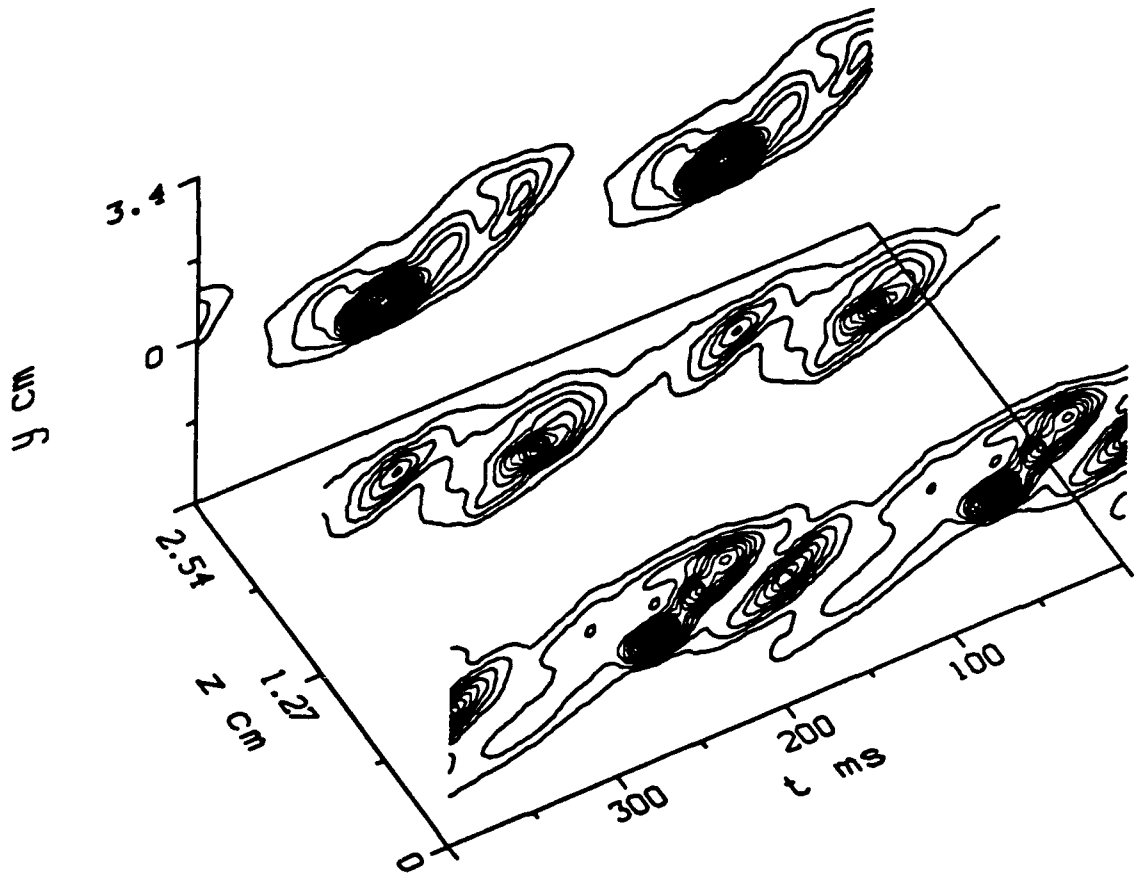

Figure 4.8

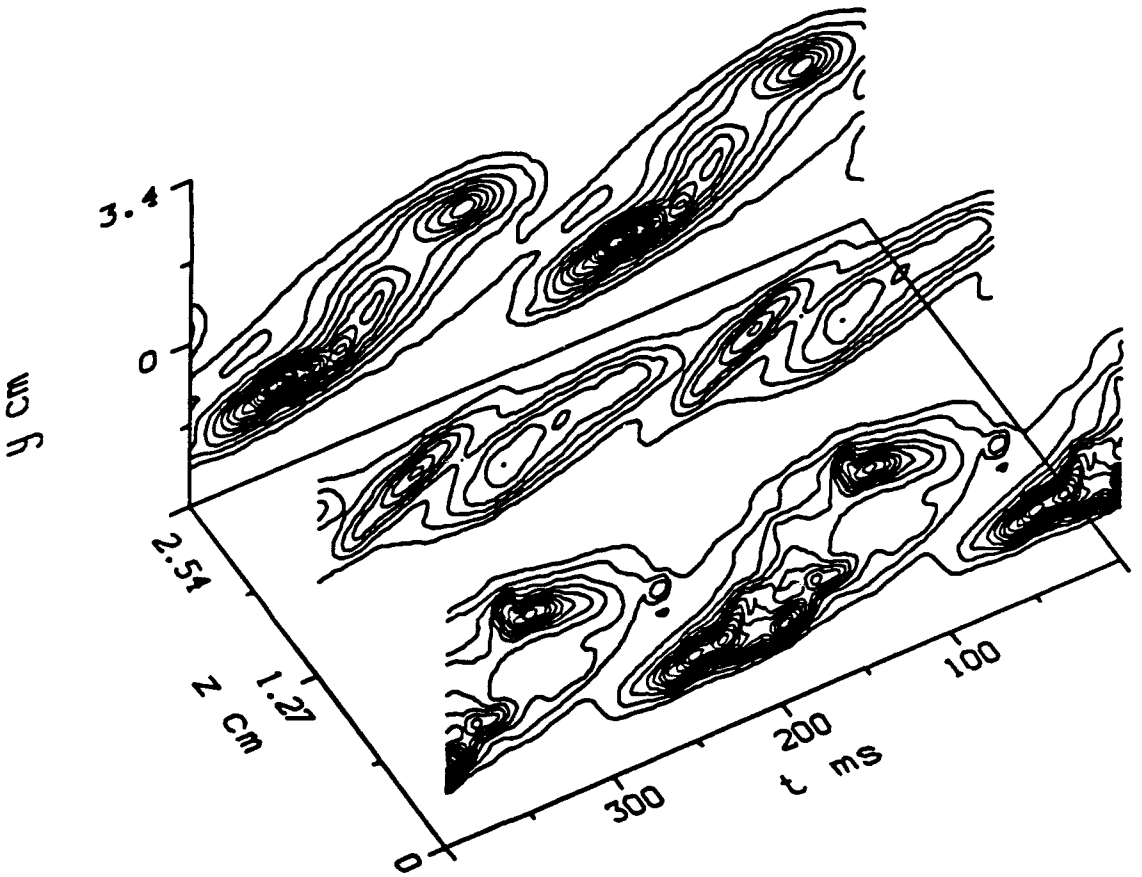

Figure 4.9

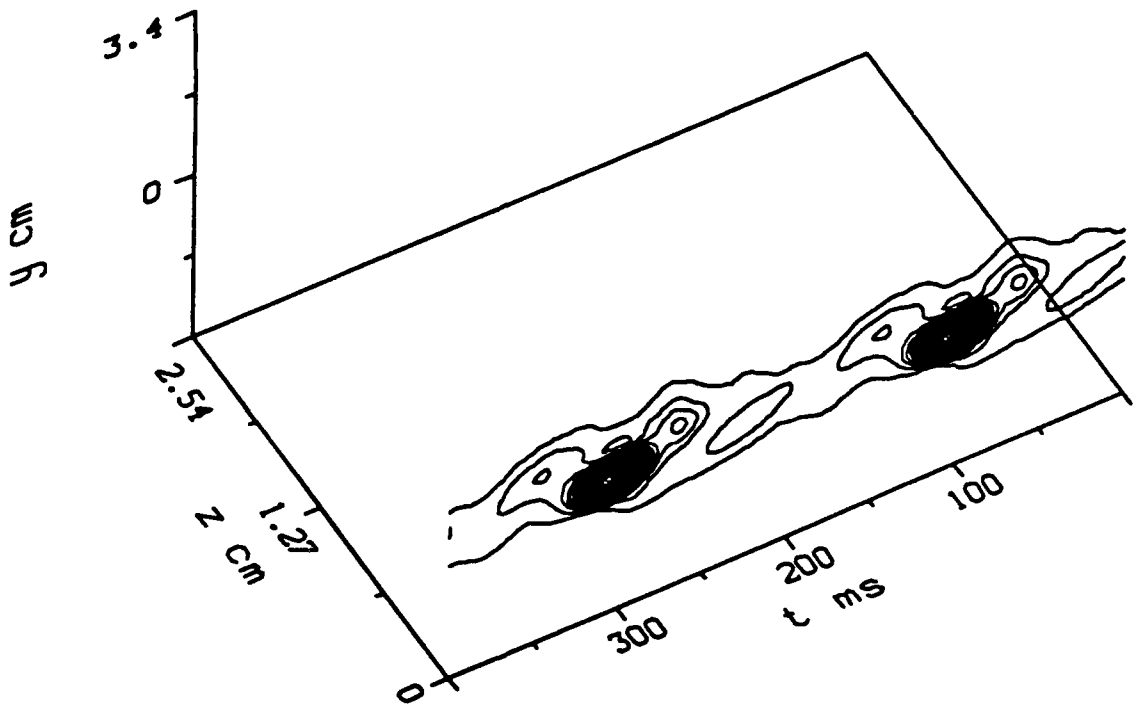

Figure 4.10

the excitation waveform is spanwise-uniform (figure 4.10), passage of the spanwise vortices at the measurement station can be recognized by concentrations of small-scale velocity fluctuations. At this streamwise position, the cross-stream distribution of $\langle u'_{trms} \rangle$ within the spanwise vortex exhibits a fairly broad, large peak displaced toward the low-speed edge of the spanwise vortex.

When $\Delta\Phi = \pi/2$, the y-t planes, $z = z_1$, z_2, and z_3, intersect a secondary vortical structure at its upstream edge (the "tail"), at its leg in the braid regio: and at its downstream edge (the "head"), respectively (figure 4.8). Note that the cross section of the primary vortex at $z = z_3$, which corresponds to its upstream bend, is almost unchanged, compared to the unforced case. At $z = z_2$, the primary vortex appears to be somewhat weaker and, at $z = z_1$, which corresponds to the downstream bend of the primary vortex, its core is clearly distorted by the secondary vortex. Concentrations of $\langle u'_{trms} \rangle$ corresponding to the tail ($z = z_1$) and head ($z = z_3$) of the secondary vortex appear at the high-speed and low-speed edges of the shear layer, downstream and upstream of the bends of the primary vortex, respectively. Note that, because of the upstream bend of the primary vortex, the secondary vortex is spatially less developed at $z = z_3$ than at $z = z_1$, and, hence, the peak of concentration of $\langle u'_{trms} \rangle$ corresponding to the head of the secondary vortex appears to be weaker than the corresponding peak at its tail. A cross-section capturing of the leg of the secondary vortex in the braid region is shown at $z = z_2$.

When $\Delta\Phi = \pi$ (figure 4.9), the planes $z = z_1$ and z_3 are y-t cross sections through successive streamwise corners of the staggered diamond-shaped cells in the x-z planview of figure 4.7, while the plane $z = z_2$ is a y-t cross section through the sides of these cells, halfway between z_1 and z_3. Concentrations of $\langle u'_{trms} \rangle$ in the y-t planes $z = z_1$ and z_3 are reasonably similar and displaced in time by $T_f/2$. The centers of the cross sections of the vortical structures in the y-t planes z_1 and z_3 alternate in time between y-elevations near the high- and low-speed edges of the shear layer; in the

plane $z = z_2$, the centers of successive cross sections have approximately the same y-elevations. Figure 4.9 also shows that cross sections of vortical structures in each of the y-t planes appear twice during each excitation cycle, suggesting that, when $\Delta\Phi = \pi$, the rollup of the primary vortices occurs at twice the forcing frequency. The relative position in time of the cross sections of the vortices in the y-t planes $z = z_1$ and z_3 suggests that the corners of the diamond-shaped cells in the x-z planview are formed by upstream and downstream bends of successive spanwise vortices. These bends occur in planes that are tilted around the z-axis such that the downstream and upstream edges of the bends are close to the high- and low-speed streams, respectively (see also figure 4.4).

As discussed above, spanwise phase excitation results in spanwise-nonuniform rollup of the primary vortices. When $\Delta\Phi = \pi$ and for a relatively short excitation wavelength, the rollup of a given spanwise vortex begins (say, at $t = t_0$) at the centers of segments of constant phase of the excitation wave train and continues along lines of constant phase within the vortex sheet between the two streams. At spanwise positions of phase discontinuities, lines of constant phase (within the vortex sheet) are inclined relative to the streamwise direction toward spanwise segments that begin their rollup at $t_1 = t_0 + T_f/2$. The rollup at $t = t_1$ forces the branches of the spanwise vortex, which began its rollup at $t = t_0$, to be pushed downward toward the low-speed side such that, at spanwise locations corresponding to centers of segments of constant phase of Φ_{sp}, there is a double rollup into two separate vortices. The rollup of a given spanwise vortex is completed when the branches are joined that form at phase discontinuities on each side of a spanwise segment of constant phase of the excitation waveform. Figure 4.11 shows a cross-stream view of the shear layer visualized by dye, which is injected into the low-speed-side boundary layer at midspan (i.e., $z = z_1$). This photograph clearly shows the double rollup of the primary vortices and, furthermore, indicates that spanwise-nonuniform pairing interactions may occur farther downstream.

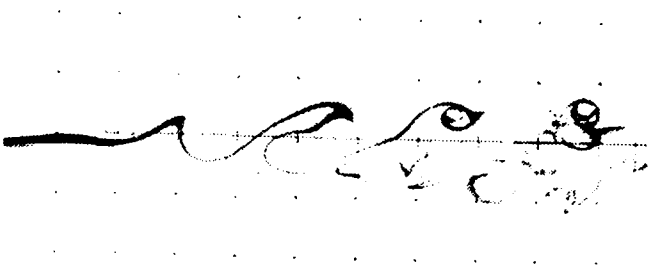

Figure 4.11

We next consider the amplification of perturbations at the forcing frequency and its first harmonic by using streamwise distributions of cross-stream-integrated amplitudes of the spectral components of u_{pert} (denoted A_1 and A_2, respectively). It is clear that this amplification includes *all* modes at the excitation frequency and its first harmonic. Figure 4.12 shows A_1 (closed symbols) and A_2 (open symbols) for spanwise-uniform excitation and phase excitation with $\Delta\Phi = \pi/2$ and π. The data corresponding to spanwise-uniform excitation were obtained at $z = z_1$ and are also plotted for reference at $z = z_2$ and z_3. When the flow is excited with a spanwise-uniform wave train, A_1 increases somewhat between $x = 5.1$ and 7.6 cm and then remains almost unchanged through $x = 15.2$ cm, where it begins to decay. The streamwise distributions of $A_1(z = z_1)$ and $A_1(z = z_3)$ for $\Delta\Phi = \pi$ are reasonably similar, as may be expected from the similarity of the flow at these x-y planes. These distributions suggest that, at these spanwise stations, the perturbation wave train is amplified for $x < 7.5$ cm, decays somewhat for 7.5 cm $< x <$ 15 cm, and then continues to amplify through the streamwise domain considered here. However, the corresponding distribution of $A_1(z = z_2)$ is substantially different and exhibits a decay for $x > 10$ cm. The important observation here is that the amplification of pairs of oblique waves does not appear to be spanwise uniform.

The differences between $A_1(z = z_1)$ and $A_1(z = z_3)$ when the flow is forced with $\Delta\Phi = \pi/2$ are presumably associated with the differences in the evolution of the primary vortices at these spanwise stations, namely, the formation of downstream and upstream bends that are closer to the high- and low-speed edges of the shear layer, respectively. Similar to the case $\Delta\Phi = \pi$, the amplitude distributions at $z = z_1$ and z_3 are different than the corresponding distribution at $z = z_2$, thus suggesting that the oblique wave disturbances are not uniformly amplified across the span of the flow. For both cases of phase excitation, the streamwise distributions of A_2 do not appear to vary significantly across the span and are similar to the corresponding distribution resulting from spanwise-uniform excitation.

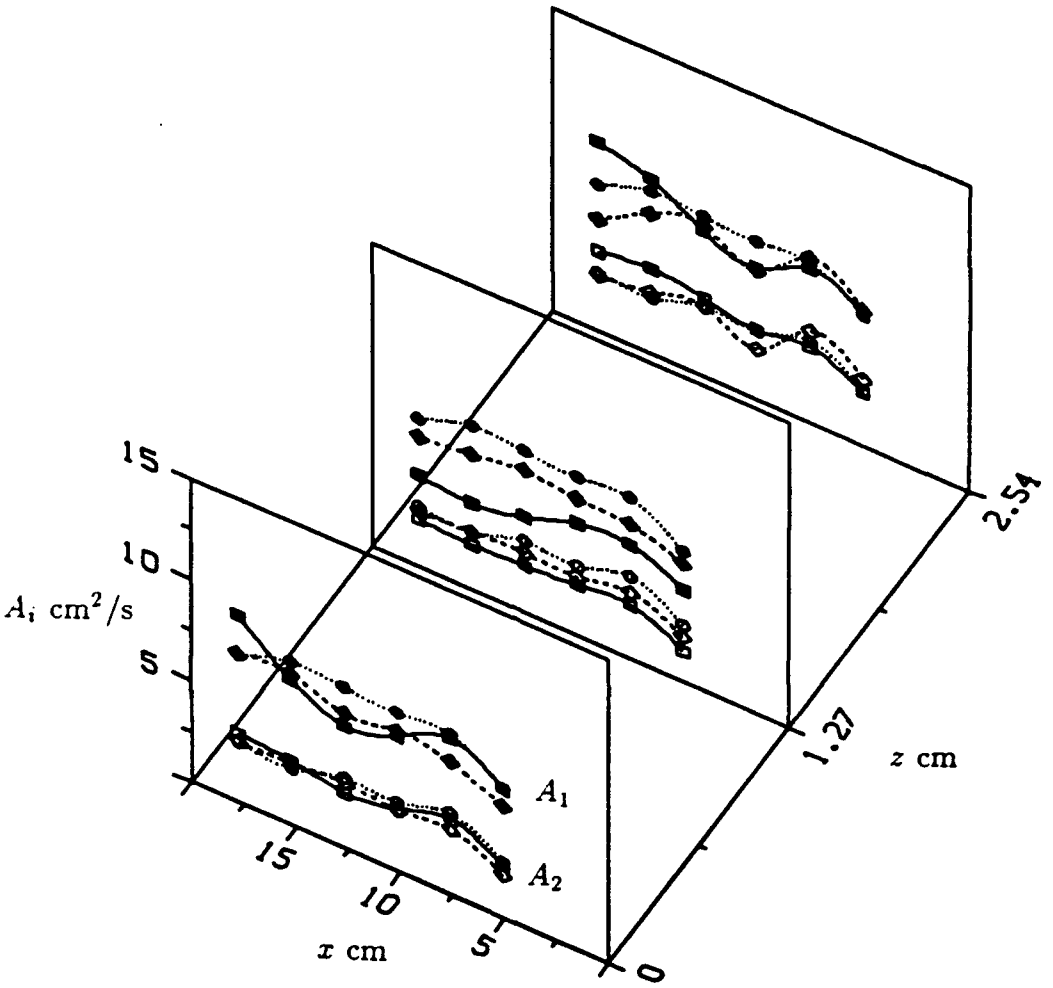

Figure 4.12

Composites of cross-stream contours of power spectra, $P(\nu, y)$, and profiles of the time-averaged streamwise velocity, $U(x, y)$, at $z = z_1$, z_2, and z_3 are shown in figures 4.13 and 4.14 for $\Delta\Phi = \pi/2$ and π, respectively. Corresponding plots for spanwise-uniform excitation at a single spanwise location are shown for reference in figure 4.15. These profiles are measured at $x = 10.2$ cm (figures 4.13*a*, 14*a*, and 15*a*) and 15.2 cm (figures 4.13*b*, 14*b*, and 15*b*). When the excitation waveform is spanwise-uniform, the power spectra have pronounced peaks at the excitation frequency and some of its higher harmonics. Note the appearance of a cross-stream band of spectral components at higher frequencies (associated with the presence of small-scale motion) close to the low-speed edge of the mixing layer (cf. figure 4.8).

When the flow is forced with $\Delta\Phi = \pi/2$ (figure 4.13), the appearance of secondary vortices is accompanied by distortions of cross-stream profiles of the mean streamwise velocity. Such a distortion is apparent at $z = z_1$, the spanwise location corresponding to the tail of the streamwise vortex. The degree of distortion of the mean velocity profiles indicates that the secondary vortices resulting from core deformations at the present excitation wavelength are weaker than corresponding streamwise vortices resulting from spanwise-nonuniform amplitude excitation (see figure 11 of Nygaard & Glezer 1991). The appearance of the secondary vortex is accompanied by spreading of small-scale motion (or propagation of turbulent interfaces) toward the low-speed side, thus indicating a spanwise-localized broadening of regions where mixing may be enhanced. At $z = z_3$, which corresponds to the head of the secondary vortex, distortion of the streamwise velocity profile is much less pronounced, and $P(\nu, y)$ is only slightly broader than the corresponding distribution for the unforced flow.

When $\Delta\Phi = \pi$ (figure 4.14), the cross-stream spreading of the mixing layer increases considerably, compared to the case of spanwise-uniform excitation. In particular, the cross-stream width (as may be judged by the mean velocity profiles) at $z = z_1$ and z_3 is greater than at $z = z_2$. Cross-stream broadening of $P(\nu, y)$ is clearly

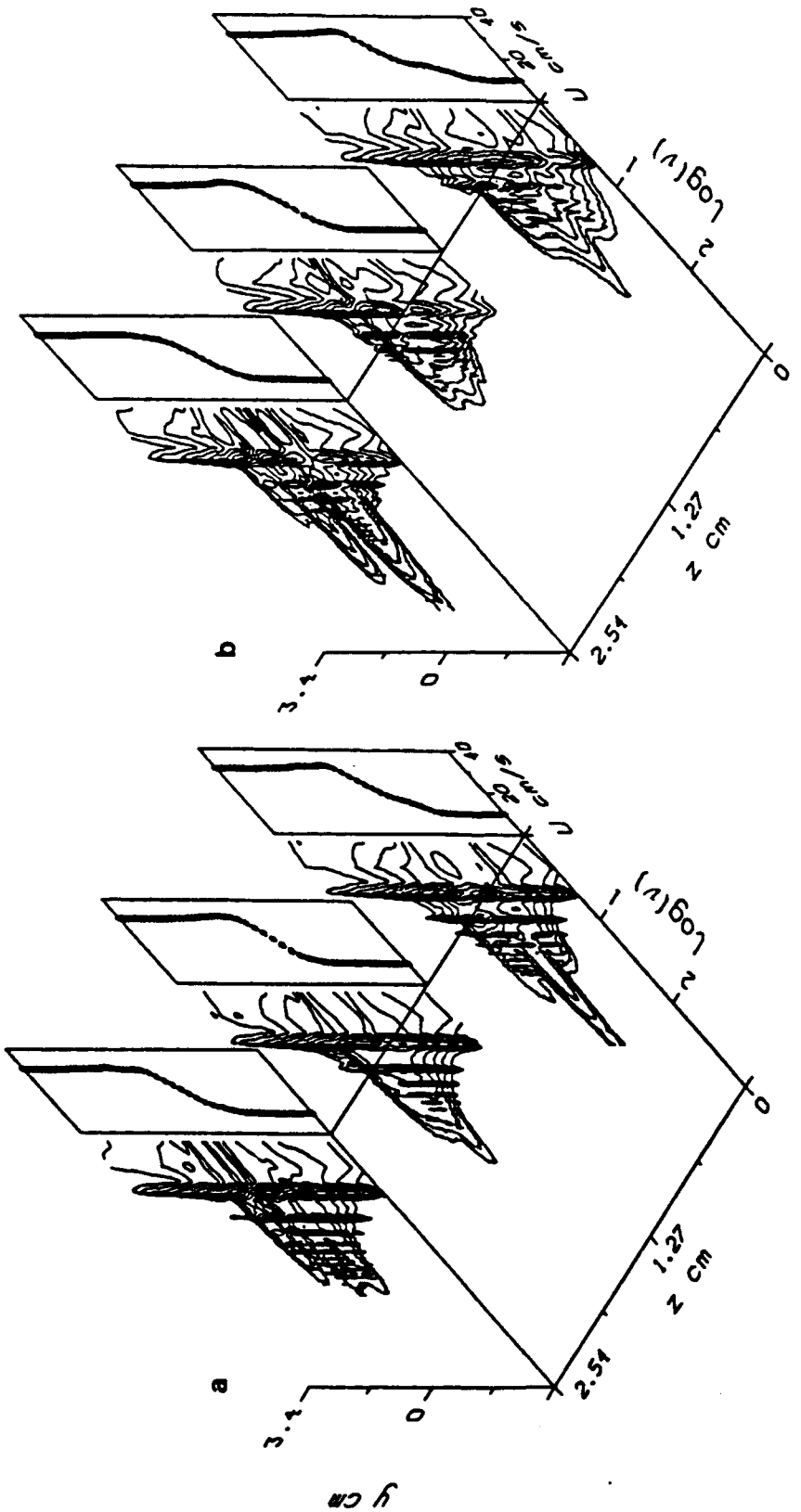

Figure 4.13

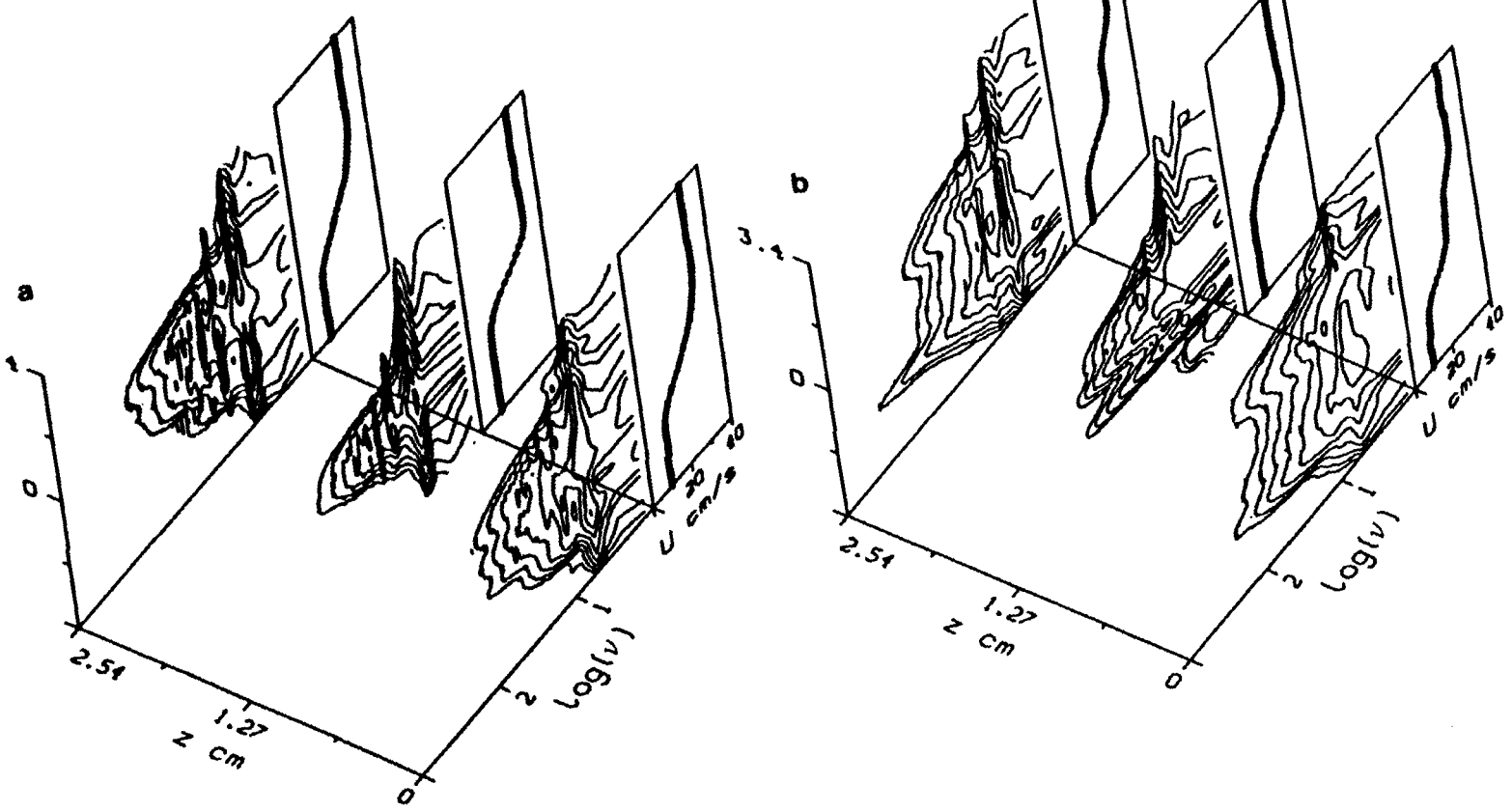

Figure 4.14

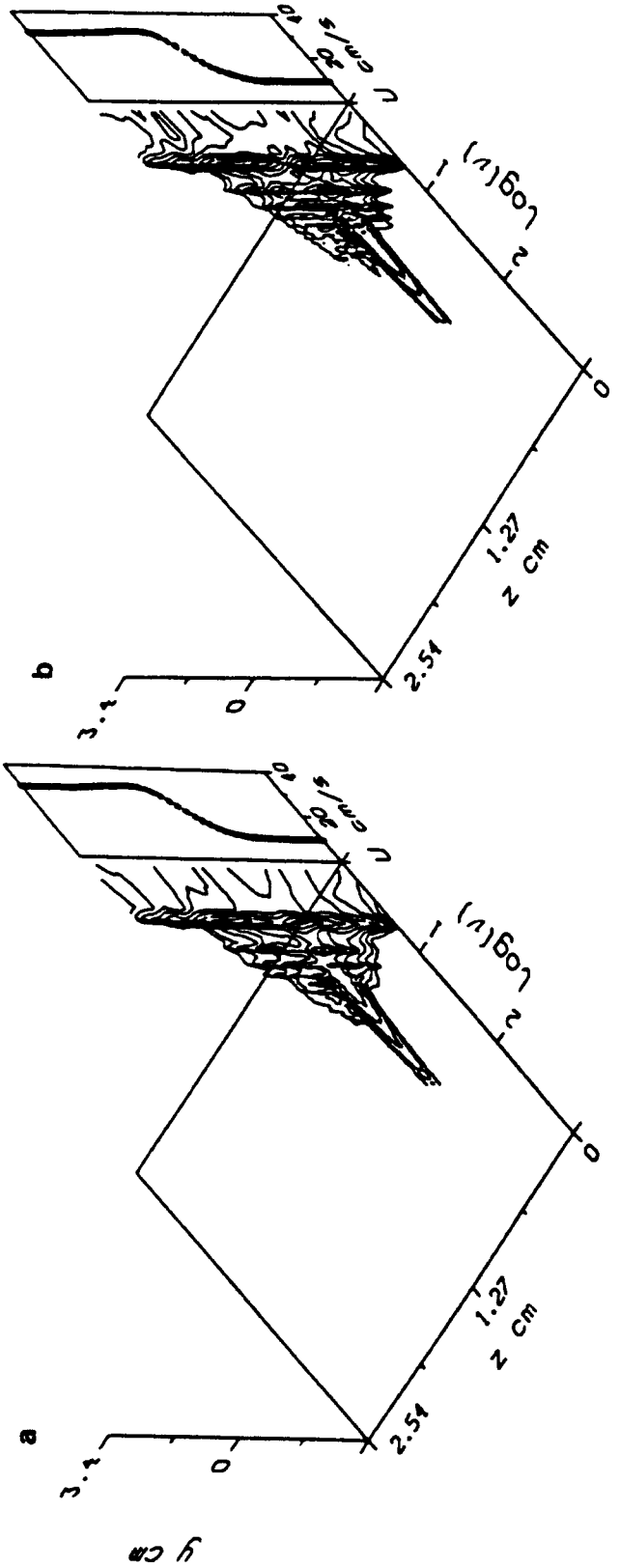

Figure 4.15

accompanied by the appearance of high-frequency spectral components. At x = 15.2 cm (figure 4.14*b*), the spectral peaks at the excitation frequency and its higher harmonics are considerably diminished and there is a pronounced cross-stream increase in the amplitude of high-frequency spectral components. These high-frequency components appear to form two cross-stream bands near the high- and low-speed edges of the flow, which, at $z = z_1$ and z_3, correspond to the appearance of additional inflection in the cross-stream distribution of U (note that cross-stream distributions of U at $z = z_1$ and z_3 are almost identical). The bands correspond to concentrations of turbulent fluctuations within the cores of the primary vortices, as evidenced by the cross-stream distributions of $\langle u'_{trms} \rangle$ in figure 4.9.

4.7. *The effect of Spanwise Phase Corrections on the Secondary Vortices*

In §3.3 we show that time-harmonic excitation having spanwise-periodic amplitude distribution, $E_0(z) = \tilde{E}(z)$, leads to the formation of pairs of streamwise counter-rotating vortical structures having spanwise spacings that are equal to the excitation wavelength, λ_z. Furthermore, as shown in figure 4.16(*a*) (same as figure 3.3*b*, λ_z = 5.1 cm), if $\lambda_z > \lambda_{KH}$, the spanwise vortices develop spanwise deformations at the excitation wavelength. Because the phase of the excitation wave train is spanwise uniform, it appears that the phase distortion necessary for the deformation of the primary vortices is induced by the formation of the streamwise vortices *upstream* of the first rollup of the primary vortices. Note that, at the downstream edge of the Schlieren view, small-scale motion is significantly increased at spanwise locations corresponding to the heads of the streamwise vortices, in comparison to the spanwise-uniform excitation of figure 2.6.

In what follows, we show that the suppression of the deformations of the primary vortices has a substantial effect on the streamwise vortices and leads to a considerable diminution in small-scale flow structure. The spanwise-periodic phase distribution,

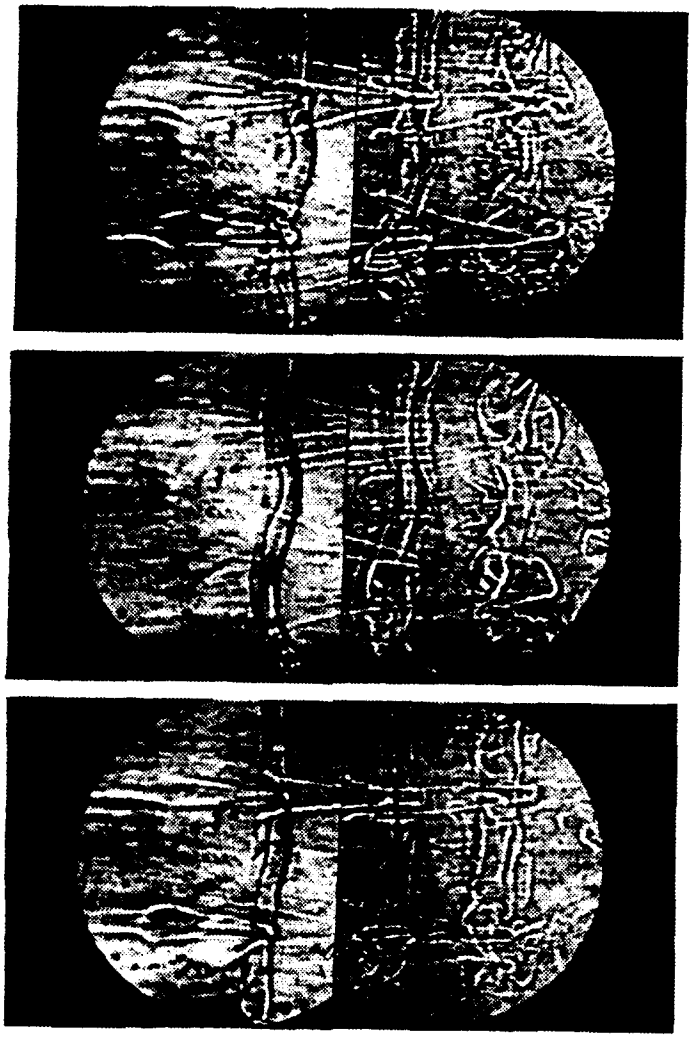

Figure 4.16

$\Phi_{sp}(z) = \tilde{\Phi}(z)$, leading to the distortion of the primary vortices in figure 4.16(*a*) is determined by using "strobed" video photography. This phase distribution is used for phase excitation having a spanwise-uniform amplitude distribution as shown in figure 4.16*b*. Note that the core deformations of spanwise vortices are almost identical to the core deformations shown in figure 4.16(*a*), except that the secondary vortices are formed *downstream* of the first rollup. As mentioned in §4.4, the shape and apparent strength of the streamwise vortices are affected by the magnitude of deformations of the primary vortices. In common with figure 4.16(*a*), figure 4.16(*b*) also shows the formation of multiple longitudinal secondary vortices having the same sense of rotation on each side of an upstream bend of the primary vortices.

In figure 4.16(*c*), we show the response of the mixing layer to an excitation waveform having both spanwise-periodic amplitude and phase distributions. While the amplitude distribution is $E_0(z) = \tilde{E}(z)$, the spanwise phase distribution is $\Phi_{su}(z) = -\tilde{\Phi}(z)$ (i.e., added out-of-phase). The most important feature in figure 4.16(*c*) is that the spanwise deformations of the primary vortices are completely cancelled. It should be emphasized that the combined excitation is not a linear superposition of the appropriate amplitude and phase disturbances, and the combined excitation waveform is generated from a single three-dimensional row of surface heaters. This is in contrast to the two-dimensional boundary layer experiments of Liepmann, Brown & Nosenchuck (1982), where a linear disturbance excited by an upstream surface heater was cancelled by a phase-delayed input to a downstream surface heater. As a result of the combined excitation, the spanwise vortex remains almost undistorted throughout the streamwise domain shown in figure 4.16(*c*). The secondary (streamwise) vortices still form upstream of the first rollup of the spanwise vortex, but the included angle between their legs is smaller compared to figure 4.16(*a*). Furthermore, the multiple streamwise vortices that are present in figures 4.16(*a,b*) are absent, and concentrations of small-scale motions within the core of the primary vortex at the downstream edge of figure 4.16(*c*) are considerably smaller than in figure 4.16(*a*).

4.8. *Spanwise-Nonuniform Pairing of Primary Vortices*

The subharmonic instability discussed by Pierrehumbert & Widnall (1982) corresponds to spanwise-localized pairing of the primary vortices and is excited by a superposition of two equal and opposite subharmonic oblique waves. These authors speculate that adjacent primary vortex cores are displaced alternately above and below the plane y = 0 and undergo spanwise-nonuniform pairing. Similar interactions were observed in the recent numerical investigation of Comte & Lesieur (1990) as a result of the addition of random three-dimensional disturbances to the two-dimensional base flow. Comte & Lesieur show that successive primary vortices develop out-of-phase spanwise undulations and assert that the undulations result in spanwise-nonuniform pairing of the primary vortices that gives rise to a "vortex-lattice" structure.

In order to demonstrate that phase disturbances can also be imposed *after the rollup of the primary vortices is completed*, the shear layer is excited simultaneously with two time-harmonic wave trains at the fundamental (most-amplified) frequency, ν_f, and its first subharmonic, $\nu_f/2$. The excitation waveform at ν_f is spanwise-uniform. The excitation waveform at $\nu_f/2$ has either amplitude (figure 4.17) or phase (figure 4.18) distributions, which are spanwise periodic and piecewise constant (as described in §4.2). The fundamental excitation results in nominally spanwise-uniform rollup of the primary vortices at ν_f. Because the spatial amplification rate of the subharmonic wave train is lower than that of the fundamental, it begins to affect the evolution of the primary vortices farther downstream and leads to their spanwise-nonuniform coalescence. In the experiments described below, the free-stream velocities are 42 and 14 cm/sec, ν_f = 9 Hz, and the spanwise wavelengths of the subharmonic wave train are λ_z^{sh} = 10.2 and 20.3 cm.

In figure 4.17(*a*), the excitation wavelength is λ_z^{sh} = 20.3 cm and the amplitude discontinuity occurs at midspan (z = 0). The normalized spanwise amplitude of the subharmonic wave train, $E_0^{sh}(z)/E_0$, is 1.0 for -20.3 cm < z < 0 (i.e., below midspan) and

a

b

Figure 4.17

0.3 for $0 < z < 20.3$ cm. Owing to the higher amplitude of the subharmonic wave train below midspan, the spanwise vortices begin to coalesce closer to the flow partition below midspan than above it. The spanwise-nonuniform pairing leads to a spanwise core deformation of the primary vortices and to the subsequent formation of secondary vortices in the braid region. The appearance of secondary vortices presumably leads to an increase in small-scale motions at the downstream edge of the Schlieren view.

When $\lambda_z^{sh} = 10.2$ cm (figure 4.17*b*), the center segment of the subharmonic excitation wave train for which $E_0^{sh}(z)/E_0 = 1.0$ is symmetric relative to midspan and leads to earlier pairing of corresponding segments of spanwise vortices. As a result, spanwise cells of paired vortices, which are reminiscent of Comte & Lesieur's (1990) vortex-lattice structure (their figure 1b), are formed around midspan. The streamwise length of each cell is approximately $2\lambda_{KH}$. These photographs suggest that spanwise-nonuniform pairing and core deformations (or phase distortions) of the primary vortices far downstream from the flow partition of an unforced plane mixing layer can result from spanwise-amplitude nonuniformities of disturbances at the subharmonics of the fundamental frequency. Clearly, this evolution may become even more complicated if the streamwise amplification rate of these disturbances is spanwise nonuniform. This may explain the wide variety of spanwise-nonuniform pairing interactions apparent in plane mixing layers in the absence of subharmonic excitation (e.g., Chandrsuda *et al.* 1978; Browand & Troutt 1980, 1985; Keller *et. al.* 1988).

The evolution of spanwise phase nonuniformities of the subharmonic excitation wave train is shown in figures 4.18(*a,b*). The spanwise distributions of $\Phi_{sp}^{sh}(z)$ for each of the two excitation wavelengths are similar to the corresponding distributions of $E_0^{sh}(z)$ and $\Delta\Phi = \pi$. Recall that, for $\Delta\Phi = \pi$, the subharmonic wave train is a linear superposition of pairs of equal and opposite oblique waves. Assuming that the amplitude immediately downstream of the flow partition and the streamwise amplification rate of adjacent segments of the subharmonic wave train are the same,

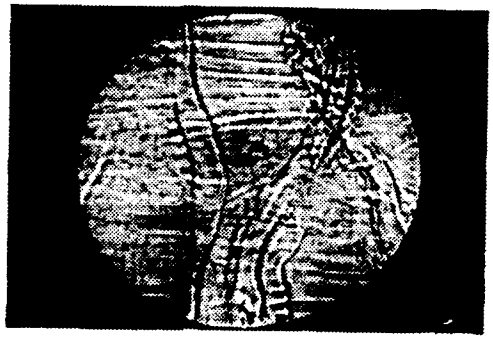

a

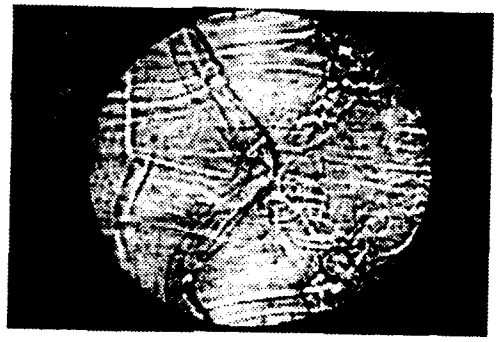

b

Figure 4.18

then pairing of spanwise segments of the spanwise vortices begins at the same streamwise position downstream from the flow partition. Pairing of adjacent spanwise segments alternates in time (every half period of subharmonic wave train) resulting in pairing interactions that are clearly reminiscent of Pierrehumbert & Widnall's (1982) subharmonic instability. Similar to the evolution of secondary streamwise vortices in figure 4.17, the primary core deformation due to spanwise-nonuniform subharmonic phase excitation also leads to the formation of secondary vortical structures and enhancement of small-scale motions.

4.9. *Conclusions*

Previous experimental evidence (e.g., Chandrsuda *et al.* 1978; Browand & Troutt 1980, 1985) has suggested that the plane shear layer is receptive to spanwise-nonuniform perturbations resulting from variations in the phase speed or frequency of the fundamental instability of the two-dimensional base flow. The present work builds on these findings and focuses on spanwise-nonuniform excitation of phase disturbances at the flow partition that result in significant core deformations of the ensuing primary vortices. An important consequence of these deformations is the appearance of secondary vortical structures in the braid region, the shape, orientation, and strength of which depend on the magnitude of the core deformation of the primary vortices.

When the spanwise phase distribution is spanwise-linear, the excitation wave train is a single oblique wave resulting in primary vortices that are inclined in the streamwise direction at the wave angle of the excitation wave train and are advected in the streamwise direction. The rollup of each primary vortex progresses along a line of constant phase (i.e., inclined relative to the trailing edge of the flow partition) of the excitation wave train. A flow visualization study indicates that all oblique waves having wave angles smaller than 29° have the same the streamwise amplification. This wave angle corresponds to streamwise inclination of approximately $3\lambda_{KH}$ across the span

of the test section. Secondary longitudinal vortices are formed in the braid region at spanwise locations corresponding to discretization discontinuities in the excitation wave train. These vortices are approximately normal to the axes of the primary vortices, indicating the direction of principal strain in the braid region between adjacent primary vortices.

Spanwise-periodic core deformations of the primary vortices are excited when the phase distribution of the excitation wave train is spanwise periodic. In the present experiments, Φ_{sp} is piecewise constant (0.5 duty cycle) with variable phase discontinuity, $\Delta\Phi$, and spanwise wavelength, λ_z. The excitation waveform is a linear superposition of a two-dimensional time-harmonic wave train and a family of pairs of equal and opposite oblique wave trains of decreasing amplitudes and increasing wave numbers. The relative amplitudes and phase of the two-dimensional and oblique waves are prescribed by the magnitude of $\Delta\Phi$. In particular, when $\Delta\Phi = 0$, the excitation is reduced to a two-dimensional wave train and, when $\Delta\Phi = \pi$, the excitation waveform consists only of the oblique waves. In the latter case, the primary vortices appear to be unstable to phase excitation that has a characteristic spanwise wavelength exceeding λ_{KH}, or a spanwise wave number below $\beta = 4\pi\nu_f/(U_1+U_2)$ (figure 4.6).

The effect of the magnitude of $\Delta\Phi$ on the evolution of secondary vortices is studied using an excitation waveform having a spanwise-periodic piecewise-constant frequency distribution where the spanwise frequency discontinuity is small. As a result, $\Delta\Phi$ is time periodic and slowly varying (at the beat frequency between adjacent segments). When $\Delta\Phi > \pi$ or $\Delta\Phi < \pi$, the streamwise vortices resemble counter-rotating vortex pairs that form in the unforced mixing layer, however, their strength and the inclination of their axes relative to the streamwise direction increase with $\Delta\Phi$ (and the deformations of the primary vortices). When $\Delta\Phi = \pi$, the "secondary" vortices are indistinguishable from the primary vortices, and the vortex system in a Schlieren x-z planview resembles chain-link-like cells. Measurements of turbulence intensity and

flow visualization in the cross-stream plane show that the spanwise-undulated vortices are formed at twice the excitation frequency. The spanwise-periodic deformations of successive vortices are offset by $\lambda_z/2$ in the spanwise direction, yielding out-of-phase deformations between adjacent primary vortices. Hence, the primary vortices appear to undergo spanwise-periodic pairings at streamwise edges of the cellular structures.

Similar to spanwise-nonuniform amplitude excitation, spanwise-nonuniform phase excitation can result in significant spanwise and cross-stream distortion of time-averaged profiles of the streamwise velocity. The appearance of higher-order inflectional instabilities, where broadband perturbations already present in the base flow are amplified, results in spanwise-nonuniform concentrations of small-scale motion. Power spectra of the streamwise velocity component show that, when $\Delta\Phi = \pi$, the width of the mixing layer increases substantially, as indicated by cross-stream spreading of high-frequency spectral components associated with small-scale motion.

As was shown by Nygaard and Glezer (1991), the excitation of streamwise vortices at spanwise wavelengths that are greater than λ_{KH} can result in deformations of the primary vortices and in the appearance of additional streamwise vortices. The importance of core deformations of the primary vortices to the generation of small-scale motion was demonstrated by its cancellation using proper phase excitation. As a result, the strength of the secondary vortices in the braid region is apparently reduced, and spanwise concentrations of small-scale motions farther downstream are substantially diminished.

Deformations of the primary vortices can also occur downstream of the first pairing of the primary vortices if the pairing is spanwise nonuniform. This may be caused by a subharmonic disturbance (natural or forced) having spanwise phase or amplitude nonuniformities. As a result, the ensuing (paired) primary vortices deform and induce the formation of streamwise vortical structures. Core deformations and spanwise-nonuniform coalescence of the primary vortices is effected using linear

superposition of two time-harmonic excitation wave trains at the fundamental frequency and its first subharmonic. The fundamental wave train is spanwise-uniform, while the subharmonic has a spanwise-nonuniform phase distribution. This excitation leads to controlled spanwise-nonuniform pairing. The primary vortices develop spanwise undulations and induce secondary vortical structures that are ingested into the cores of the coalesced primary vortices and lead to enhancement of concentrations of small-scale motion farther downstream compared to spanwise-uniform pairing. Because the secondary vortices are critical to the maintenance of small-scale mixing, this is a plausible mechanism for the continuation of mixing downstream of mixing transition.

4.10. *References*

Browand, F. K. & Ho, C.-M. 1987 Forced unbounded shear flows. *Nuclear Physics B* 2, 139-158.

Browand, F. K. & Prost-Domasky,S. 1990 Experiment on pattern evolution in the two-dimensional mixing layer. In *New Trends in Nonlinear Dynamics and Patterning Phenomena: The Geometry of Non-Equilibrium* (ed. P. Coullet & P. Huerre). NATO ASI Series 8, Plenum.

Browand, F. K. & Troutt, T. R. 1980 A note on spanwise structure in the two-dimensional mixing layer. *J. Fluid Mech.* **97**, 771-781.

Browand, F. K. & Troutt, T. R. 1985 The turbulent mixing layer: geometry of large vortices. *J. Fluid Mech.* **158**, 489-509.

Chandrsuda, C., Mehta, R. D., Weir, A.D. & Bradshaw, P. 1978 Effect of free-stream turbulence on large structures in turbulent mixing layers. *J. Fluid Mech.* **85**, 693-704.

Collis, S., Lele, S., Rogers, Moser, R. & Rogers, M. 1991 Time developing mixing layer with spanwise-nonuniform phase. *Bull. Amer. Phys. Soc.* **36**, 2660.

Comte, P. & Lesieur, M. 1990 Large and small-scale stirring of vorticity and a passive scalar in a 3D temporal mixing layer. *Phys. of Fluids A* (submitted).

Corcos, G. M. & Lin, S. J. 1984 The mixing layer: deterministic models of a turbulent flow. Part 2. The origin of the three-dimensional motion. *J. Fluid Mech.* **139**, 67-95.

Dallard, T. & Browand, F. K. 1992 Scale transitions at defect sites in the mixing layer: application of the 2D arc wavelet transform. *J. Fluid Mech.* (submitted).

Delville, J., Bellin, S., Garem, J. H. & Bonnet, J. P. 1988 Analysis of structures in a turbulent plane mixing layer by use of pseudo flow visualization method based on hot wire anemometry. *Proceedings of Berlin 88 European Turbulence Conference.* Springer.

Hama, F. R., Rist, U. & Konzelman, U., Laurien, E. & Meyer, F. 1987 Vorticity field structure associated with 3D Tollmien-Schlichting Waves. *S̃ādhanā* **10**, 321-347.

Ho, C.-M. & Huerre, P. 1984 Perturbed free shear layers. *Ann. Rev. Fluid Mech.* **16**, 365-424.

Keller, J. O., Ellzey, J. L., Pitz, R. W., Shephard, I. G. & Daily, J. W. 1988 The structure and dynamics of reacting plane mixing layers. *Exp. in Fluids* **6**, 33-43.

Lasheras, J. S. & Choi, H. 1988 Three dimensional instability of a plane free shear layer: an experimental study of the formation and evolution of streamwise vortices. *J. Fluid Mech.* **189**, 53-86.

Liepmann, H. W., Brown, G. L. & Nosenchuck, D. M. 1982 Control of laminar instability-waves using a new technique. *J. Fluid Mech.* **118**, 187-200.

Nygaard, K. J. 1991 Spanwise-nonuniform excitation of a plane mixing layer. PhD thesis, University of Arizona.

Nygaard, K. J. & Glezer, A. 1990 Core instability of the spanwise vortices in a plane mixing layer. *Phys. Fluids A* **2**, 461-464.

Nygaard, K. J. & Glezer, A. 1991 Evolution of streamwise vortices and the generation of small-scale motion in a plane mixing layer. *J. Fluid Mech.* **231**, 257-301.

Pierrehumbert, R. T. & Widnall, S. E. 1982 The two- and three-dimensional instabilities of a spatially periodic shear layer. *J. Fluid Mech.* **114**, 59-82.

Robey, H. F. 1987 The nature of oblique instability waves in boundary layer transtion. In *Turbulence Management and Relaminarization, Proceedings IUTAM Symposium, Bangalore, India* (ed. H. W. Liepmann & R. Narasima). Springer Verlag.

Roos, F. W., Kegelman, J. T. & Kibens, V. 1989 Two stream mixing layer from a swept trailing edge," AIAA Paper 89-1022.

Sandham, N. D. & Reynolds, W. C. 1991 Three dimensional simulations of large eddies in the compressible mixing layer. *J. Fluid Mech.* **224**, 133-158.

Schneider, S. P. 1989 Effects of controlled three-dimensional perturbations on boundary layer transition. Ph.D. thesis, California Institute of Technology.

5. Pulsed Excitation of the Plane Shear Layer

5.1. *Introduction*

Although the evolution of anharmonic disturbances in plane mixing layers is substantially different from time-harmonic disturbances, no previous investigation has studied the effect of the former. A fundamental understanding of the evolution of anharmonic disturbances and their interaction with the nominally two-dimensional base flow structure owes much of its importance to technological applications in chemical reaction and unsteady combustion processes.

The technology of pulse combustion was known as early as World War II. Compared to conventional combustion systems, devices using pulsed combustion yield higher heat transfer rates, combustion intensities, and thermal efficiencies, accompanied by lower emission levels of nitrogen oxides (Keller & Westbrook 1986; Keller, Bramlette, Dec & Westbrook 1989). Pulsed combustion involves a three-dimensional transient flow field that is highly turbulent and has variable physical properties (Barr, Dwyer & Bramlette 1988). Therefore, investigations of three-dimensional transient flow fields are important for the advancement of this attractive technology.

Modifications of the flow structure in plane mixing layers have been commonly achieved by manipulation of instability modes via *time-harmonic* excitation waveforms having spanwise-uniform (e.g., Oster & Wygnanski 1982) or spanwise-periodic (Nygaard & Glezer 1991) amplitude distributions. Other types of time harmonic excitation have utilized spanwise-nonuniform phase or frequency distributions (Nygaard 1991). It is important to recognize that, within the streamwise domain of influence of the time harmonic excitation, the flow can only evolve spatially and its temporal evolution is restricted to the forcing frequency and its higher harmonics.

In real-time control applications of mixing layers of practical interest, the fact that these flows are not only irregular both in time and space, but are also subjected to temporally and spatially complex disturbances with important consequences to the

mixing, is not a trivial problem. In fact, in an unforced shear layer, the large coherent vortical structures do not appear at regular time intervals and may develop both in time and space.

The importance of this difference in boundary layer transition was established by Gaster & Grant (1975), who studied the evolution of a wave packet formed in a laminar Blasius boundary layer by a momentary acoustic pulse. The flow disturbances caused by the passage of the packet were detected by a hot-wire anemometer positioned just outside the boundary layer. The authors observed, that at some distance downstream from the pulse generator, the packet, which was initially smoothly contoured and with peak amplitudes close to its center, gradually distorted and developed nonlinear characteristics, which eventually led to the breakdown to turbulence. The authors further stated: "The non-linear development of a wave packet and its final breakdown into a turbulent spot involves processes akin to those of natural transition and a controlled experiment of this regime may provide fresh insight into the various interactive mechanisms that arise."

A theoretical linear model of a wave packet in a flat-plate boundary layer was proposed by Gaster (1975), who compared the experimental and analytical (based on the linear stability theory) evolutions of frequency-wave-number spectra of a flat-spectrum input. It was found that the overall shapes of the disturbed region of the wave packet and the manner in which it spreads as it travelled downstream could be predicted by the model. Gaster later (1987) concluded that *an isolated wave packet may lead to transition to turbulence much faster than a continuous wave train* (Gaster, private communication).

In an experimental study of an axisymmetric free shear layer of an air jet, Kleis, Hussain & Sokolov (1981) showed that a momentary disturbance, resulting from the triggering of a three-dimensional turbulent spot by a spark at the nozzle boundary layer upstream of the exit, is amplified much faster than the flow instabilities of the surrounding axisymmetric shear layer. In an earlier study, Sokolov, Hussain, Kleis &

Husain (1980) found that the spot is a large-scale, elongated, turbulent structure spanning the entire width of the shear layer, but does not appear to exhibit self-similar characteristics.

Balsa (1989) studied analytically the evolution of three-dimensional disturbances in a parallel mixing layer having a piecewise-linear velocity profile (Rayleigh profile). He showed that, in contrast to the boundary layer, a wave packet that develops in a plane shear layer has wave fronts that are approximately parallel to the spanwise direction. Balsa also studied the receptivity of the shear layer to pulsed-type and harmonic excitations and concluded that the shear layer is most receptive to external forcing near its centerline ($y = 0$).

In an experiment on pattern evolution in the two-dimensional mixing layer, Browand & Prost-Domasky (1990) studied the development of natural and artificially forced vortex defects. The forced defects were acoustically introduced by a row of 16 loudspeakers mounted along the span of the wind tunnel ceiling. The most prominent feature of such defects or dislocations is the occurrence of an interconnection of two vortex structures (or waves). The authors observed that the influence of the original defect appeared to spread laterally across the span as a propagation disturbance field, which extended both upstream and downstream from the original defect.

The evolution of a momentary, spanwise-uniform disturbance in a plane mixing layer was studied by Glezer, Wygnanski & Gu (1989). The experiment was conducted in an open-return air facility, and the streamwise velocity component at midspan was measured using a rake of hot-wire probes. The flow was forced by pulsed amplitude modulation of a time-harmonic wave train using a spanwise-uniform thin flap mounted at the trailing edge of the flow partition. The response to the modulating pulse was decomposed to a family of modal wave packets. It was found that the fundamental wave packet is advected with the mean velocity of the two streams, and its streamwise extent and dominant frequencies remain virtually unchanged with downstream distance.

An important observation of Glezer *et al.* was that the passage of the disturbance is accompanied by a spatial and temporal change in the momentum thickness of the harmonically excited flow. Cross-stream distributions of the streamwise velocity perturbation within the spatially amplified region of the disturbance are similar to those of the harmonically excited flow at streamwise stations having the same momentum thickness. The authors also discovered that high turbulence levels, not prevalent in the harmonically excited shear layer, are detected within the disturbance and suggest the possibility of transient mixing enhancement.

The purpose of the experimental work described in §5 was to study the spatial and temporal evolutions of three-dimensional pulsed disturbances in a plane mixing layer, their role in the development of the flow, and the extent of their interaction with the nominally two-dimensional flow structures.

5.2. *The Excitation Waveform and Measurement Procedure*

The disturbance is effected by spanwise-nonuniform pulsed amplitude modulation of a two-dimensional time-harmonic carrier wave train. The excitation waveform is pulsed amplitude modulation of a time-harmonic carrier wave train (figure 5.1) and is synthesized by a mosaic of surface film heaters. This waveform is chosen because temporal and spatial irregularities in the unforced mixing layer result in a substantial scatter in the amplitude and arrival time of a pulsed disturbance at the measurement station. In order to minimize this difficulty, a clear phase reference is provided by the low-level, two-dimensional, time-harmonic wave train (Glezer *et al.* 1989).

Similar to §2, the excitation power is comprised of a linear superposition of spanwise-uniform time-harmonic wave train and a time-periodic pulse,

$$E(z,t) = E_0 \, [1 + \sin(2\pi f_0 t)] + E_p \, (z,t) \, ,$$

where E_0 is constant. The pulse $E_{p(z,t)}$ is defined as

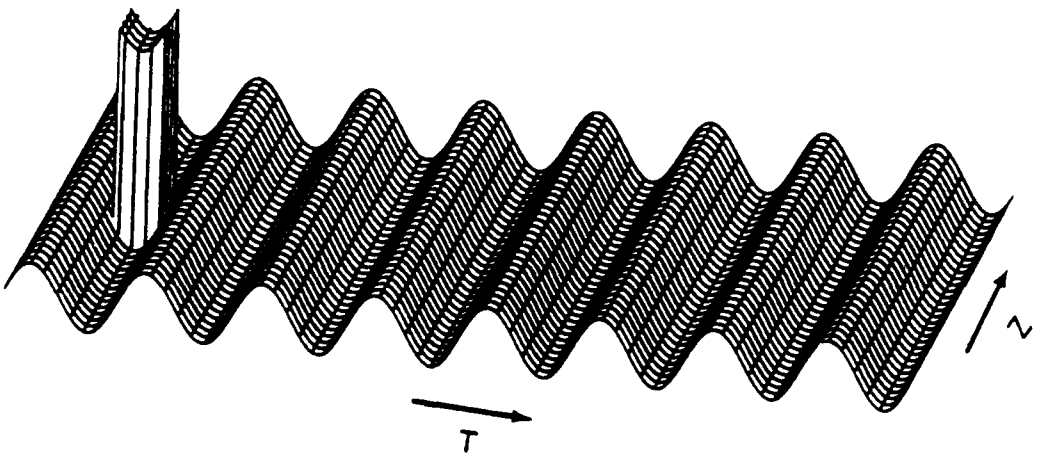

Figure 5.1

$$E_p(z,t) = \begin{cases} \gamma E_0, & \text{for } -2\Delta Z \le z \le +2\Delta Z \text{ and } t_c-\sigma T \le t \le t_c+\sigma T \\ 0, & \text{otherwise} \end{cases}$$

where γ is a positive constant, ΔZ is the width of a heating element (6.35 mm), 2σ equals the ratio between the duration of the pulse and the period of the wave train, and $t_c-\sigma T$ and $t_c+\sigma T$ are the rise and fall times of the pulse, respectively. We define

$$t_c = (\Delta + nM_p)T_f, \qquad n = 0, 1, 2, 3, \ldots ,$$

where ΔT_f is a time delay ($\Delta<1$) between the pulse (at time t_c) and a previous zero crossing of the time-harmonic wave train, and M_p is a positive integer (the frequency of the pulse train is f_0/M_p).

In the present experiments, the free-stream velocities are 30 and 10 cm/sec, and the excitation frequency of the two-dimensional wave train is $f_0 = 5$ Hz, which corresponds to a streamwise wavelength $\lambda_{KH} \cong 4$ cm. The resistance of each heating element is 3.6 Ω, and the average power dissipated by each heating element for the time-harmonic wave train is 5.9 watts (rms).

Cross-stream measurements of the streamwise velocity are taken with a rake of 31 hot-wire sensors, which is traversed 40 mm on each side of midspan. The pulsed disturbance is synthesized by a group of four adjacent heating elements centered at the midspan, i.e., $4\Delta Z = 25.4$ mm. The ratio between the power of a pulsed disturbance and the power dissipated by the time-harmonic wave train over one period ($2\sigma\gamma$) is selected to be 2, based on previous experience with two-dimensional pulsed disturbance (Glezer *et al* 1989). However, unlike the previous experiments in which the duration of the pulsed disturbance was the period of the time-harmonic wave train, in the present experiments, 2σ is 0.4 and $\gamma = 5$. The time delay, ΔT_f, between the pulsed disturbance at $t = t_c$ and the zero crossing of the excitation wave train is selected using Schlieren visualization downstream of the flow partition. The evolution of the disturbance depends critically on ΔT_f. For example, when $\Delta = 1/4$ the ensuing pulsed disturbance

is hardly visible. The disturbance appears to be strongest when $\Delta = 3/4$. A reduction in the duration or the amplitude of the pulse does not appear to alter substantially the characteristic evolution of the ensuing disturbance, although the disturbance becomes weaker, which makes its detection more difficult. The pulsed disturbances are repeated every eight cycles of the two-dimensional time-harmonic wave train ($M_p = 8$). This repetition rate was chosen so that successive pulsed disturbances will not affect each other.

The streamwise velocity component is measured phase-locked to the excitation waveform at equally spaced grid points (2 mm apart) in the y-z plane. The grid is symmetric relative to the y- and z-axes and measures 60 mm × 80 mm, respectively. These measurements are repeated at six streamwise stations (25.4 mm apart) between $x = 51$ mm ($\cong 1.3\lambda_{KH}$) and 178 mm ($4.45\lambda_{KH}$). The first streamwise measurement station, $x = 51$ mm, approximately corresponds to the location where the first rollup of the primary vortices occurs. The sampling frequency is 300 Hz, which is equivalent to 60 data points per period of the time-harmonic wave train. Each velocity data record contains 1024 data points and includes 17 periods of the time-harmonic wave train and two consecutive pulsed disturbances. Fifteen hot-wire channels are sampled simultaneously.

5.3. *Evolution of Vortices: Flow Visualization*

The spatial evolution of the pulsed disturbance is visualized in the x-z plane using a double-pass Schlieren system by exploiting the small changes in index of refraction due to the surface heaters (Nygaard & Glezer 1991). The Schlieren view may be thought of as a planar projection of streaklines of slightly heated fluid elements. Figure 5.2 shows a sequence of composite Schlieren photographs, each consisting of two partially overlapping images having nominal diameters of 132 mm and centered at midspan. The flow direction in each frame is from the left to the right, and the

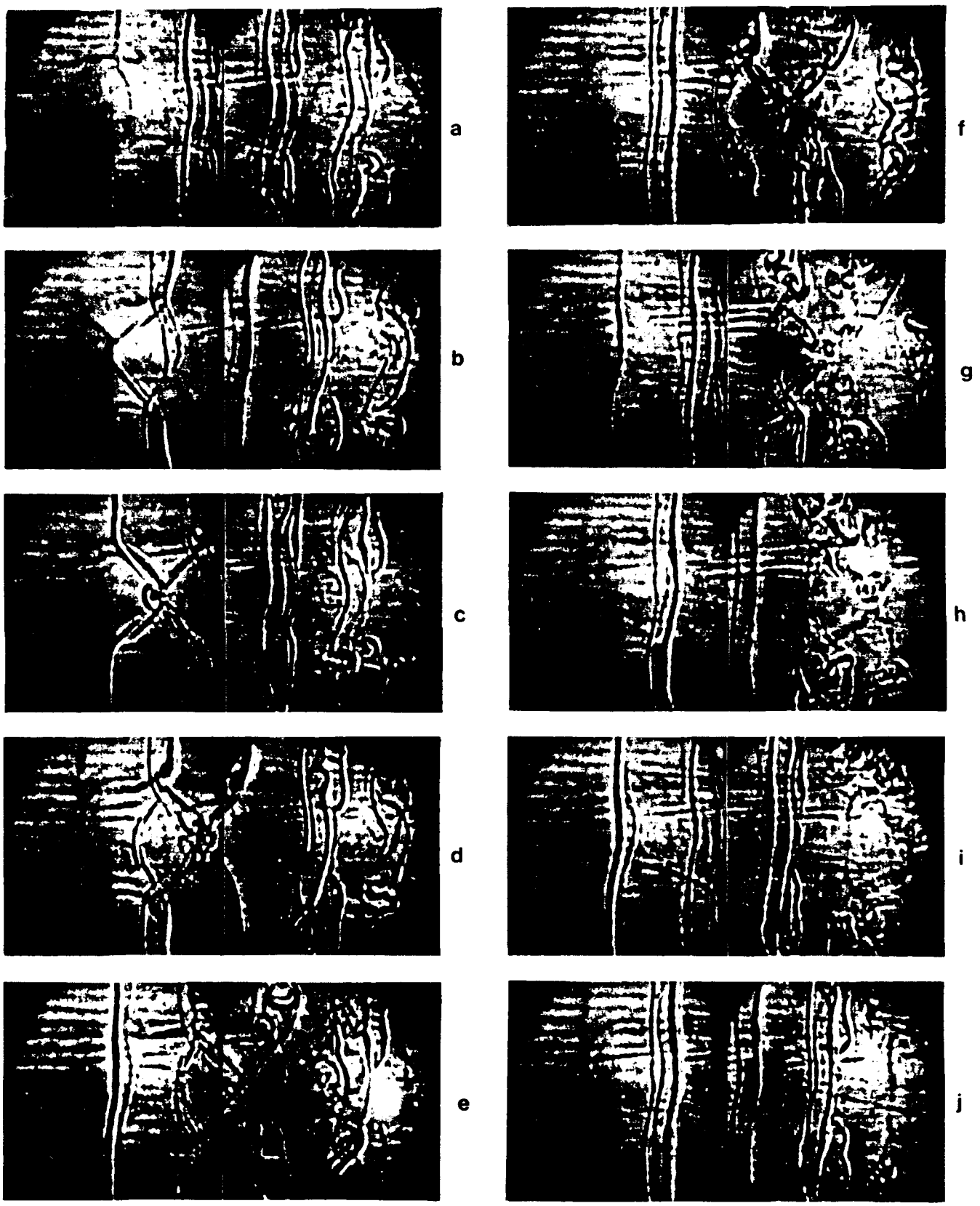

Figure 5.2

streamwise domain of each composite is 10 mm < x < 218 mm (the first rollup of the spanwise vortices in the absence of the disturbance occurs at x ≅ 50 mm). The Schlieren images were obtained from a high-speed (1000 frames per second) video movie. The time interval between two consecutive composites is 0.1 sec (≅ T/2). Figure 5.2(*a*) was taken before the pulsed disturbance appeared in the field of view, and the primary vortices are uniform along the span. In figure 5.2(*b*), the disturbance is seen at the left-hand (upstream) edge, and the deformation of the primary vortex immediately downstream of the disturbance is visible. The pulsed disturbance first appears in the braid region between two spanwise vortices, as shown in figure 5.2(*c*), and leads to an "X"-shaped vortex, which is connected with the upstream and downstream spanwise vortices. In figure 5.2(*d*), the vortex structure upstream of the "X"-shaped vortex forms a diamond-shaped cell around midspan. Note that the spanwise domain of influence of the disturbance is still limited at this streamwise station. The primary vortex upstream of the disturbance is apparently not affected by the pulse, as can be seen from figure 5.2(*e*). Figures 5.2(*f-j*) show that the pulsed disturbance spreads symmetrically along the spanwise direction as it is advected downstream, and it seems to lead to a local pairing of the two adjacent primary vortices, which is accompanied by the generation of small-scale motions. One can expect that the domain of influence of the pulsed disturbance is characterized by higher turbulence levels compared to the two-dimensional base flow. Figure 5.2(*j*) shows that the primary vortex upstream of the pulsed disturbance is remarkably uniform along its span. Figures 5.2(*a-j*) clearly indicate that the streamwise domain of influence of the pulsed disturbance is limited to 1-2 wavelengths of two-dimensional base flow.

5.4. *The Phase-Averaged Pulsed Disturbance*

The streamwise variation of the momentum thickness, $\theta(x)$, of the flow when it is subjected to two-dimensional time-harmonic excitation is shown in figure 5.3. The

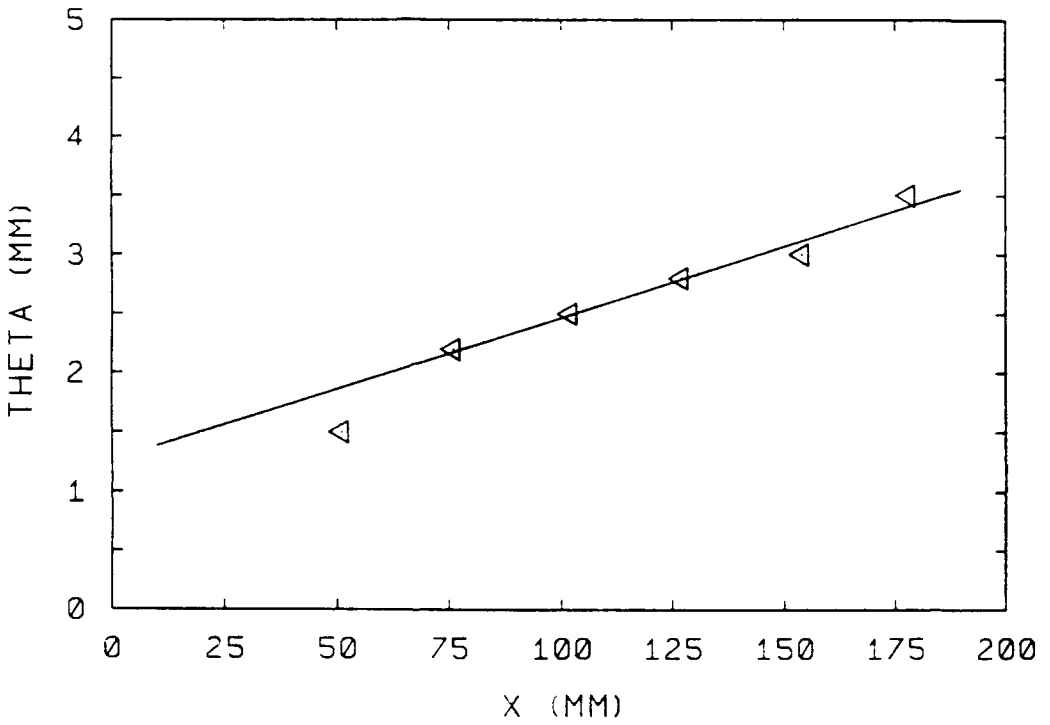

Figure 5.3

momentum thickness is calculated from the time-averaged data of ensemble-averaged velocity records. The slope of the linear fit to the data is $d\theta/dx \cong 0.012$ and, for $x > 76$ mm ($1.9\lambda_0$), θ increases linearly with x. At $x = 178$ mm ($4.45\lambda_0$) , $\theta \cong 3.5$ mm, which is approximately twice the value at $x = 51$ mm. Hence, within the streamwise domain of the measurements, the Reynolds number, based on $\theta(x)$ and the averaged free-stream velocity of the base flow U_c, varies from 300 to 700. Time-averaged cross-stream profiles of the streamwise velocity U(x), for 51 mm < x < 178 mm, are shown in figure 5.4 in similarity variables $(y-y_0)/2\theta$ ($U = U_c$ @ $y = y_0$) and $(U-U_1)/(U_2-U_1)$. Almost all data points fall onto a single curve, which means that the streamwise velocity profiles of the base flow are self-similar. The spanwise uniformity of the base flow is illustrated by surface plots of time-averaged streamwise velocity, U(x), in the y-z plane at x= 76, 127, and 178 mm, in figure 5.5. The base flow is quite uniform across the span at upstream stations and becomes slightly distorted farther downstream due to small imperfections in the experimental apparatus.

Surfaces of ensemble-averaged cross-stream velocity profiles, $\langle u(x;t) \rangle$, measured at midspan (z=0) at x= 76, 127, and 178 mm, are shown in the y-t plane in figure 5.6. Note that, in the absence of the disturbance, the phase of the streamwise velocity fluctuations across the mixing layer changes approximately by π, as can be seen, for example, by following a line of constant time when the velocity perturbation has a peak on the high-speed side and a valley on the low-speed side. The temporal change in the streamwise velocity due to passage of the pulsed disturbance is clearly distinguishable from the response to the time-harmonic wave train, and is felt across the entire width of the shear layer. Of particular note is the temporal evolution of the three velocity peaks on the high-speed side associated with passage of the disturbance at the measurement station. These peaks appear closer in time farther downstream, indicating a possible occurrence of "local pairing" of the primary vortices.

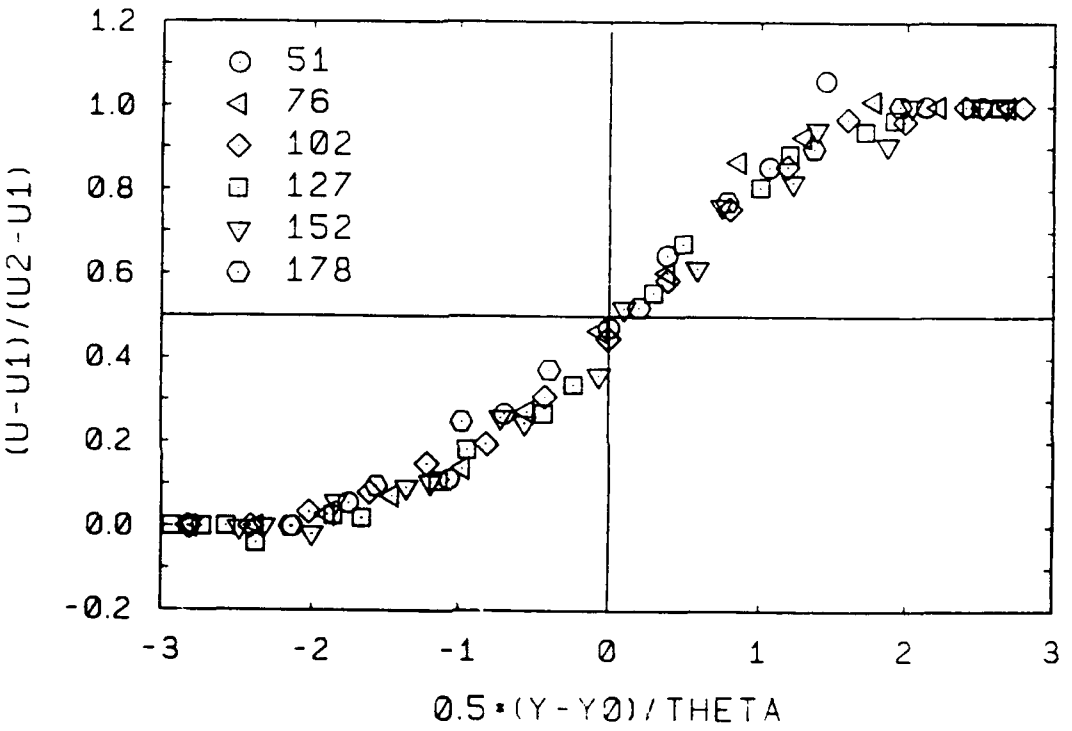
1.2
1.0
0.8
0.6
0.4
0.2
0.0
-0.2
(U-U1)/(U2-U1)
51
76
102
127
152
178
-3
-2
-1
0
1
2
3
0.5*(Y-Y0)/THETA

Figure 5.4

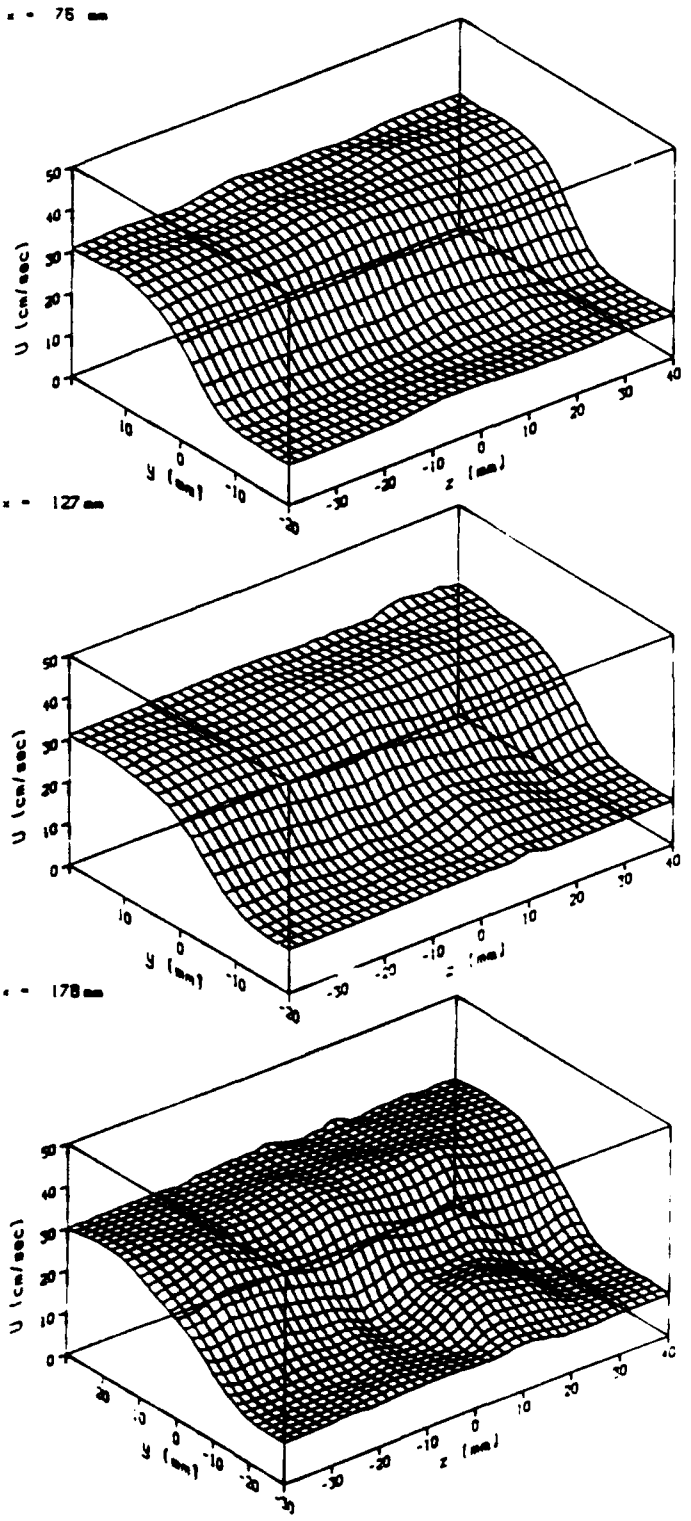
x = 76 mm
U (cm/sec)
y (mm)
z (mm)
x = 127 mm
U (cm/sec)
y (mm)
z (mm)
x = 178 mm
U (cm/sec)
y (mm)
z (mm)

Figure 5.5

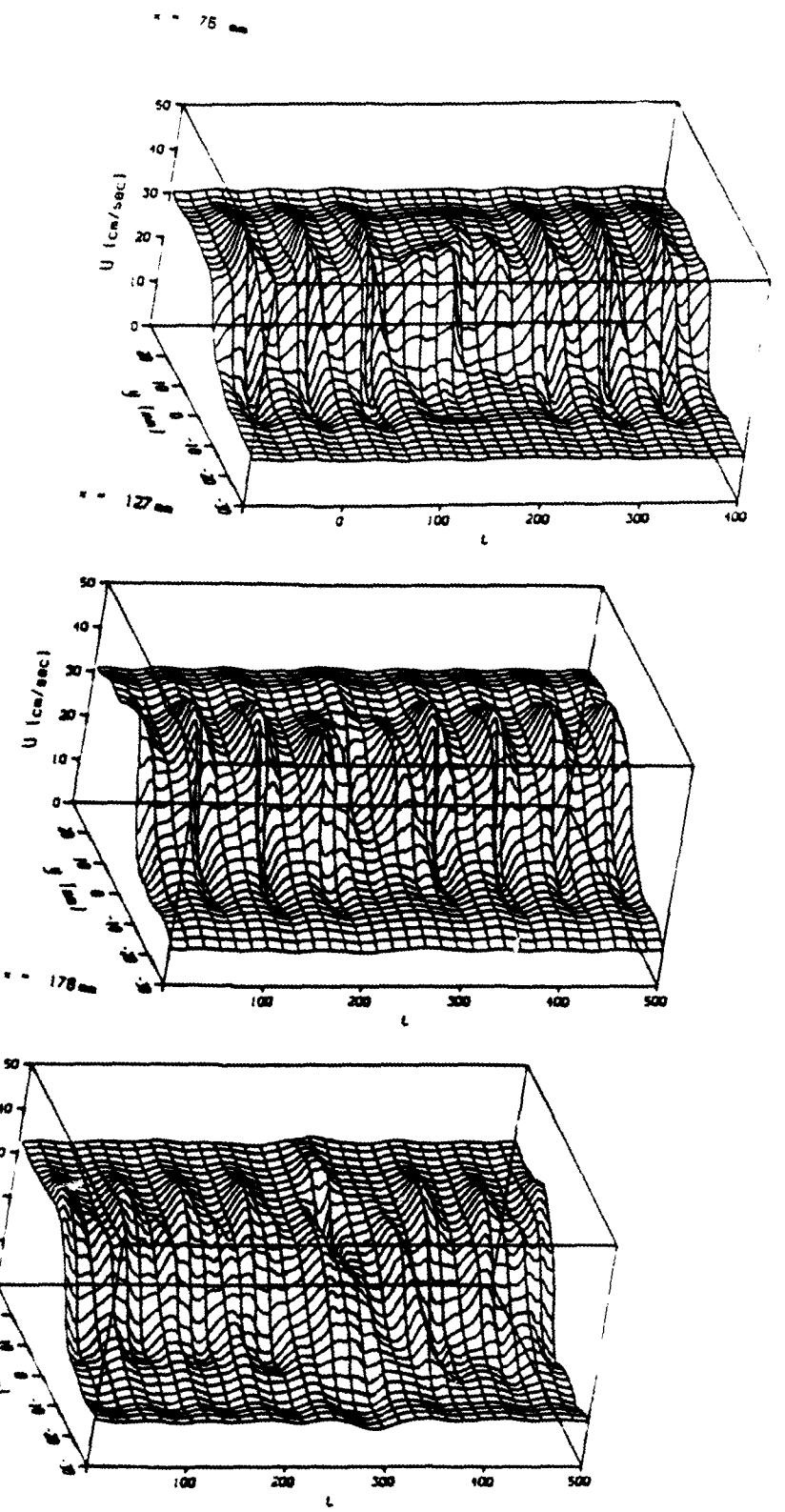

Figure 5.6

Ensemble-averaged profiles of the streamwise velocity perturbations, $\langle u_{pert}(x,t)\rangle = \langle u(x,t)\rangle - U(x)$, in the z-t plane y = 10 mm at x = 76, 127, and 178 mm, respectively, are shown in figure 5.7. Spanwise profiles of $\langle u_{pert}\rangle$ are plotted at equally spaced time intervals in figure 5.7(*a*), while time series of $\langle u_{pert}\rangle$ are plotted at equally spaced spanwise stations in figure 5.7(*b*). These data emphasize temporal and phase variations, respectively. Figure 5.7 shows that the pulsed disturbance affects approximately three wavelengths of the fundamental wave train, and outside of this domain of influence the time-harmonic wave train is spanwise-uniform. The pulsed disturbance is advected downstream at approximately U_c, as can be determined from the delays in its arrival time at the downstream measurement stations. The "X"-shaped disturbance spreads both in time (and thus in x) and in the spanwise (z) direction as it is advected downstream and, at x = 178 mm, it affects the entire spanwise width of the measurement domain. The streamwise length of the pulsed disturbance, however, does not seem to grow as dramatically and appears to be limited by the fundamental instability of the base flow. A similar observation was also made by Glezer *et al.* (1989) regarding a two-dimensional disturbance. Dallard & Browand (1992), who studied the evolution of vortex structure of plane mixing layers in the vicinity of a vortex dislocation, reported that the vortical "defect" grows more rapidly in the spanwise direction than in the streamwise direction--thus preserving a tendency for two-dimensionality.

The evolution of the pulsed disturbance is studied using surface plots of $\langle u'_{trms}(x,t)\rangle$ in y-z-t coordinates (figures 5.8*a-c* measured at x = 76, 127, and 178 mm, respectively) and plotted during three periods of the excitation wave train. These data allow for a detailed study of the three-dimensional features of the flow structure induced by the disturbance and its interaction with the spanwise vortices. As demonstrated by the photographs of figure 5.2, at x = 76 mm, an "X"-shaped structure is formed in the braids region, between two adjacent primary vortices, that is connected

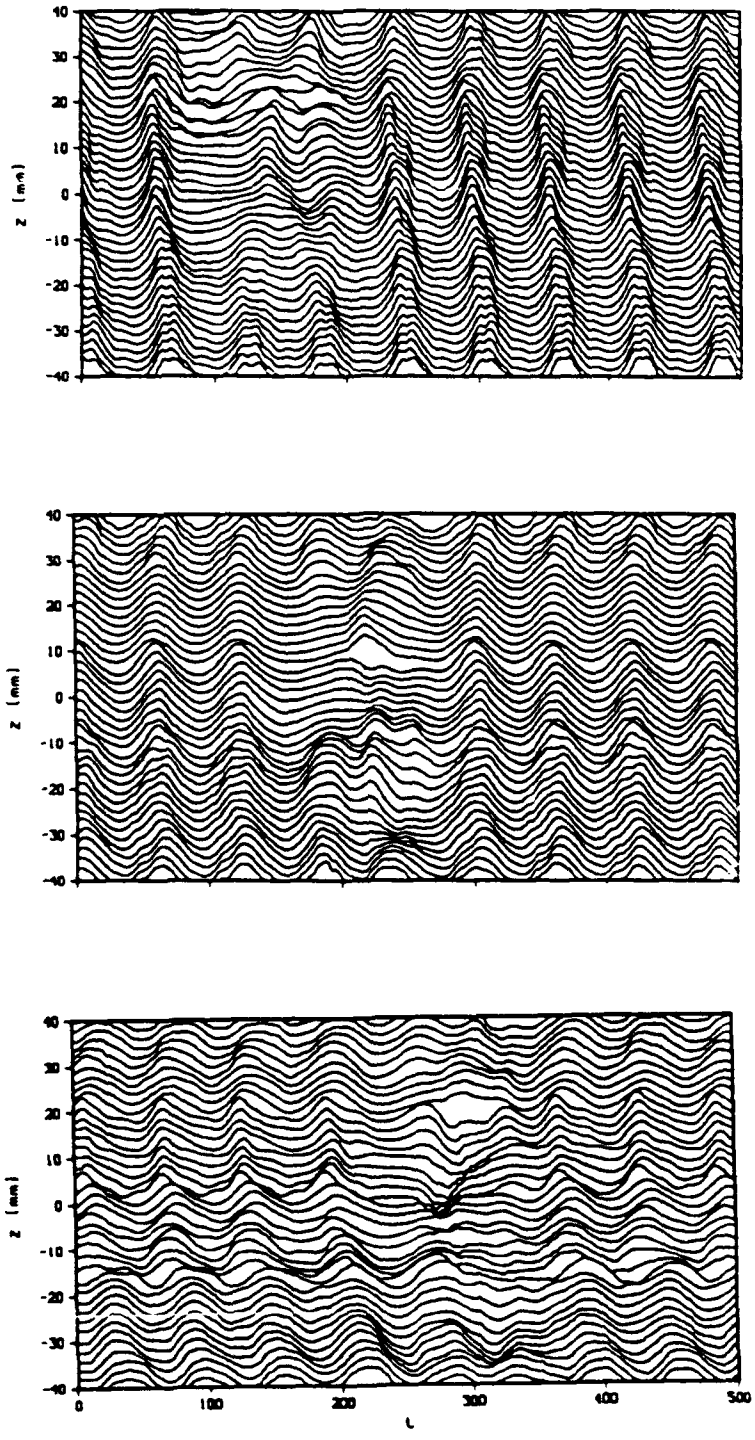

Figure 5.7a

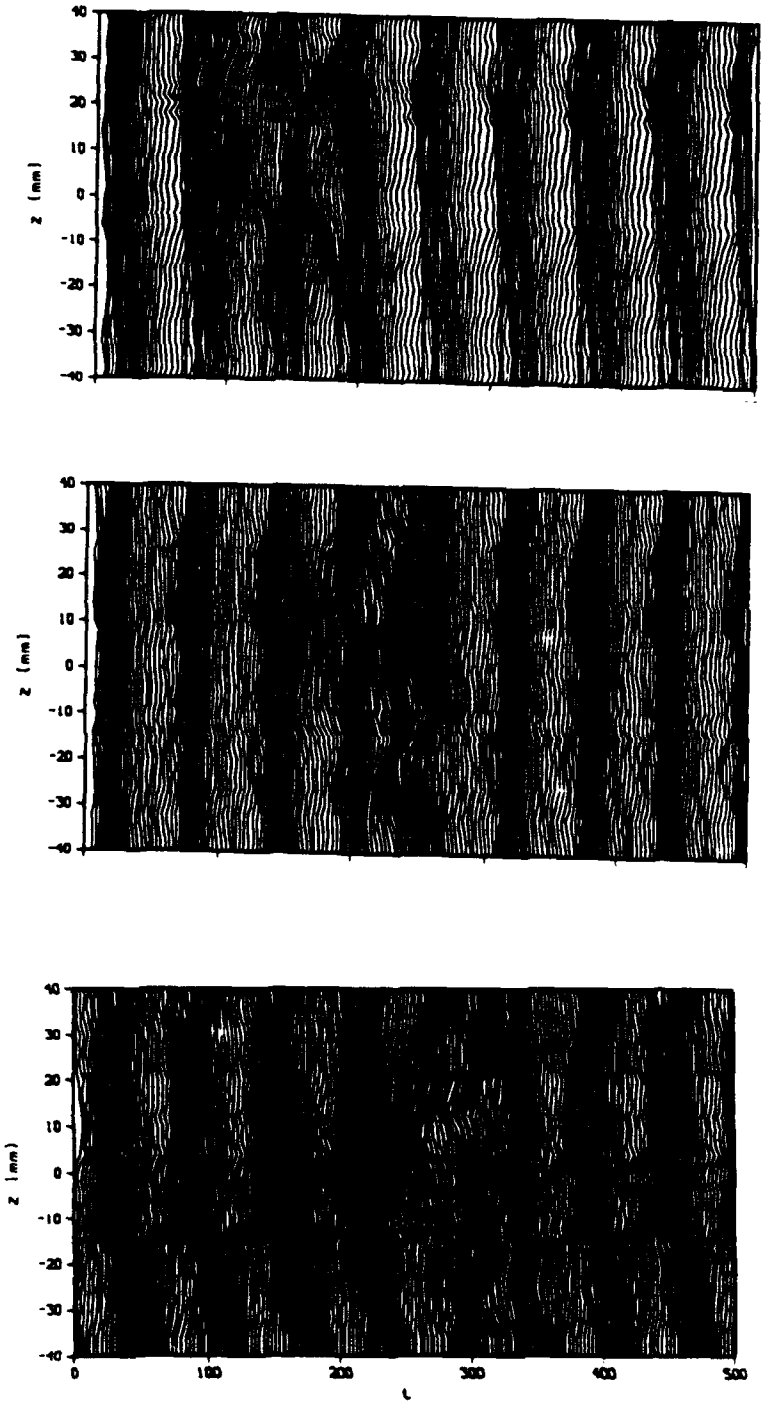

Figure 5.7b

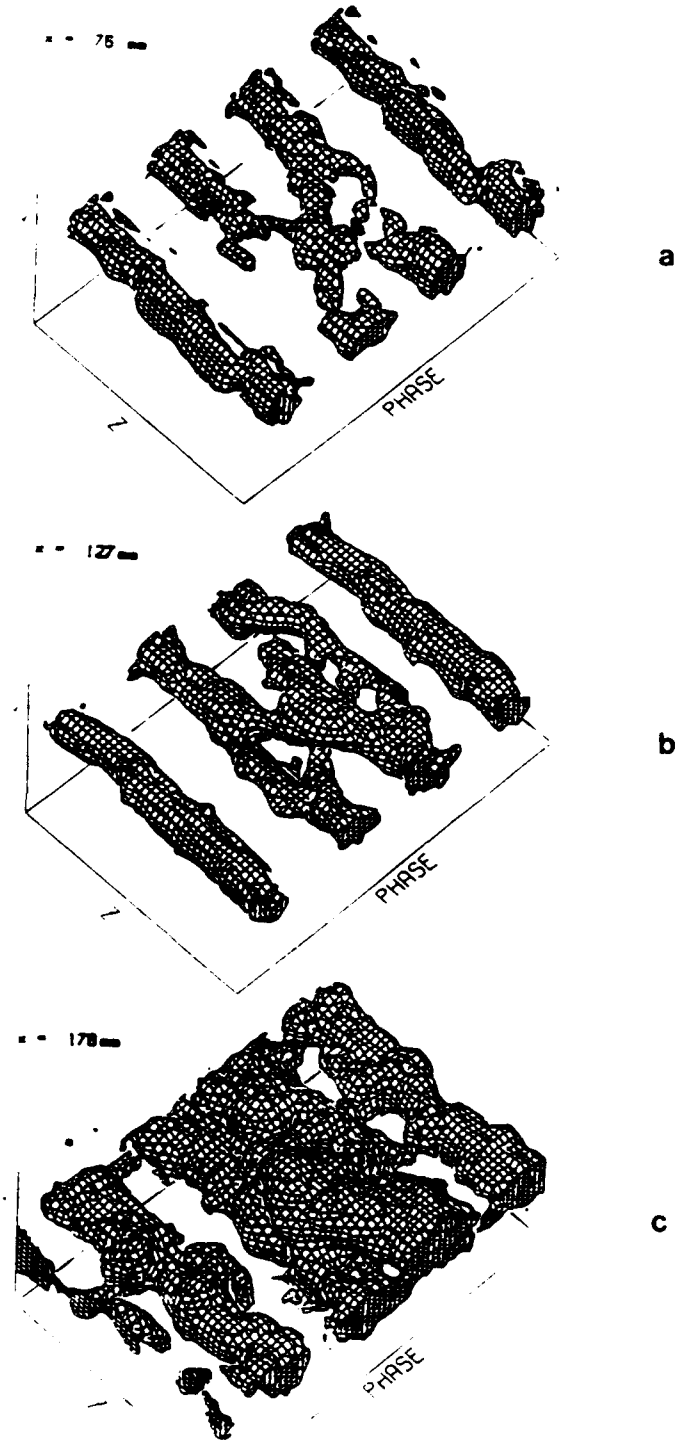

a

b

c

Figure 5.8

with the upstream and downstream primary vortices. Farther downstream (x = 127 mm), the central region of the "X" structure moves closer to the high-speed side and appears to be catching up with the downstream primary vortex in a way that resembles spanwise-localized pairing. This process is accompanied by a striking increase in rms velocity fluctuations induced by the disturbance (x = 178 mm).

Contours of $\langle u'_{trms}(x,t)\rangle$ in the y-t plane z = 0, at x = 76, 127, and 178 mm, are shown in figure 5.9. At x = 76 mm, the cross-stream width of the disturbance is comparable to that of the harmonically forced flow, and it appears between two vortices of the base flow. The elapsed time between passage of primary vortices upstream and downstream of the disturbance corresponds to three wavelengths of the fundamental wave train. At x = 127 mm, the cross-stream extent of the pulsed disturbance is approximately 1.5 times that of the two-dimensional wave train, and local pairing of the spanwise vortices is apparent during passage of the disturbance. At x = 178 mm, the disturbance is about twice as wide in the cross-stream direction as in the harmonically forced flow. Furthermore, the turbulence intensity within the pulsed disturbance is much higher than at the upstream locations.

The spanwise spreading rate of the disturbance may be inferred from the distortion of the shape of the streamwise velocity profiles of the nominally two-dimensional base flow. A cross-stream integral measure of such distortion is the temporal momentum thickness, $\Theta(x,z;t)$, defined as

$$\Theta(x,z;t) = \int_{-\infty}^{+\infty} \tilde{U}(x;t)[1 - \tilde{U}(x;t)]dy$$

where

$$\tilde{U}(x;t) = \frac{U(x;t) - U_1}{U_2 - U_1}$$

and

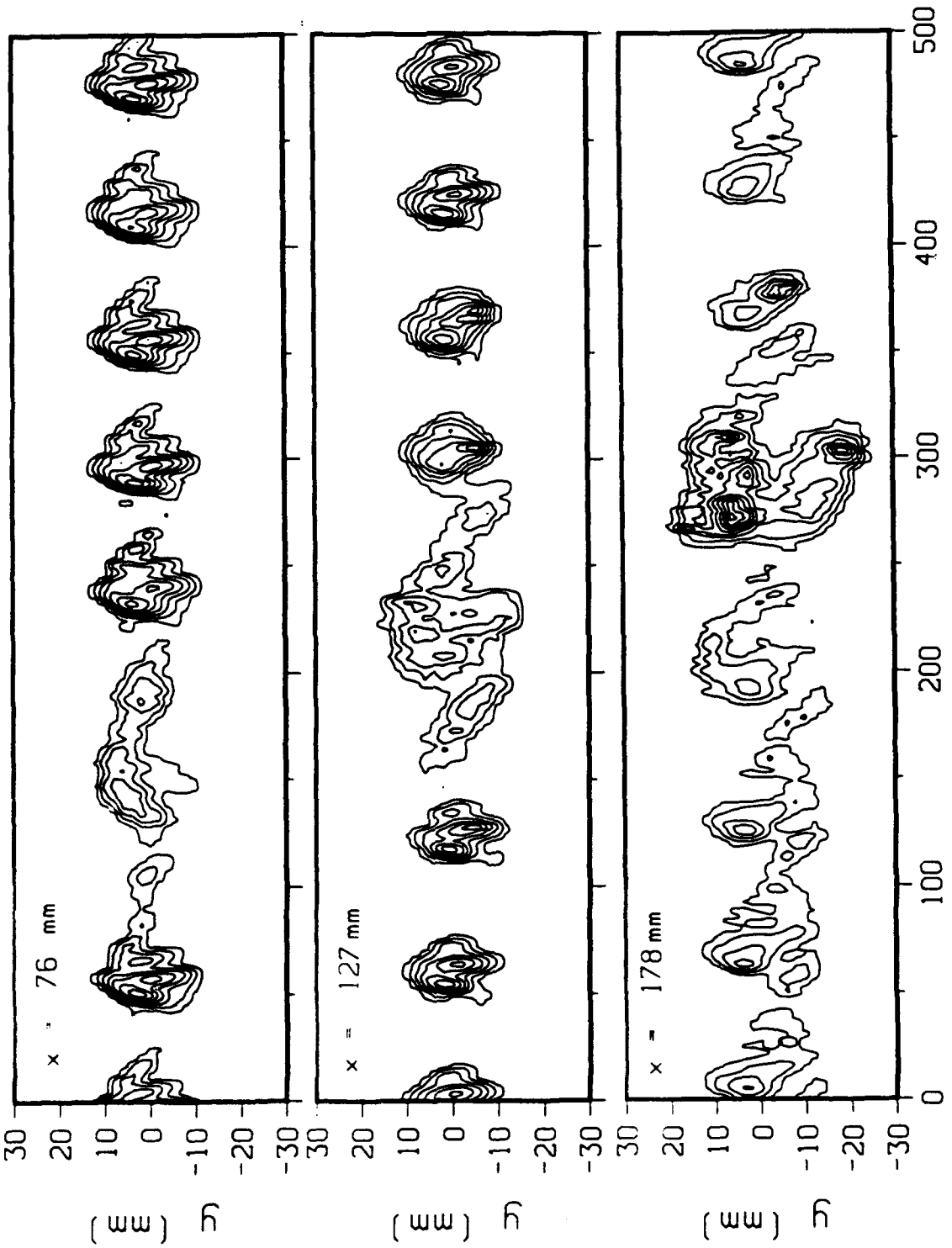
x = 76 mm
x = 127 mm
x = 178 mm
y (mm)
30
20
10
0
-10
-20
-30
0
100
200
300
400
500
t

Figure 5.9

$$U(x;t) = \frac{1}{T_f} \int_{t-T_f/2}^{t+T_f/2} \langle u(x;\tau) \rangle d\tau \quad .$$

It should be noted that, if the entire integration interval of the last equation is well removed from the disturbance, or if the flow is excited by the carrier signal only, $U(x;t) = U(x)$ and thus $\Theta(x,z) = \theta(x,z)$. Figure 5.10 is a sequence of contour plots of $\Delta\theta(x,z;t) = \Theta(x,z;t) - \theta(x,z)$ at a number of streamwise stations. In each frame, $\Delta\theta(x,z;t)$ is shifted in time by $\Delta x/U_c$. The contours in each frame, for a given x, are shown in the z-t plane. Although an estimate that is based on an integral measure of the distortion of the base flow may be conservative, it exhibits a strong spreading rate in the spanwise direction. The slope $\Delta z/\Delta x \cong 0.2$, indicating that the disturbance spreads in both spanwise directions at a speed approximately equal to $0.2U_c$.

5.5. *Demodulation of the Pulsed Disturbance: The Fundamental Wave Packet*

A demodulation technique is used to discriminate between the response of the flow to the carrier signal and to the modulating pulse (see Appendix), and to decompose the response of the flow to pulsed excitation into a family of modal wave packets.

Cross-stream distributions of amplitude and phase of streamwise velocity fluctuations at the forcing frequency ν_f are shown in figure 5.11 (solid lines) for 6 streamwise stations. These data correspond to a *single* frequency component in the power spectrum of $\langle u_{pert} \rangle$. Figure 5.11(*a*) shows that the amplitude of the streamwise velocity fluctuations decays exponentially with y when the base flow is subjected to two-dimensional time-harmonic excitation. The phase of the streamwise velocity fluctuations of the base flow changes continuously across the mixing layer, and the phase difference across the shear layer is approximately 180° (figure 5.11*b*). This phase reversal is caused by the two-dimensional spanwise primary vortices. Also shown in figure 5.11 (using symbols) are cross-stream profiles of the amplitude, A_{c_0}, and the

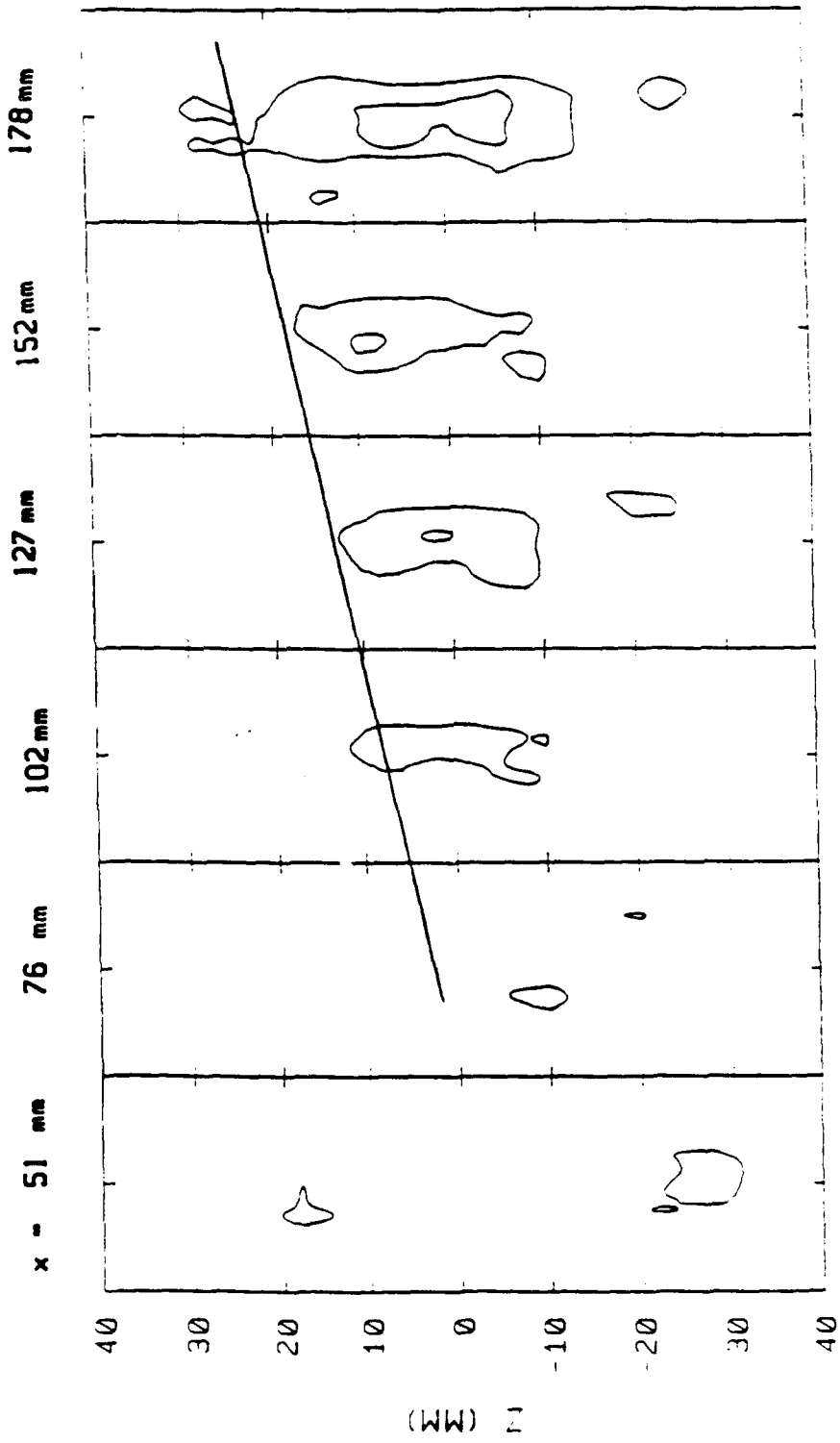

Figure 5.10

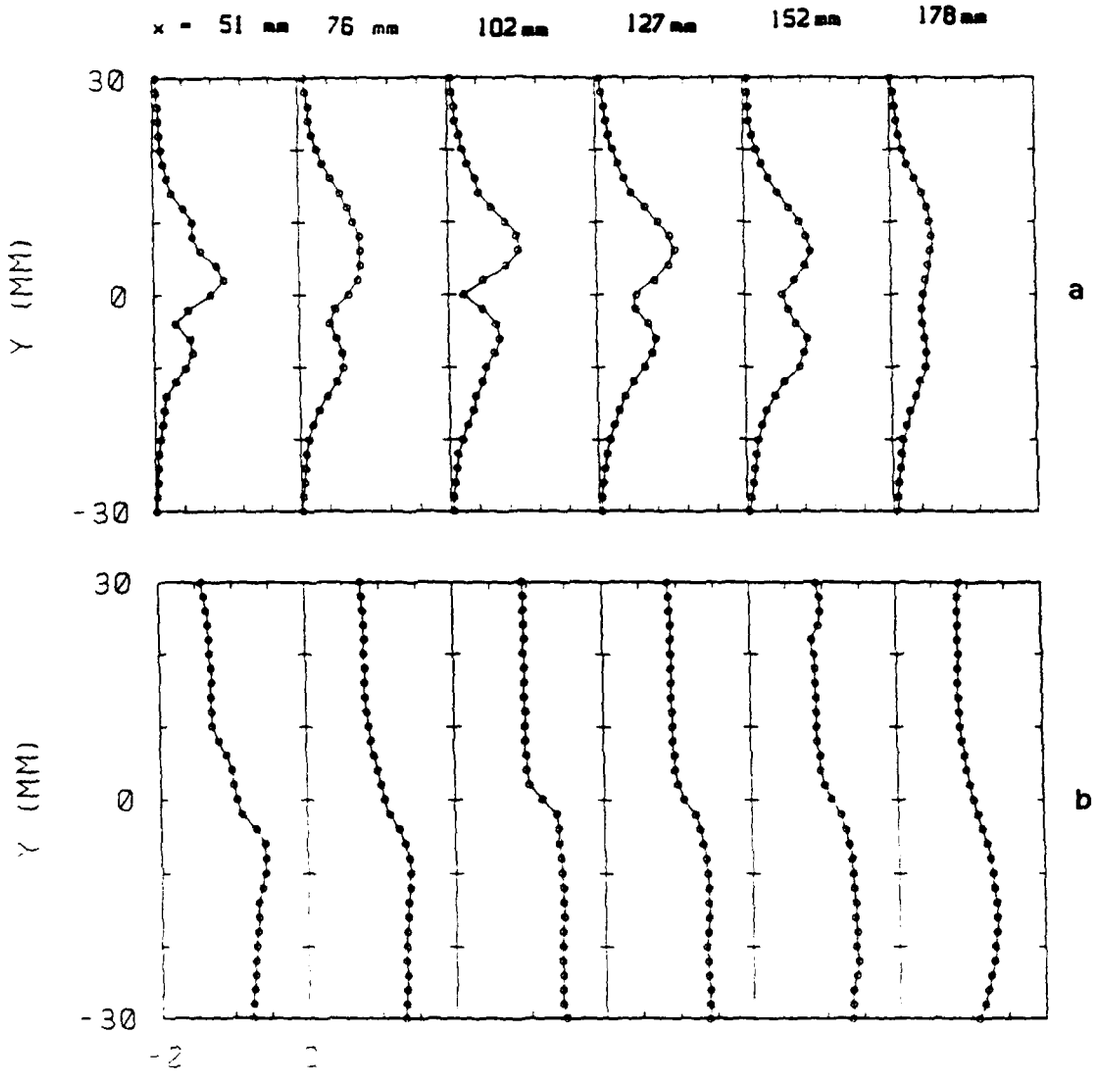

Figure 5.11

phase, Ψ_{c_0}, of a modulated velocity signal, $S_0(x,t)$, when the flow is subjected to time-harmonic excitation. The excellent agreement between the pairs of profiles is noteworthy because $S_0(x,t)$ includes *all* spectral components within the frequency band, $\Delta\omega$, centered at the fundamental frequency, ν_f. This indicates that much of the spectral broadening around the forcing frequency and its higher harmonics is due to the pulsed amplitude modulation of the harmonic excitation signal. It should also be mentioned that the calculation of the amplitude and the phase of $S_0(x,t)$ is actually a one-dimensional wavelet transform in time at the fundamental frequency (see Appendix). The wavelet transform, however, cannot discriminate between the wave packet and the harmonic wave train.

Perspective views of the fundamental wave packet, $W_{p_0}(x,t)$, at a fixed cross-stream elevation in the z-t plane are shown in figure 5.12 for 6 streamwise stations, 25.4 mm apart (51 mm < x < 178 mm). Also shown in figure 5.12 are the corresponding contour plots of $W_{p_0}(x,t)$. Note that, at the first 3 upstream stations, the packet has one peak close to its center, while farther downstream (x = 152 mm), the packet develops two peaks away from its spanwise center. At x = 178 mm, there are a number of spanwise maxima having a spanwise wavelength of approximately 12.5 mm ($\cong 0.31\lambda_{KH}$). The wave packet apparently develops nonlinear characteristics, which subsequently lead to its breakdown to turbulence. It is interesting to note that, in contrast to wave packets in boundary layers where wave fronts in the spanwise direction are highly curved (Gaster & Grant 1975), the wave fronts within the packet in the plane shear layer are almost parallel to the spanwise direction.

Similar to figure 5.7, profiles of velocity perturbations associated with the fundamental wave packet are plotted in the y-t plane z = 0 (figure 5.13) for x = 76, 127, and 178 mm. Amplitude features of the packet are emphasized using a time sequence of cross-stream profiles, while cross-stream phase features are emphasized using time profiles at a number of equally spaced cross-stream elevations. The amplitude of the

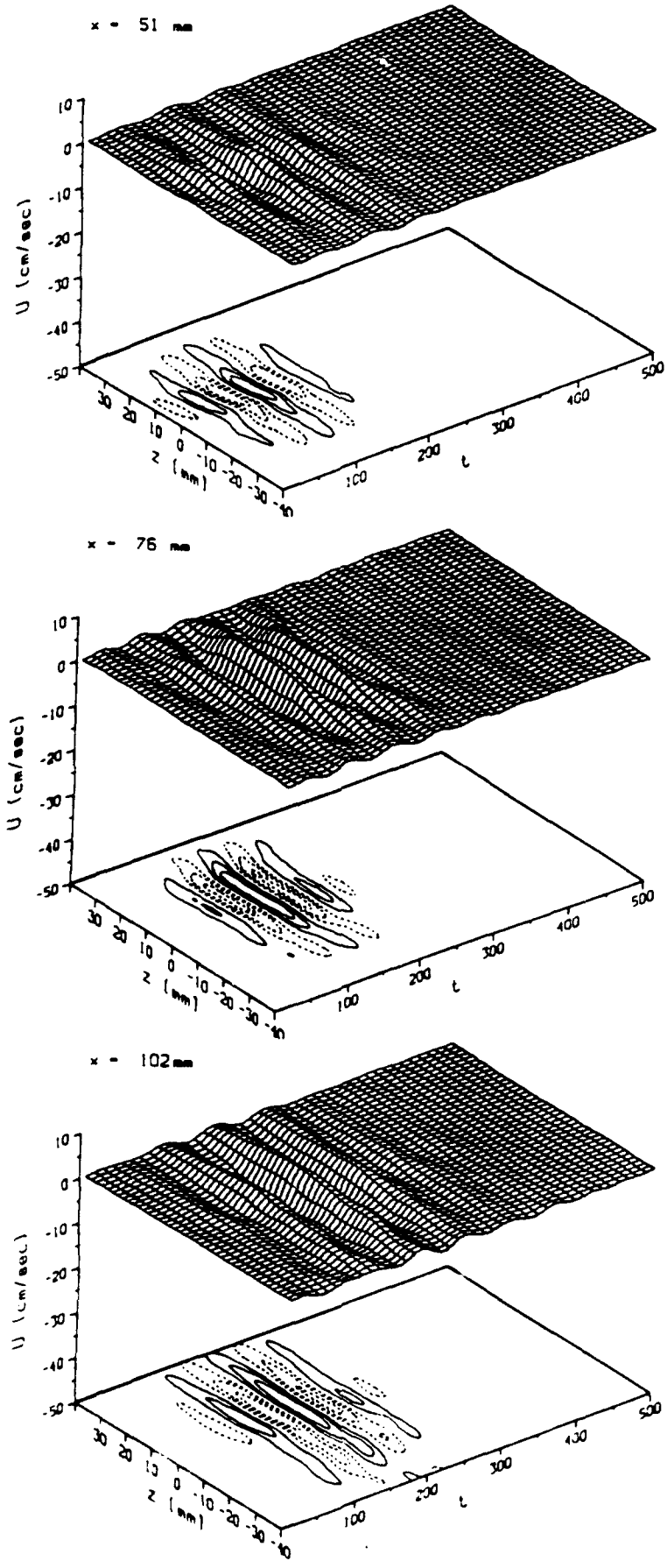
x = 51 mm
x = 76 mm
x = 102 mm
U (cm/sec)
z (mm)
t
10
0
-10
-20
-30
-40
-50
30
20
10
0
-10
-20
-30
-40
100
200
300
400
500

Figure 5.12a

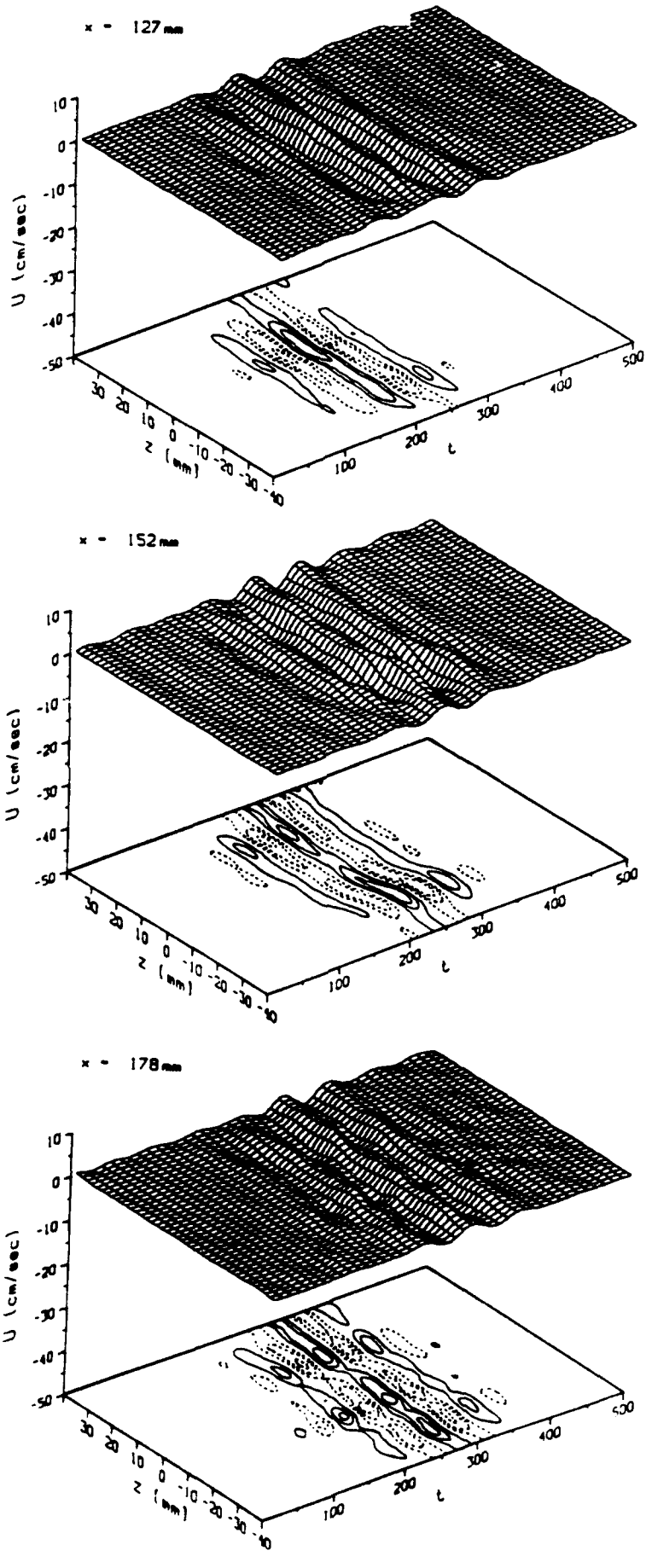
x = 127 mm
x = 152 mm
x = 178 mm
U (cm/sec)
10
0
-10
-20
-30
-40
-50
z (mm)
30
20
10
0
-10
-20
-30
-40
t
100
200
300
400
500

Figure 5.12b

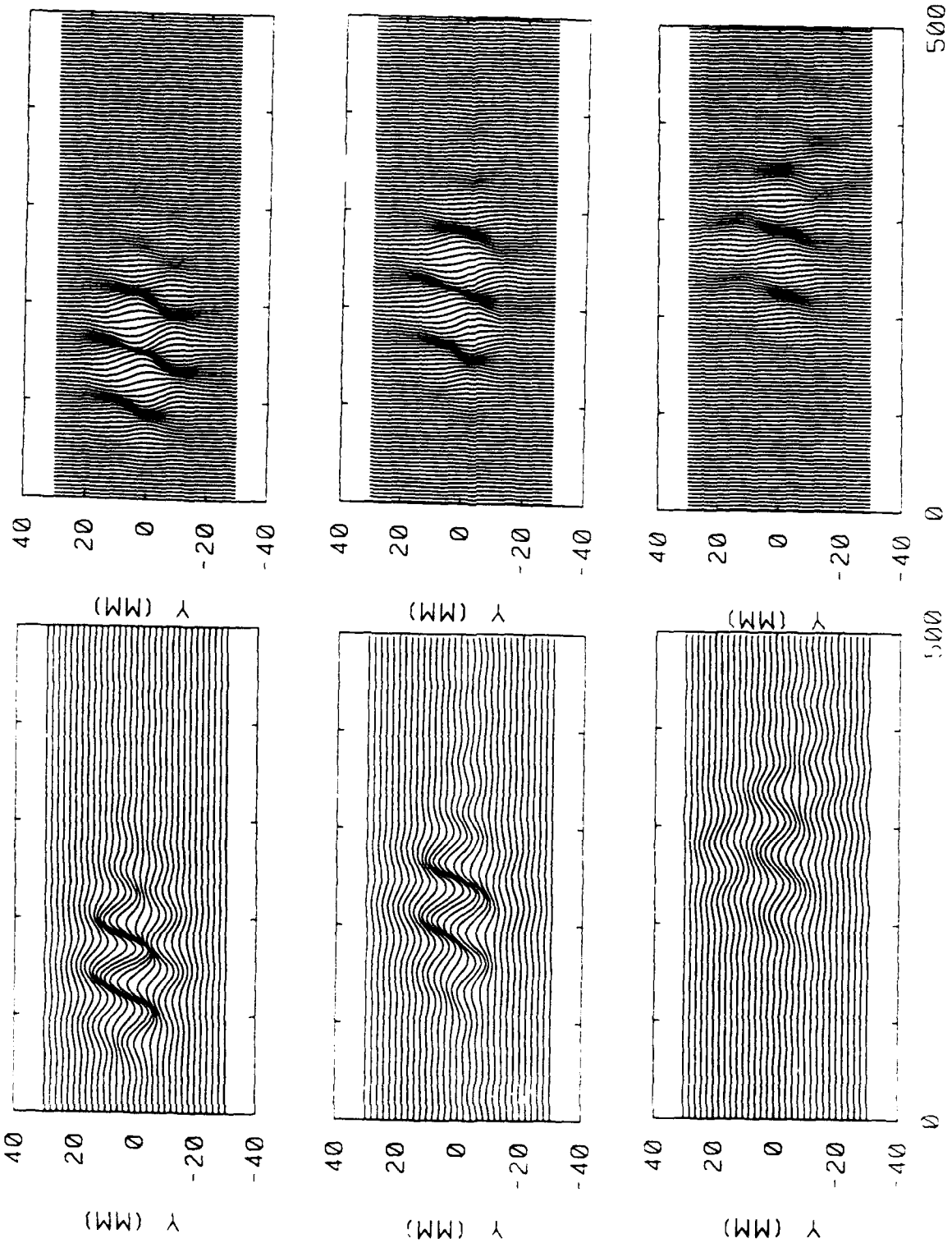

Figure 5.13

packet is largest near $y = 0$, and it decreases with downstream distance. Similar to the two-dimensional base flow, the cross-stream phase shift is approximately π.

The spanwise spreading rate of the packet is measured using the spanwise expansion of a selected contour level at a given cross-stream elevation. The packet's envelope at $y = 10$ mm at each streamwise station is normalized to the local maximum, and the spanwise extent of the contour level, 0.6, is used to determine the streamwise spreading. Figure 5.14 shows that the spreading is approximately linear with downstream distance, having a slope $2\Delta z/\Delta x = 2U_z/U_c = 0.4$, where U_z is the spanwise spreading velocity of the fundamental wave packet in either spanwise direction and $U_z = 0.2U_c$. This is consistent with the momentum thickness measure (§5.4).

We next determine the dispersion relation for the fundamental wave packet. Since there is no traveling wave in the cross-stream direction for plane mixing layers, the wave number component α_y may be ignored. Because the packet in the plane shear layer appears to be almost two-dimensional, we postulate that α_z must be very small compared to α_x. Therefore, only the streamwise wave number α_x was determined by measuring the streamwise variation of phase for a given frequency ω. This method is also used by Corke & Mangano (1989) in a Blasius boundary layer. Figure 5.15(*a*) shows the streamwise variation in phase of the time-harmonic wave train at the fixed (y,z) station for different frequencies. For a given ω, the corresponding (local) wave number α_x is determined by the (local) slope of the curve fitted to the same set of data (figure 5.15*a*). Since all local slopes in figure 5.15(*a*) are the same, α_x is independent of x. The normalization with ω_f/ω in figure 5.15(*a*) is helpful because for, a non-dispersive wave, all data in figure 5.15(*a*) should fall onto one straight line, the slope of which is the wave number α_f:

$$\frac{\Delta\phi(\omega)}{\Delta x}\,\frac{\omega_f}{\omega} = \alpha_x(\omega)\,\frac{\omega_f}{\omega} = \frac{\omega_f}{V_{cr}(\omega)} = \frac{\omega_f}{V_{cr}(\omega_f)} = \alpha_f.$$

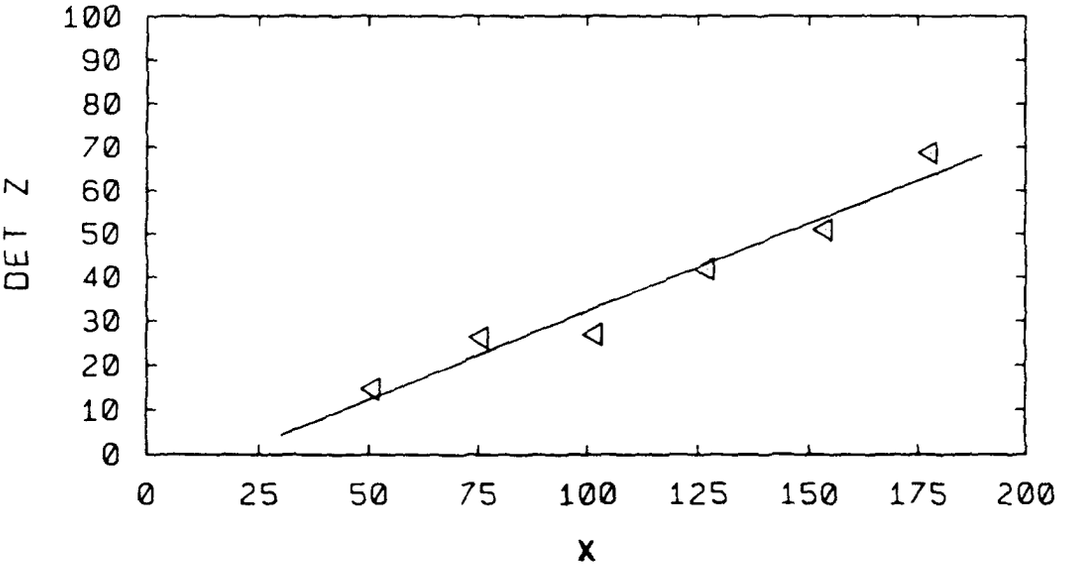

Figure 5.14

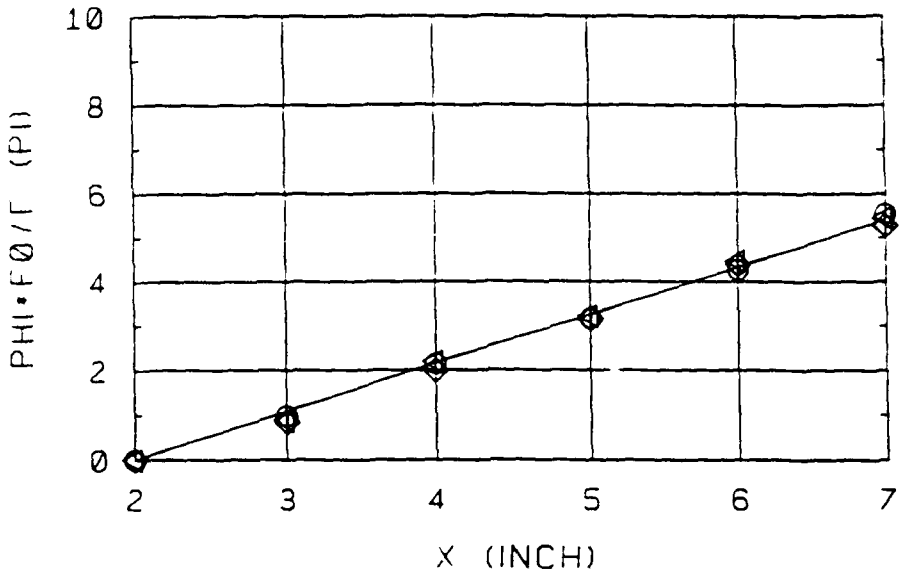

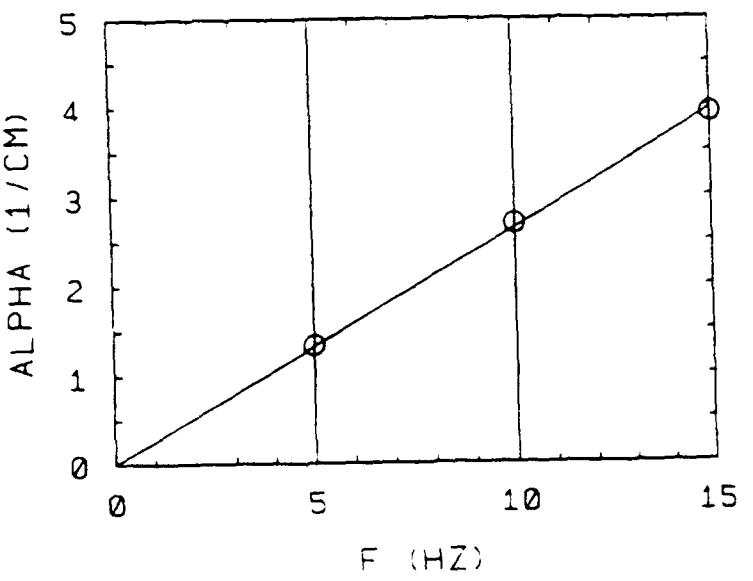

Figure 5.15

where the subscript f indicates a reference to the fundamental frequency of the time-harmonic wave train and V_{cr} is the crest velocity.

The dispersion relation for the time-harmonic wave train is shown in figure 5.15(*b*). The crest velocity, $V_{cr} = \omega/\alpha_x$ (which is also the phase velocity for one-dimensional plane waves), is constant for all frequencies. The group velocity is also equal to the crest velocity, as can be seen from the straight line in figure 5.15(*b*), meaning that wave trains at different frequencies all travel at the same speed.

Similarly, the streamwise development of the phase of the fundamental wave packet is shown in figure 5.16(*a*) for frequencies within the band-pass filter, and the dispersion relation of the wave packet is shown in figure 5.16(*b*). The crest speed of the wave packet at a given frequency within the frequency window is the same as the speed of the packet. Hence, the wave packet is non-dispersive, and kinematic wave theory may be applied (Landahl 1982). Balsa (1988) pointed out that, for free shear layers subjected to two-dimensional external excitation, the unstable modes are non-dispersive. The phase speed of the packet is $(U_1+U_2)/2 = const$, and its streamwise spreading arises from variations in the growth rate rather than from variations in phase velocity with wave number. The present experimental results are in general agreement with his conclusions.

5.6. *Temporally and Spanwise-Periodic Pulsed Disturbances*

A spanwise and streamwise staggered pattern of three-dimensional pulse trains is superimposed on a two-dimensional time-harmonic wave train ($\nu_f = 6$ Hz), as shown in figure 5.17. The top frame of the figure shows a pulse train superimposed on the two-dimensional wave train and, in the bottom frame, dotted lines corresponding to peaks of the two-dimensional wave train are plotted parallel to the span. The rectangles in the bottom frame represent the relative sizes and locations of pulses in the spanwise and streamwise directions. In the present experiments, the free-stream velocities of the base

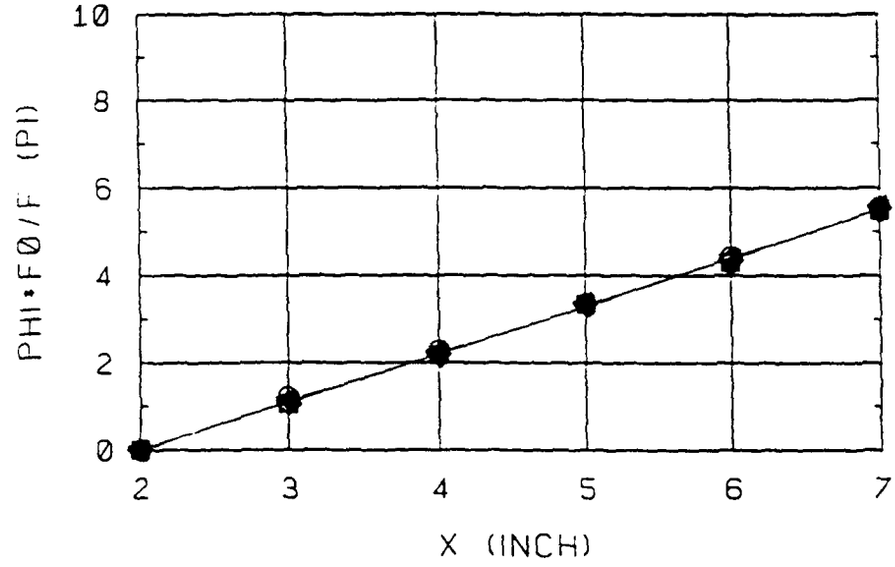

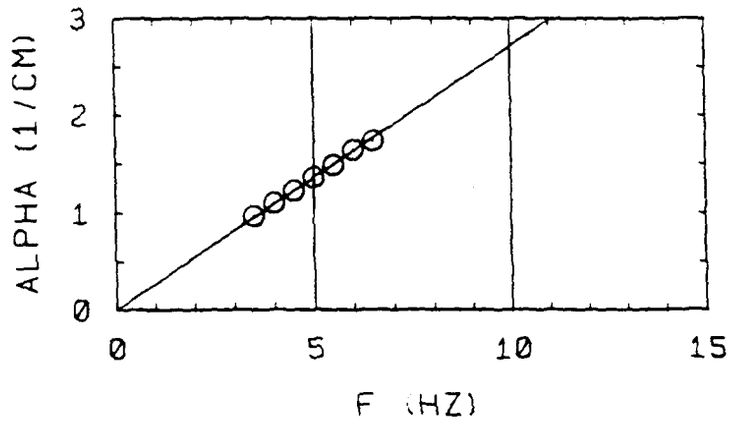

Figure 5.16

flow are 36 and 12 cm/s, and $\lambda_{(KH)} = U_c/\nu_f = 4$ cm. Similar to the procedure described in §5.2, the pulsed input to spanwise segments of four surface heaters is repeated every four cycles of the harmonic wave train (i.e, $M_p = 4$). The individual pulses are identical to the single pulse described in §5.2 (i.e., each pulse is synthesized by four heating elements, $\gamma = 5$, and the pulse duration is $0.4T_f$). As can be seen from figure 5.17, the pulse trains are spanwise periodic. Because of the rapid spanwise growth of pulsed disturbances, the smallest spanwise spacings between the (centers) of two pulse trains of the same phases are chosen to be equal to the length of 12 heating elements (76 mm), or $1.9\lambda_{KH}$. The staggered pattern is achieved by a phase shift between two adjacent pulse trains that corresponds to half a period. The spanwise range of measurement of the streamwise velocity component is 120 mm, centered at the midspan.

The surface $\langle u'_{trms} \rangle = 0.055U_c$ in the y-z-t coordinates at x = 125 mm is shown in figure 5.18. Each pulse is located in the braid region between adjacent primary vortices and induces clear deformations. The pulses form a spanwise and streamwise periodic and staggered pattern. As shown in the previous section, a single pulsed disturbance spreads rapidly in the spanwise direction. This is no longer the case when neighboring pulsed disturbances are allowed to interact. The present experiments show that the spanwise growth of the individual disturbances is quenched, and surface plots of $\langle u'_{trms} \rangle$ exhibit almost no variations with x.

Figure 5.19(*a*) shows a time sequence of spanwise profiles of $\langle u_{pert} \rangle$, measured at y = 0 and x = 125 mm, when the flow is excited with the pattern of pulsed disturbances described above. The harmonically excited flow is shown for comparison in figure 5.19(*b*). Figure 5.19(*a*) shows three spanwise pulse trains. Velocity fluctuations at the top and at the bottom of the frame are similar and in-phase, but out-of-phase with respect to the velocity perturbations at the center. The elapsed time between two peaks at z = 0, for example, is approximately equal to the period of the pulse train. Within this time, there are three cycles with relative lower amplitude. This

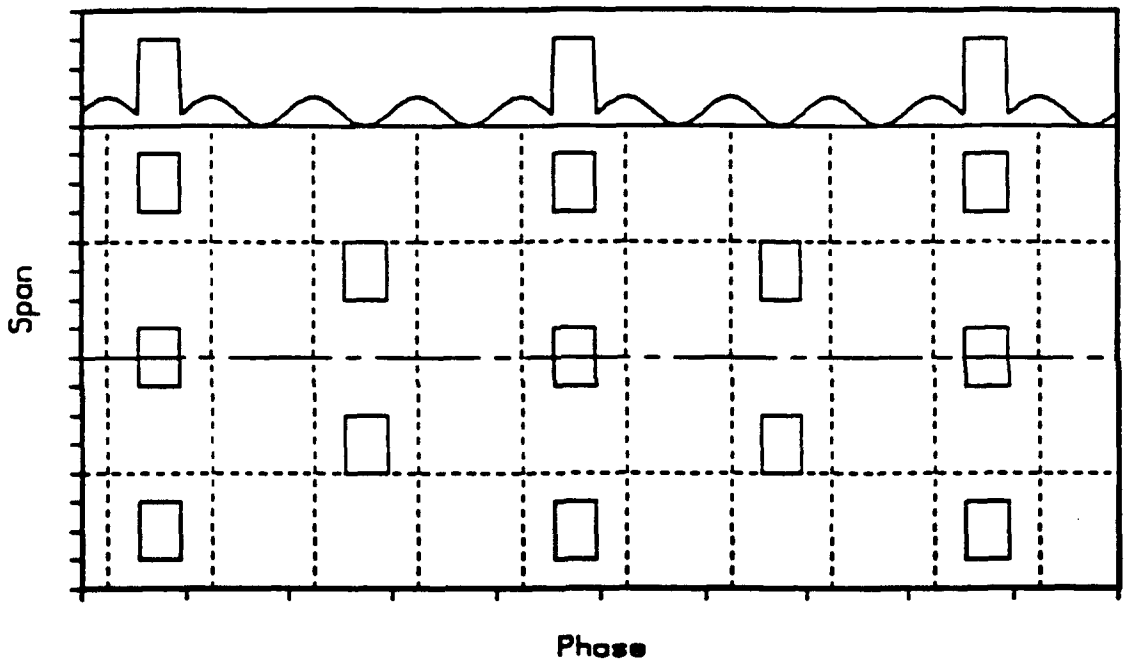

Figure 5.17

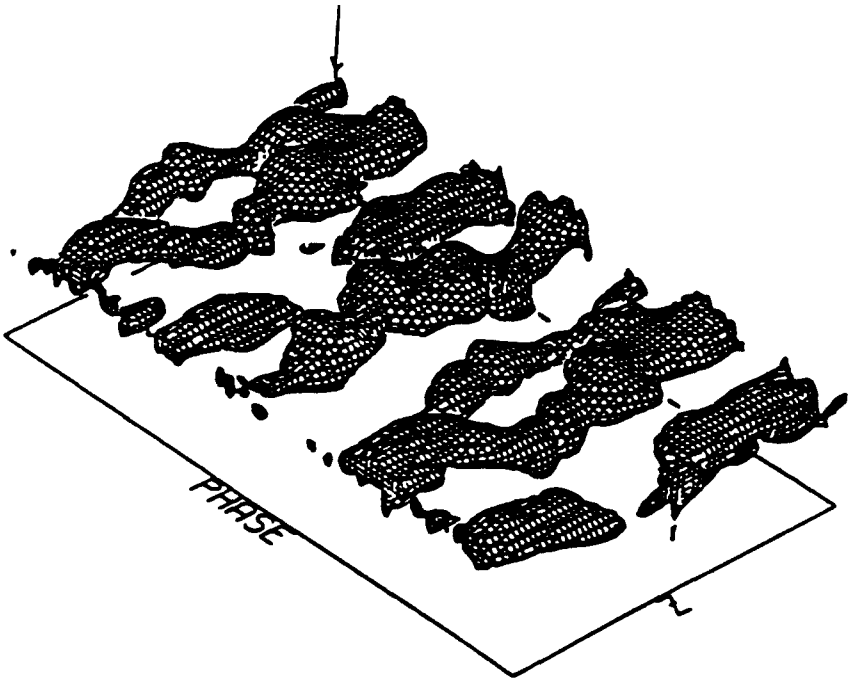

Figure 5.18

indicates that the power spectra of velocity fluctuations at the spanwise locations of the pulse train should have very large components, not only at frequency $\nu_f/4$, but also at $3\nu_f/4$, where ν_f is the fundamental frequency of the wave train. Notice that not only is the flow no longer two dimensional, but there are no visible remnants of the two-dimensional wave train. There are interactions between two adjacent (phase-shifted) pulse trains, and between the pulse train and the fundamental wave train.

Contours of the power spectra of $\langle u_{pert} \rangle$ at y = 0 and x = 75, 125, and 175mm are shown in the z-frequency plane (figure 5.20). As expected, in spanwise locations of the pulse train, there are three peaks at frequency $\nu_f/4$ = 1.5 Hz, which is the frequency of pulse trains, and at $3\nu_f/4$. The power spectral component at the fundamental wave train frequency, ν_f = 6 Hz, is very small at x = 75 mm, and it becomes somewhat stronger farther downstream. There are two strong peaks in the power spectrum at $\nu_f/2$ at spanwise stations between two adjacent pulse trains. This subharmonic component is probably generated by spanwise interaction of staggered pulse trains. As can be seen from the surface plot of $\langle \tilde{u}' \rangle$ in figure 5.19, the time between passage of two vortical structures at the interface between two adjacent pulse trains is approximately equal to 2T. Finally, figure 5.21 shows power spectra of $\langle u_{pert} \rangle$ of the harmonically and pulsed excited flow (bottom) at x = 175 mm, (y,z) = 0. It is clear that the pulsed disturbance leads to a drastic increase in the amplitude of spectral components at high frequencies, suggesting a premature transition to turbulence.

5.7. *Conclusions*

The investigation reported in §5 appears to be the first experimental study of three-dimensional pulsed disturbances in a plane mixing layer, although related experiments have been conducted for the flat-plate boundary layer (Gaster & Grant 1975) and for an axisymmetric jet (Sokolov *et al.* 1980).

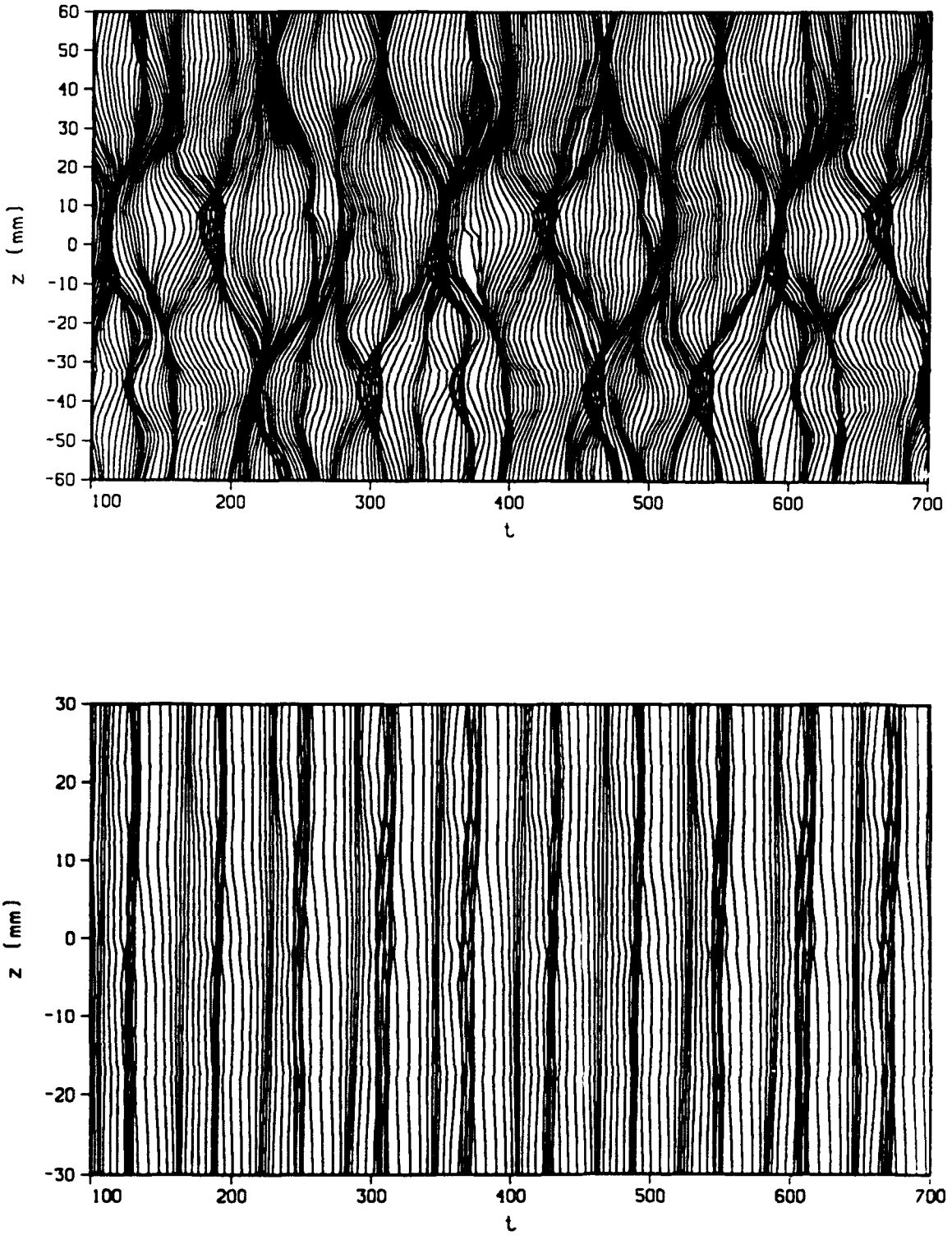
60
50
40
30
20
10
0
-10
-20
-30
-40
-50
-60
z (mm)
100
200
300
400
500
600
700
t
30
20
10
0
-10
-20
-30
z (mm)
100
200
300
400
500
600
700
t

Figure 5.19

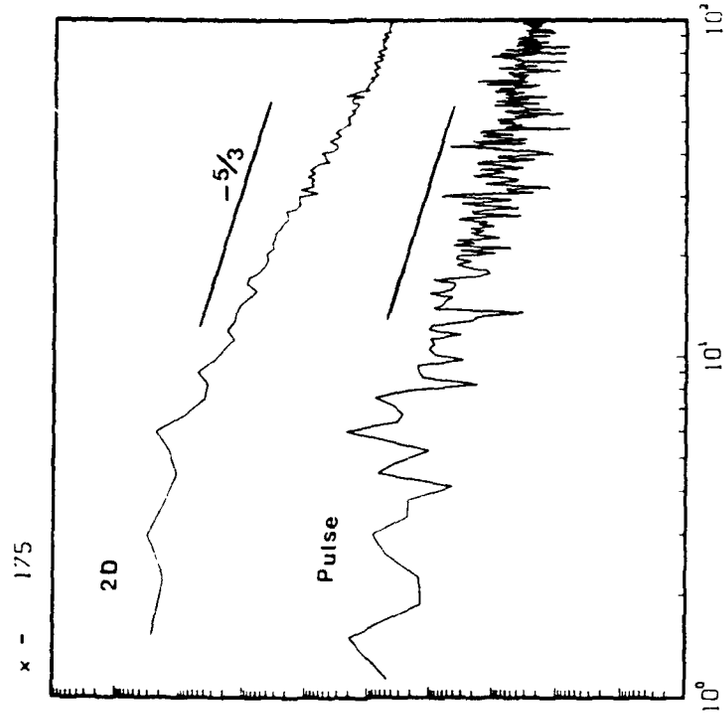

Figure 5.21

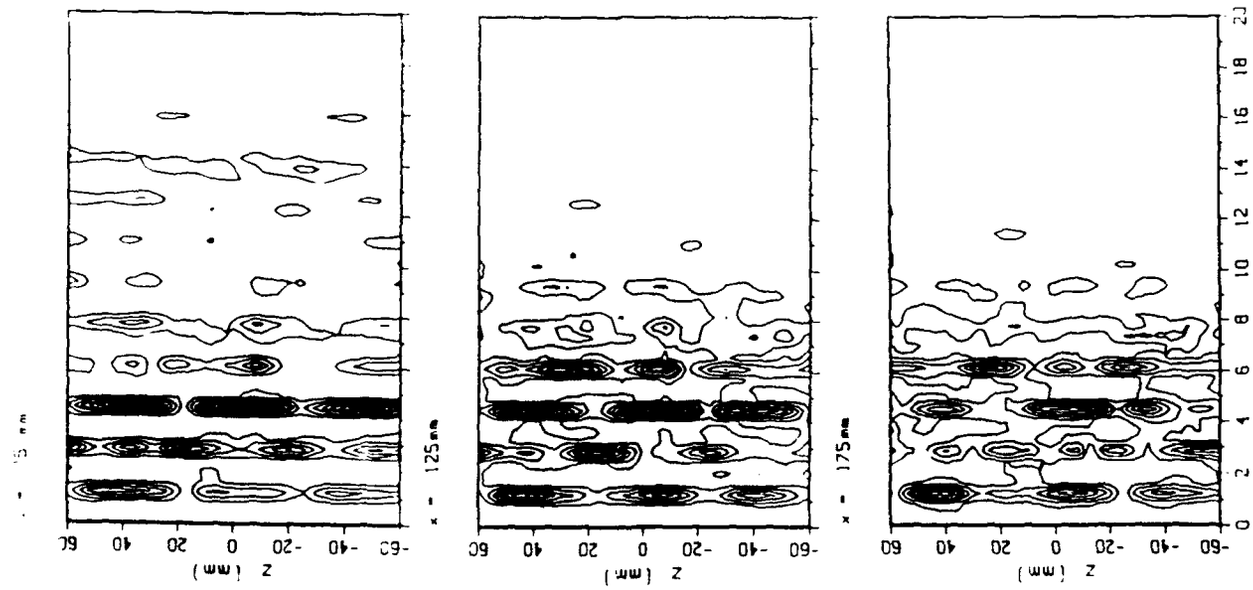

Figure 5.20

The present experiments consisted of two parts: In the first part, the evolution of a single three-dimensional pulsed disturbance in the shear layer was studied in detail. The second part focused on a cluster of temporally and spatially regular patterns of pulsed disturbances. The disturbances were effected via amplitude modulation of a spanwise-uniform time-harmonic wave train, which provided a clear phase reference for the phase-locked velocity measurements. The amplitude of the pulse was five times the amplitude of the wave train, and its duration was $0.4T_f$. We have found that the evolution of the pulsed disturbance depends crucially on the time delay between the modulation pulse and the carrier wave train, and that the plane mixing layer is most receptive to pulsed excitation when the pulse appears in the braid region between adjacent primary vortices of the base flow. The temporal change in ensemble-averaged cross-stream profiles of the streamwise velocity due to passage of the disturbance is clearly distinguishable from the response to the wave train alone, and it is felt across the entire width of the shear layer.

The evolution of vortex structures was studied using flow visualization and three-dimensional distributions of turbulence intensity of the streamwise velocity component. The pulsed disturbance resulted in a spanwise-localized pairing of the primary vortices that occurred much farther upstream than for the nominally two-dimensional pairing of the harmonically forced flow. The high levels of turbulence intensity suggests a transient increase of mixing. An amplitude demodulation technique was used to decompose the modulated velocity signals into a family of modal wave packets, and the evolution of the fundamental wave packet was studied in detail. We found that the wave packet spreads more rapidly in the spanwise direction than in the streamwise direction. In fact, its growth in the streamwise direction is limited by the primary two-dimensional instability of the base flow, which is in agreement with the findings of Glezer *et al.* (1989) and Dallard & Browand (1992). The wave fronts of the wave packet in plane mixing layers, as predicted by Balsa (1989), are almost parallel to the

spanwise direction (z-axis), in contrast to a boundary layer wave packet (Gaster & Grant 1975), where wave fronts of the packet are bowed. This feature of the shear layer wave packet is due to the fact that the cross-stream distribution of the mean streamwise velocity is almost antisymmetric relative to the cross-stream elevation where $U = U_c$. The fundamental wave packet in the present experiment spread in the spanwise direction at a rate approximately equal to $0.2U_c$. The dispersion relation of the fundamental wave packet shows that the wave packet in the plane shear layer is non-dispersive, in agreement with the results of Balsa (1989).

In the second part of the present experiments, three-dimensional pulsed disturbances forming a temporally and spatially periodic and staggered pattern were superimposed on the two-dimensional time-harmonic wave train. Contour plots of power spectra of the streamwise velocity exhibit strong spectral components at the frequency of the pulse train, $\nu_f/4$, as well as at $3\nu_f/4$, which is a direct result of the streamwise nonlinear interaction between the pulse train and the wave train. Also prominent are spectral components at the subharmonic, $\nu_f/2$, which are due to spanwise interaction between two adjacent, staggered pulse trains. Finally, compared to the harmonically excited flow, the pattern of pulsed disturbances causes a drastic increase in the amplitudes of high frequency, suggesting turbulent mixing enhancement.

5.8. *References*

Balsa, T. F. 1988 On the receptivity of free shear layers to two-dimensional external excitation. *J. Fluid Mech.* **187**, 155-177.

Balsa, T. F. 1989 Three-dimensional wave packets and instability waves in free shear layers and their receptivity. *J. Fluid Mech.*. **201**, 77-97.

Barr, P. K., Dwyer, H. A. & Bramlette, T. T. 1988 A one-dimensional model of a pulse combustor. *Combust. Sci. and Tech.* **58**, 315-336.

Browand, F. K. & Prost-Domasky,S. 1990 Experiment on pattern evolution in the two-dimensional mixing layer. In *New Trends in Nonlinear Dynamics and Patterning Phenomena: The Geometry of Non-Equilibrium* (ed. P. Coullet & P. Huerre). NATO ASI Series 8, Plenum.

Corke, T. C. & Mangano, R. A. 1989 Resonant growth of three-dimensional modes in transitioning Blasius boundary layers. *J. Fluid Mech.* **209**, 93-150.

Dallard, T. & Browand, F. K. 1992 Scale transitions at defect sites in the mixing layer: application of the 2D arc wavelet transform. *J. Fluid Mech.* (submitted).

Gaster, M. 1975 A theoretical model of a wave packet in the boundary layer on a flat plate. *Proc. Roy. Soc. Lond. A* **347**, 253-261.

Gaster, M. & Grant, I. 1975 An experimental investigation of the formation and development of a wave Packet in a laminar boundary layer. *Proc. R. Soc. Lond. A.* **347**, 253-261.

Glezer, A., Wygnanski, I. J. & Gu, X. 1989 Amplitude modulated excitation of a turbulent mixing layer. *Phys. Fluids A* **1**, 1007-1020.

Grossmann, A. & Morlet, J. 1984 Decomposition of Hardy functions into square integrable wavelets of constant shape. *SIAM J. Math. Anal.*, 723-736.

Grossmann, A. & Morlet, J. 1985 Decomposition of functions into wavelets of constant shape, and related transforms. *Mathematics + Physics, Lectures on Recent Results* (ed L. Streit), Vol. 1, pp. 135-165.

Keller, J. O., Bramlette, T. T., Dec, J. E. & Westbrook. C. K. 1989 Pulse combustion: the importance of characteristic times. *Combustion and Flame* **75**, 33-44.

Keller, J. O. & Westbrook, C. K. 1986 Response of a pulse combustor to changes in fuel composition. *21st Symposium (International) on Combustion*, pp. 547-555. The Combustion Institute.

Kim, Y. C., Khadra, L. & Powers, E. J. 1980 Wave modulation in a nonlinear dispersive medium. *Phys. Fluids* **23**, 2250.

Kleis, S. J., Hussain, A. K. M. F. & Sokolov, M. 1981 A turbulent spot in an axisymmetric free shear layer; part 3. azimuthal structure and initiation mechanism. *J. Fluid Mech.* **111**, 87-106.

Landahl, M. T. 1982 The application of kinematic wave theory to wave trains and packets with small dissipation. *Phys. Fluids* **25**, 1512-1516.

Miksad, R. W., Jones, F. L., Powers, E. J., Kim, Y. C. & Khadra, L. 1982 Experiments on the role of amplitude and phase modulations during transition to turbulence. *J. Fluid Mech.* **123**, 1-29.

Nygaard, K. J. 1991 Spanwise-nonuniform excitation of a plane mixing layer. PhD thesis, University of Arizona.

Nygaard, K. J. & Glezer, A. 1991 Evolution of streamwise vortices and the generation of small-scale motion in a plane mixing layer. *J. Fluid Mech.* **231**, 257-301.

Oster, D. & Wygnanski, I. 1982 The forced mixing layer between parallel streams. *J. Fluid Mech.* **123**, 91-130.

Sokolov, M., Hussain, A. K. M. F., Kleis, S. J. & Husain, Z. D. 1980 A turbulent spot in an axisymmetric free shear layer; part 1. *J. Fluid Mech.* **98**, 65-95.

Appendix: *Demodulation Technique*

A demodulation technique was developed to discriminate between the response of the flow to the carrier signal and to the modulating pulse. The objective was to decompose the response into a family of modal wave packets, each having a narrow band of frequencies centered around the excitation frequency and its higher harmonics. A similar technique was used by Kim, Khadra & Powers (1980) to study modulated waves in a weakly ionized plasma, and by Miksad, Jones, Powers, Kim & Khadra (1982) to study the interaction of two harmonic wave trains of different frequencies in a two-dimensional wake.

Consider an ensemble-averaged time series of the velocity perturbation

$$\langle u_{pert}(t)\rangle = \langle u(t)\rangle - U \,, \tag{A.1}$$

where $\langle u(t)\rangle$ is the ensemble-averaged velocity and U represents the time-averaged mean velocity. This time series (figure A.1*b*) has a power spectrum $|\langle \hat{u}_{pert}(\omega)\rangle|$ (figure A.1*a*), which suggests that the response of the flow to the excitation is primarily concentrated in relatively narrow frequency bands, $\Delta\omega$, around the carrier frequency, ω_0, and its harmonics, $(j+1)\omega_0$, where j is an integer. The spectral components within these frequency bands may be obtained by applying a band-pass filter $\hat{g}^*(\omega)$, centered at $(j+1)\omega_0$, to $\langle \hat{u}_{pert}(\omega)\rangle$. Figure A.1(*a*) shows one example of such a filter. Taking the inverse Fourier transform, the filtered signal around the fundamental frequency ω_0 is

$$S_0(t) = 2\int_{\omega_0-\Delta\omega}^{\omega_0+\Delta\omega} \langle \hat{u}_{pert}(\omega)\rangle\, \hat{g}^*(\omega)\, e^{i\omega t} d\omega \,. \tag{A.2}$$

Note that since $\langle u_{pert}(t)\rangle$ is real and its Fourier transform is complex conjugate in ω $[\langle \hat{u}_{pert}(-\omega)\rangle = \langle \hat{u}_{pert}{}^*(\omega)\rangle]$ and, because the filter $\hat{g}^*(\omega)$ is real and only has non-zero values in the interval $[\omega_0-\Delta\omega, \omega_0+\Delta\omega]$, the inverse Fourier transform of $\langle \hat{u}_{pert}(\omega)\rangle\, \hat{g}^*(\omega)$ is complex. The amplitude and the phase of $S_0(t)$ can be easily determined by its real and imaginary parts.

On the other hand, $S_0(t)$ in Eq.(A-2) may also be expressed as

$$S_0(t) = A_{M_0}(t)\, e^{i[\omega_0 t + \Psi_0(t)]} \,, \tag{A.3}$$

where

$$A_{M_0}(t) = |S_0(t)| \tag{A.4}$$

and

$$\Psi_0(t) = \tan^{-1}(Re\{S_0(t)\}/Im\{S_0(t)\}) - \omega_0 t \,. \tag{A.5}$$

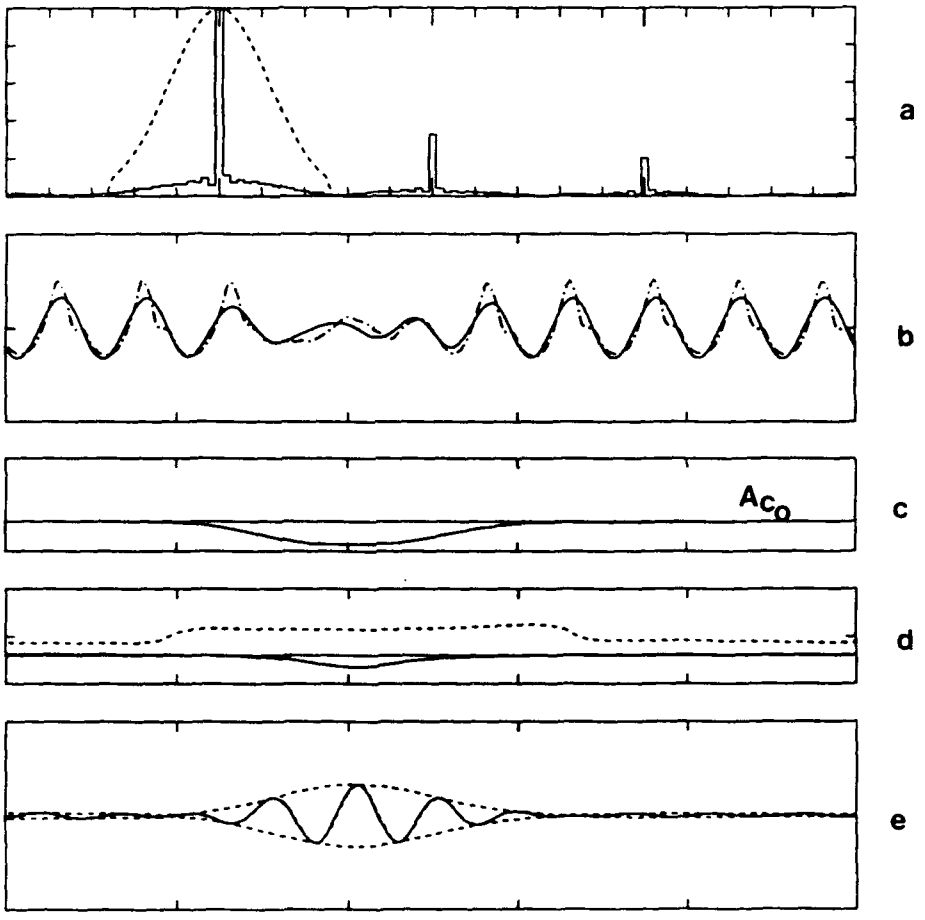

Figure A-1

The amplitude and phase of the modulated fundamental modal signal can be written as

$$A_{M_0}(t) = A_{c_0}[1 + c_0(t)] \tag{A.6}$$

and

$$\Psi_0(t) = \Psi_{c_0} + \phi_0(t) , \tag{A.7}$$

where A_{c_0} and Ψ_{c_0}, which are independent of time, are the amplitude and phase of the spectral component of $\langle u_{pert}(t) \rangle$ within $\Delta\omega$. When the flow is excited by the carrier signal only, $|c_0(t)|$ is the degree of amplitude modulation of $S_0(t)$ resulting from passage of the disturbance, and $\phi_0(t)$ represents the change in phase. The temporal variation of c_0 and ϕ_0 reflects the passage of the disturbance at the measurement station. Notice that $A_{c_0} c_0(t)$ is not the amplitude of the fundamental modal wave packet if $\phi_0(t)$ varies in time.

Figure A.1(*b*) shows the real part of $S_0(t)$ (as dotted curve), whereas its amplitude $A_{M_0}(t)$ is plotted in figure A.1(*c*) in which the amplitude of the fundamental carrier signal, A_{c_0}, is also indicated. The phase $\Psi_0(t)$ is shown in figure A.1(*d*). Note that A_{c_0} and Ψ_{c_0} are the asymptotic values of $A_{M_0}(t)$ and $\Psi_0(t)$ before or after the disturbance passes the measurement station. Furthermore, $c_0(t)$ may be negative (but $1+c_0(t) \geq 0$), indicating that the amplitude of flow response to the carrier signal may be diminished by the disturbance.

The modulated fundamental modal wave $S_0(t)$ can be thought of as the sum of a (complex) fundamental modal wave train, $W_{c_0}(t)$, and a (complex) wave packet, $W_{p_0}(t)$:

$$S_0(t) = W_{c_0}(t) + W_{p_0}(t) \tag{A.8}$$

with

$$W_{c_0}(t) = A_{c_0} \exp[i(\omega_0 t + \Psi_{c_0})] \tag{A.9}$$

and

$$W_{p_0}(t) = A_{p_0}(t) \exp[i(\omega_0 t + \Psi_{c_0} + \delta_0(t))] , \tag{A.10}$$

where A_{c_0} and $A_{p_0}(t)$ represent, respectively, amplitudes of the fundamental modal carrier wave train and the wave packet, and $\delta_0(t)$ is the relative phase between the wave packet and the wave train.

From Equations (A-3) and (A-6) to (A-10), one obtains

$$A_{p_0}(t)\, e^{i\delta_0(t)} = A_{M_0}(t)\, e^{i\phi_0(t)} - A_{c_0} \ . \tag{A.11}$$

Therefore,

$$A_{p_0}(t) = \sqrt{A_{M_0}(t)^2 + A_{c_0}{}^2 - 2A_{M_0}(t)A_{c_0}\cos(\phi_0(t))} \tag{A.12}$$

and

$$\tan\delta_0(t) = \frac{A_{M_0}(t)\sin\phi_0(t)}{A_{M_0}(t)\cos\phi_0(t) - A_{c_0}} \ . \tag{A.13}$$

Notice that when $\phi_0(t) = 0$, Eqs. (A.12) and (A.13) become

$$A_{p_0}(t) = A_{M_0}(t) - A_{c_0} = A_{c_0}\, c_0(t)$$

and

$$\delta_0(t) = 0 \ .$$

The fundamental wave packet, $Re\{W_{p_0}(t)\}$, and its amplitude $A_{p_0}(t)$ are shown in figure A.1(*e*). The j-th modal wave packet can be calculated similarly using the same procedure by replacing the subscript 0 with j and letting $\omega_j = j\omega_0$.

A final note. The function S_0 in Eq.(A.2) is, up to a normalization factor, a *wavelet transform* of $\langle u_{pert}(t)\rangle$ using a wavelet g[(t-b)/a] whose Fourier transform is $\hat{g}(a\omega)$ (which has finite supports) at *the* scale a corresponding to the *resonance frequency* ω_0. The *admissibility condition* for the wavelet is also satisfied, i.e., $\int g(t)dt = \hat{g}(\omega = 0) = 0$. More information about the wavelet transform can be found, for example, in Grossmann & Morlet (1984, 1985).

6. Publications Acknowledging AFOSR Grants 86-0324 and 88-0271

6.1 *Papers*

Fiedler, H. E., A. Glezer and I. J. Wygnanski, "The Control of the Plane Mixing Layer--Some Novel Experiments," in AIAA Series on Progress in Astronautics and Aeronautics, *Current Trends in Turbulence Research* (H. Branover, M. Mond, and Y. Unger, eds.), 112, 30-64, 1988.

Glezer, A., I. J. Wygnanski and X. Gu, "Amplitude Modulated Excitation of a Turbulent Mixing Layer," *Physics of Fluids A* 1, 1007-1020, 1989.

Nygaard, K. J. and A. Glezer, "On the Spanwise Structure of a Plane Mixing Layer," in *Advances in Turbulence 2* (H.-H. Fernholtz and H. E. Fiedler, eds.), 461-466, Berlin: Springer, 1989.

Nygaard, K. J. and A. Glezer, "Core Instability of the Spanwise Vortices in a Plane Mixing Layer," *Physics of Fluids A* 2, 461-464, 1990.

Nygaard, K. J. and A. Glezer, "Spanwise Nonuniform Excitation of a Plane Mixing Layer," AIAA Paper 91-0625.

Nygaard, K. J. and A. Glezer, "Evolution of Streamwise Vortices and the Generation of Small-Scale Motion in a Plane Mixing Layer," *Journal of Fluid Mechanics* 231, 257-301, 1991.

6.2 *Papers in Preparation*

Nygaard, K. J. and A. Glezer, "Phase Excitation of a Plane Mixing Layer," to be submitted to *Journal of Fluid Mechanics*.

Gu, X. and A. Glezer, "Three-Dimensional Anharmonic Forcing of a Plane Shear Layer," to be submitted to *Journal of Fluid Mechanics*.

6.3 *Conference Presentations*

Gu, X., A. Glezer, and I. J. Wygnanski, "Spatial and Temporal Evolution of Momentary Disturbances in an Excited Turbulent Mixing Layer," presented at APS/DFD Meeting, Columbus, Ohio, November 1986.

Gu, X., A. Glezer, and I. J. Wygnanski, "Evolution of a Pulsed Two-Dimensional Disturbance Superimposed on an Excited Turbulent Plane Mixing Layer," presented at the APS/DFD Meeting, Eugene, Oregon, November 1987.

Nygaard, K. J., A. Glezer, and I. J. Wygnanski, "Concurrent Streamwise and Spanwise Forcing of a Turbulent Mixing Layer," presented at the APS/DFD Meeting, Eugene, Oregon, November 1987.

Nygaard, K. J. and A. Glezer, "Experimental Investigation of a Spanwise Forced Mixing Layer," presented at the Second European Turbulence Conference, Berlin, August 1988.

Nygaard, K. J. and A. Glezer, "Spanwise Nonuniformly Forced Plane Mixing presented at the APS/DFD Meeting, Buffalo, New York, November 1988.

Nygaard, K. J. and A. Glezer, "Spanwise Amplitude-, Phase-, and Frequency-Modulated Excitation of a Plane Mixing Layer," presented at the AIAA 2nd Shear Flow Conference, Tempe, Arizona, March 1989.

Nygaard, K. J. and A. Glezer, "Excitation of Spanwise Instabilities in a Plane Mixing Layer," presented at the International Conference on Organized Structures and Turbulence in Fluid Mechanics, Grenoble, France, September 1989.

Gu, X. and A. Glezer, "Three-Dimensional Pulsed Excitation of a Plane Mixing Layer," presented at the APS/DFD Meeting, NASA-Ames Research Center, California, November 1989.

Nygaard, K. J. and A. Glezer, "Spanwise Instabilities in a Forced Plane Mixing Layer," presented at the APS/DFD Meeting, NASA-Ames Research Center, California, November 1989.

Nygaard, K. J. and A. Glezer, "Spanwise Instabilities and the Generation of Small-Scale Motion in a Plane Mixing Layer," presented at the Third European Turbulence Conference, Stockholm, Sweden, July 1990.

Nygaard, K. J. and A. Glezer, "Spanwise Core Instability of the Primary Vortices in a Plane Mixing Layer," presented at the APS/DFD Meeting, Ithaca, New York, November 1990.

Gu, X. and A. Glezer, "Three-Dimensional Pulsed Disturbance in a Turbulent plane Mixing Layer," presented at the APS/DFD Meeting, Arizona State University, Scottsdale, Arizona, November 1991.

Nygaard, K. J. and A. Glezer, "Coalescence of Primary Vortices in a Plane Mixing Layer--Three Dimensioanl Aspects," presented at the APS/DFD Meeting, Arizona State University, Scottsdale, Arizona, November 1991.

6.4 *Theses and Dissertations*

Kris J. Nygaard (M.S. 1987): "Construction, Instrumentation and Testing of a Spanwise Forced Plane Mixing Layer Facility"

Kris J. Nygaard (Ph.D. August, 1991): "An Experimental Investigation of a Spanwise Forced Mixing Layer"

Xiaogang Gu (Ph.D. June, 1992): "Temporally and Spatially Nonperiodic Excitation of a Plane Mixing Layer"